

Late-Paleocene paleoenvironmental and temperature changes at Point Margaret, South-East Australia, derived from dinoflagellate cysts, isotope and organic biomarker analyses

C.C.M. Rem

Abstract

A good understanding of the climate dynamics of the transition from the cold mid-Paleocene to the early Eocene hothouse is essential. This entails being able to recreate the reconstructed hothouse conditions in climate models. However, there is a mismatch between reconstructed and modelled sea surface temperatures for hothouse conditions at the Southern Ocean. An outcrop section of Late Paleocene age called Point Margaret, located in the Otway Basin, South-East Australia – paleolatitude $\sim 56^\circ$ S, was investigated to check whether the discrepancy between models and reconstructed SSTs is also present at the Australo-Antarctic Gulf (AAG). Branched and isoprenoidal GDGT concentrations were measured, elemental and $\delta^{13}\text{C}$ analyses were performed to and dinoflagellate cysts were counted to reconstruct the paleoenvironment. During the Late Paleocene, Point Margaret was located near shore close to a river which provided a high nutrient load. The FCO of *Apectodinium* occurred ~ 300 kyr before the PETM, this early acme is not related to the PETM but to changing conditions of the Proto-Leeuwin Current and/or AAG. Point Margaret and ODP Site 1172, Tasman Plateau, show a very similar response from ~ 100 kyr before to the onset of the PETM. This means that the sites must have been more connected than is possible with a closed Tasmanian Gateway and the ocean configuration related to this. Differences between SST and MAT records in the Southern Ocean, concerning especially absolute changes during the PETM, are extremely large. Thus MAT proxies with higher calibration ranges are needed to enable the reconstruction of higher absolute temperatures during hothouse conditions and to improve the comparison between MAT and SST. The relative temperature increase during the PETM at all Southern Ocean sites is in accordance with the increase obtained from models ($\sim 4^\circ\text{C}$) and the maximal global mean surface temperature anomaly ($\sim 5^\circ\text{C}$). However, models underestimate absolute temperatures of the entire Southern Ocean during the Late Paleocene and PETM with differences that cannot only be explained by calibration errors. Problems with models concerning the climate sensitivity and feedback mechanisms but also the application of a low latitudinal gradient and a greater polar amplification at more acceptable CO_2 conditions must be solved before they can be applied to the present day 'greenhouse world'.

1. Introduction

From the relatively cold mid-Paleocene (~ 58 Ma) to the Early Eocene Climatic Optimum (EECO; ~ 52 - 50 Ma) Southern Ocean surface and global deep-water temperatures increased drastically (Zachos et al., 2008; Bijl et al., 2009, 2013; Hollis et al., 2012). Atmospheric CO_2 concentrations in the mid-Paleocene seem comparable to those we measure today (although the information about Paleocene pCO_2 is scarce; Beerling &

Royer, 2011; Fig. 1). Whereas CO₂ values in the Eocene are similar or even higher than the most extreme Representative Concentration Pathway (RCP) scenario (RCP 8.5; IPCC, 2014) for the end of this century (i.e. ±1000 ppm; Fig. 1). The Eocene ‘hothouse’ is often considered as an end-member climate state regarding CO₂, which bears analogy to the predicted future CO₂ values. In order to better understand the development and implications for future climate of such hothouse climate states, a good understanding of the climate dynamics of the transition from the cold mid-Paleocene to the early Eocene hothouse is essential. This includes the reconstruction of these conditions in climate models and the role of ocean heat transport. Hollis et al. (2012) described two Eocene coupled climate model simulations, with 2240 and 4480 ppmv CO₂-equivalent representing middle Eocene and EECO (early Eocene Climatic Optimum; described later) conditions. However, there seems to be a mismatch between reconstructed and modelled sea surface temperatures (SST) for both these periods at the Southern Ocean (Hollis et al., 2012 and references therein; Fig. 2).

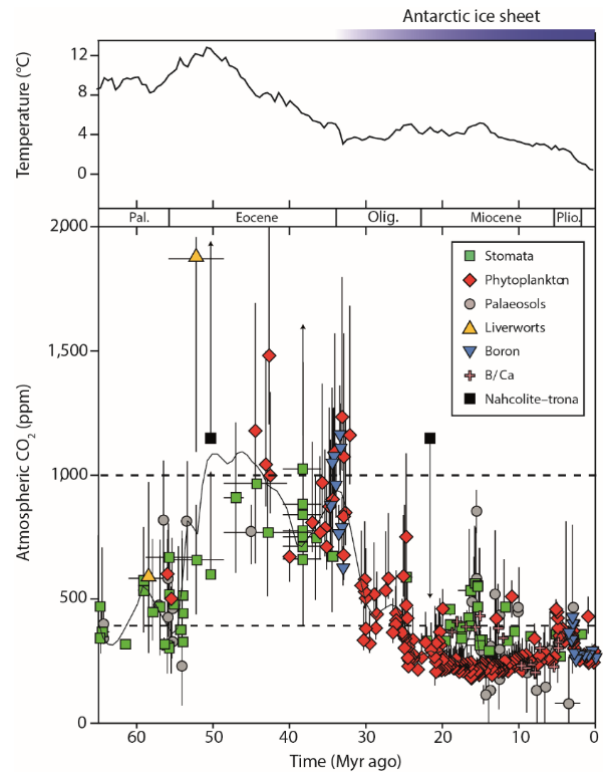


Figure 1: Earth's Cenozoic atmospheric CO₂ history reconstructed from terrestrial and marine proxies (Beerling and Royer 2011). The horizontal dashed line represents a CO₂ concentration of 390 ppm which is close to the present-day CO₂ value.

To compare the model results with our data, we assume that there were similar greenhouse conditions during the Late Paleocene and middle Eocene and during the EECO and PETM (Paleocene Eocene Thermal Maximum). Where the PETM is a short-lived period in the geological history, starting at 56 Ma (Gradstein et al., 2012), in which the temperature of the Earth rose with 5-8 °C (Sluijs et al., 2007a). Also, large changes in ocean chemistry and biotic response occurred during this event (Sluijs et al., 2007b) due to

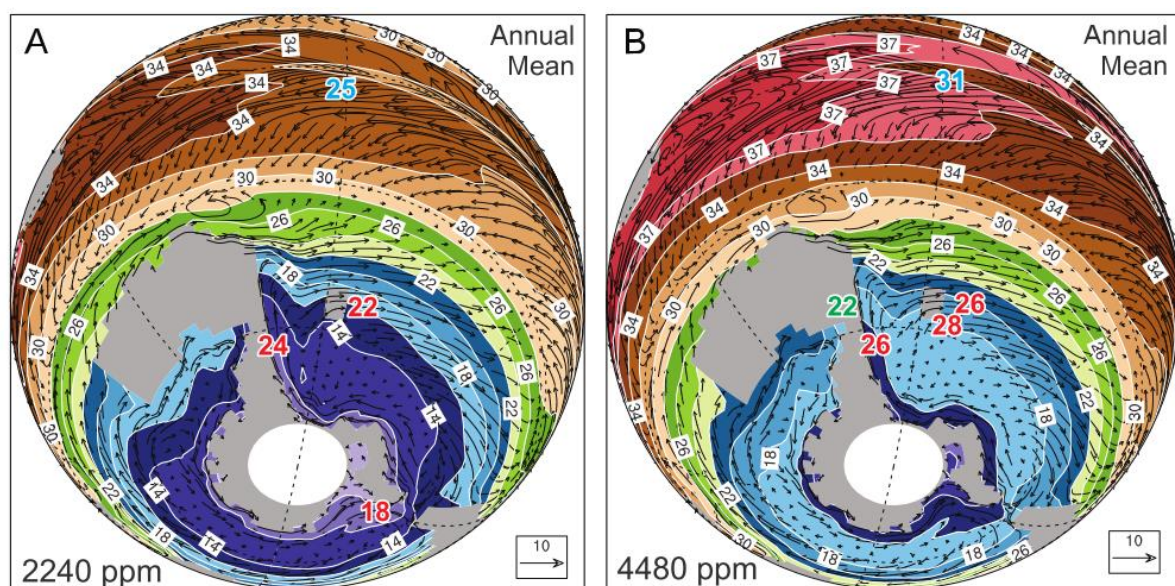


Figure 2: Eocene annual mean SST Model results for lower (A. 2240 ppm) and higher (B. 4480 ppm) greenhouse forcing compared to reconstructed mean SSTs (blue and red) and MATs (green) from the middle Eocene (A.) and EECO (B.) from Hollis et al., (2002).

rapid, at geological scale, and massive injections of ^{13}C -depleted carbon into the ocean atmosphere system (Dickens et al., 1997; Panchuk et al., 2008; Zeebe et al., 2009). The PETM was a hyperthermal which occurred during a long-term warming trend which build up to a period of extreme warmth called the EECO (Zachos et al., 2001; Zachos et al., 2008; Bijl et al., 2009; Westerhold & Röhl, 2009). During this period, lasting from ~ 50 to ~ 52 Ma, the warmest temperatures in the Cenozoic were recorded (Zachos et al., 2008).

Here we investigate an outcrop section called Point Margaret (coordinates: $38^\circ 43' 28.8'' \text{ S}$, $143^\circ 10' 35.0'' \text{ E}$), located in the Otway Basin, South-East Australia – paleolatitude $\sim 56^\circ \text{ S}$ (using Van Hinsbergen et al., 2015; Fig. 3), to check whether this discrepancy between models and reconstructed SSTs is also present at other locations in the Southern Ocean. Previous stratigraphic studies in this area have shown that the Pebble Point Formation (consisting of the Margaret, Buckley and Coble Cove Members) and the overlying Pember Mudstone (part of the Dilwyn Formation) are of Late Paleocene age (McGowran 1965; Holdgate & Gallagher, 2003; and references therein).

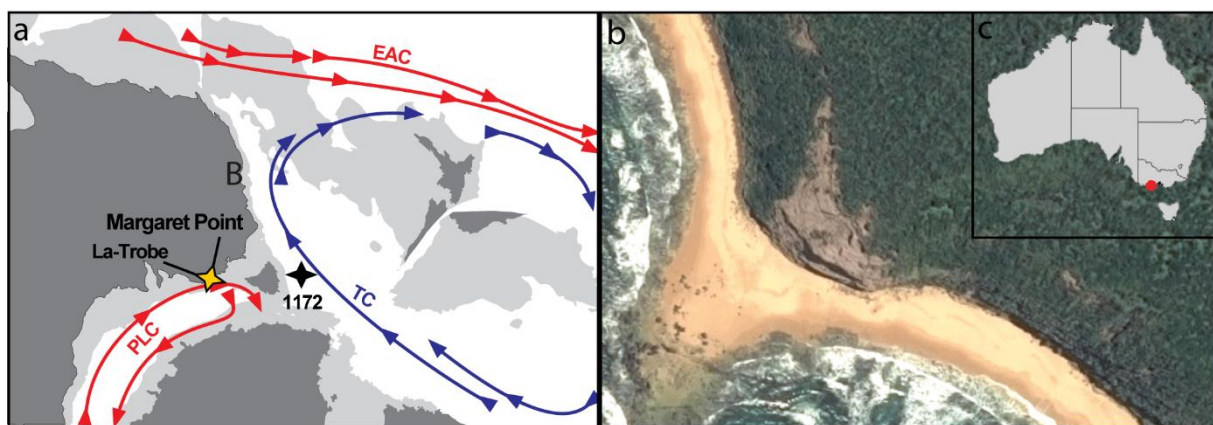


Figure 3: a) The location of the Point Margaret outcrop, La-Trobe core and ODP Site 1172 at the Late Paleocene with indicated ocean currents Proto-Leeuwin Current (PLC, Tasman Current (TC) and East Antarctic Current (EAC). b) The outcrop section of Point Margaret from Google Maps. c) The current location of Point Margaret in Australia

As the Tasmanian Gateway was still closed during the Late Paleocene (Bijl et al., 2013a), Point Margaret was located in the Australo-Antarctic Gulf (AAG) on the left side of the Tasman Rise (Fig. 3). Relatively warm low latitude-derived Indian Ocean waters were transported to this region by the Proto-Leeuwin Current (PLC; Huber et al., 2004). Whereas the Tasman Current (TC) transported relatively cool Antarctic-derived water towards Ocean Drilling Program (ODP) Site 1172, East Tasman Plateau (ETP) $\sim 58^\circ \text{ S}$ (using Van Hinsbergen et al., 2015), on the other side of the Tasman Rise (Sluijs et al., 2011, Fig. 3). During the Late Cretaceous and Paleocene the eastern end of the AAG was characterized by input of abundant terrestrial organic matter (OM) from adjacent landmasses, warm climatic conditions, low oxygenation of waters and possibly high marine biological productivity in eutrophic conditions (Exon et al., 2001).

To reconstruct temperatures the concentration of Glycerol Dialkyl Glycerol Tetraethers (GDGTs) in the sediment was measured. These GDGTs are membrane lipids from certain types of archaea, crenarchaeota, euryarchaeota and thaumarchaeota, and bacteria (e.g. Schouten et al. 2013). There are two main types of GDGTs, isoprenoidal (iGDGTs) and branched (brGDGTs). Isoprenoid GDGT lipids are mainly biosynthesized by Marine Group I Crenarchaeota and contain 0 to 3 cyclopentane moieties (GDGT-0 to GDGT-4) and crenarchaeol (Cren), which has a characteristic cyclohexane moiety as well as 4 cyclopentane moieties (Schouten et al., 2000, 2008; Sinninghe Damsté et al., 2002). A regio isomer of crenarchaeol (Cren') is also biosynthesized by these organisms. The

number of cyclopentane moieties is correlated to temperature as more cyclopentane moieties indicate higher temperatures. With this correlation SSTs can be calculated using proxies such as TEX₈₆ (Schouten et al., 2002; Liu et al., 2009; Kim et al., 2010).

BrGDGTs are membrane-spanning lipids which are abundantly present in mesophilic settings (Schouten et al., 2013), such as soils, lakes, rivers, marine sediments and peat deposits (Naafs et al., 2017a; and references therein). They are produced by (acido)bacteria which adjust the membrane fluidity to the different soil conditions they are found in (Weijers et al., 2009; Sinninghe Damsté et al., 2011). The alkyl core chain of these lipids is a straight chain comprising two to three methyl groups (Ia, IIa, IIIa; Fig. 4), which can undergo internal cyclization resulting in the presence of one or two cyclopentane moieties (Weijers et al., 2006a; Ib, Ic, IIb, IIc, IIIb, IIIc; Fig. 4). The changes in methylation are correlated to changes in soil pH and the changes in cyclisation to changes in mean annual air temperature (MAT; Weijers et al., 2007). It is likely that temperature has a direct effect on the membrane fluidity whereas the proton gradient across the membrane influences soil pH (Weijers et al., 2007a). De Jonge et al. (2013) found brGDGT isomers which have a different position of the methyl groups on the branched carbon skeleton. This occurs in the hexa- and penta-methylated brGDGTs, where the methyl group(s) are situated at the 6 position rather than the 5 position (IIa', IIb', IIc', IIIa', IIIb', IIIc'; Fig. 4). A different chromatographic HPLC method must be used to enable separation of the 5- and 6-methyl brGDGTs (De Jonge et al., 2013).

Apart from using GDGTs to determine temperature, dinoflagellate cysts (from now on called dinocysts) were counted to improve the existing age model using biostratigraphy and to describe the palaeoenvironment of Point Margaret. Dinocysts are preserved organic walled hypnozygotic resting cysts produced by dinoflagellates (Sluijs et al., 2005), which are single-celled eukaryotic plankton occurring as motile cells in surface waters (e.g. Fensome et al., 1996). Different dinocysts species, groups or genera are assumed to reflect different environmental conditions as explained by Sluijs and Brinkhuis (2009)

Finally, elemental and $\delta^{13}\text{C}$ analyses were performed to determine changes in the total organic carbon (TOC) and $\delta^{13}\text{C}$. Changes in these parameters will show changes in the organic matter supply and can help determine the presence and magnitude of the PETM at Point Margaret.

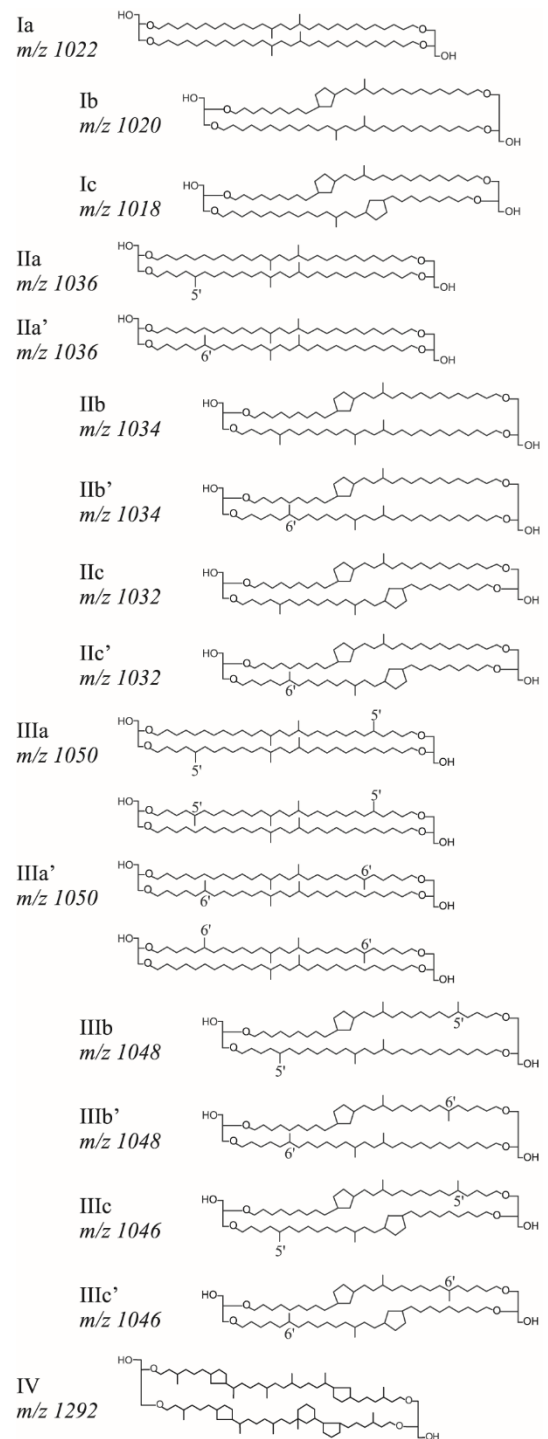


Figure 4: An overview of all the branched GDGTs and Crenarchaeol (IV) from De Jonge et al., (2014a)

2. Materials

The Otway Basin is a basin situated in the South-East of Australia (Fig. 5), which was part of the northern flank of the AAG during the Late Paleocene. During the early Paleogene, sediments in the Otway Basin were siliciclastics, organic-rich but carbonate poor (Holdgate and Gallagher, 2003). The Pebble Point Formation is the first formation of the Otway Basin (Holdgate and Gallagher, 2003) and is a late Thanetian marine ingressions (as in a relatively short transgression) which is part of a bigger ingressions sequence (McGowran, 1978, 1991; McGowran et al., 2004). Lithologically, the Pebble Point Fm. is characterized by meter-scale mud-to-sandstone alternations interpreted to represent high-energy shallow-marine environments (e.g. Keating, 1993). The Dilwyn Formation overlies the Pebble Point Fm., and its first member, the Pember Mudstone, is characterized by homogeneous silty claystones in this region (Arditto, 1995). The Pember Mudstone represents the first large transgression of the Dilwyn Fm., which also consists of the Rivernook-A and Rivernook Beds (Arditto, 1995).

The Otway Basin is of Late Paleocene age since *Globanomalina australiformis*, a foraminifer species, was found in the upper part of the Pebble Point Formation (close to Point Margaret; McGowran, 1965). *G. australiformis* has a FAD (First Appearance Datum) in the Southern Ocean between 50 and 560 kyr before the negative carbon isotope excursion (CIE) associated with the PETM (Huber & Quillev er e, 2005) and so must be of Late Paleocene age.

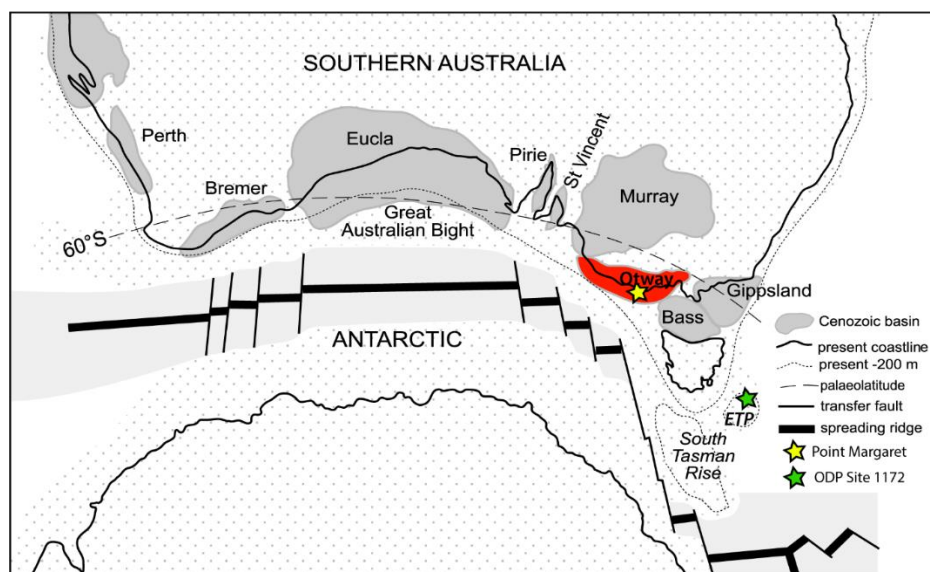


Figure 5: An overview of the Cenozoic basins of Southern Australia modified from McGowran et al., (2004).

3. Methods

3.1 Sample collection

During a field expedition in February 2016, samples were obtained from Point Margaret. The Pebble Point Formation and Pember Mudstone (part of the Dilwyn Formation) were targeted for high-resolution sampling. Preferentially fine grained, organic-rich strata were sampled in the Pebble Point Fm., to optimize the palynological yield. For the upper ~17 m of the outcrop, 35 stainless steel casings, 53x5x3 cm (length x width x depth), were hammered into the thoroughly cleaned substrate with 1-2 cm overlap. From the 365

samples, 57 were from the Pebble Point Fm and 308 from the Pember Mudstone, the topmost part of the Pember Mudstone and the overlying Rivernook Beds are not exposed or missing at Point Margaret.

The outcrop is nearly vertical in the first ~23 m (Pebble Point Formation), whereas the rest of the outcrop (Pember Mudstone) shows a 60-75 degree slope angle. This means that the thickness of the Pember Mudstone has been somewhat overestimated relative to the thickness of the Pebble Point Fm.

3.2 Palynologic analyses

Samples from Point Margaret were processed in the GML laboratory of Utrecht University. Palynological microscope slides were generated using standard palynological processing techniques, described in Brinkhuis et al. (2003); Sluijs et al. (2003); and Bijl (2011). Shortly this entails treating the manually crushed and oven dried sediment (11-14 g/sample) samples with hydrochloric (HCl) acid and hydrofluoric (HF) acid and then sieving the residue. An exotic marker spore (*Lycopodium clavatum*, Lund University batch #3862, n = 9666) was added to each sample to allow the calculation of absolute (specimens/gram dried sediment) palynomorph abundances. Carbonates and silicates were removed using a 10 and 30% treatment with HCl, followed by two treatments with 38-40% HF acid. After these treatments samples were neutralized with de-ionized water and then sieved over 10 and 250 µm nylon sieves to remove small and large particles. Finally, the 250-10 µm residue was mounted on a microscope slide using glycerine jelly and sealed. The sample residues and slides are stored at the Laboratory of Palynology and Palaeobotany, Utrecht University, Utrecht, The Netherlands.

For each sample up to 200 dinoflagellate cysts were counted. The dinocyst taxonomy described in Fensome & Williams (2004) was followed, however Sluijs et al. (2009) was used to determine the different spiny peridinioid taxa. Terrestrial palynomorphs were counted till 20 lycopodium spores and more than 200 pollen and spores were found. Dinocyst images were taken using a Leica DM2500LED microscope with a Leica MC170AD camera with 5 mega pixel resolution.

In total 81 samples from Point Margaret were counted, 61 samples (> 32.1 m) were counted by Joost Frieling and 20 samples (3.32 – 32.1 m) were counted by me. To ensure that the dinocyst data could be combined and used as one dataset, some slides were counted by both researchers and later discussed. Terrestrial palynomorphs were counted in more detail up to 32.1 m and later sorted into three main groups: gymnosperms, angiosperms and pteridophytes. For the upper part of the section only the number of terrestrial palynomorphs was counted to enable calculation of the marine/terrestrial palynomorph ratio per sample.

3.3 Elemental and $\delta^{13}\text{C}$ analyses

A representative part of the sample was freeze dried and ± 0.3 g was crushed to a powder. To decalcify the sediment, twice 7.5 ml of HCl was added to each sample after which it was shaken and centrifuged. The residue was neutralized by adding de-ionized water. Only one sample (PP31) reacted with the HCl and was therefore left out of the results. The residue was dried in the oven (50 °C). To obtain the total organic carbon (TOC) content, the remainder of the sample was crushed to powder and measured with an Elemental Analyzer (EA), Fisons 1500 CMS, at the GML laboratory at Utrecht University. From this same powder stable carbon isotopes were measured on a ThermoScientific DeltaV

advantage coupled to a ThermoScientific Flash 2000 EA at the Royal Netherlands Institute for Sea Research (NIOZ).

In total 246 samples were analysed from which 150 by Joost Frieling (> 33 m) and 96 (1.7 - 33 m) by me. 3 samples were excluded due to processing and measuring mistakes.

3.4 Organic biomarker analyses

Between 6 and 14 grams of freeze-dried and manually powdered sediment was used per sample to extract organic compounds out of the sediments. This was done by using a mixture of dichloromethane (DCM) and methanol (MeOH) at a ratio of 9:1 in the Dionex Accelerated Solvent Extractor (ASE) at 100 °C, 7*10⁶ Pa. Then the excess solvents were removed by a N₂ flow using the TurboVap machine. The dried extract was rinsed out of the vial with DCM/MeOH (9:1) and put to dry under a stream of N₂. After this the extract could be separated in polar and apolar fractions. This was done by using an activated Al₂O₃ column adding hexane: DCM (9:1), hexane: DCM (1:1) and DCM:MeOH (1:1) respectively. The polar fraction, which contains the GDGTs, was dissolved in hexane: isopropanol 99:1. A standard was added of C₄₈ with 99 ng/vial to the polar fractions. The redissolved fractions were subsequently filtered over a 0.45µm and 4mm diameter PTFE filter. The fractions were analysed on GDGTs on an Agilent 1290 high performance liquid chromatograph coupled to an Agilent 6130 mass spectrometer (HPLC-MS) using the settings described by Hopmans et al. (2016).

90 sediment samples were analysed on GDGTs, of which 70 (> 33.25 m) were processed by Joost Frieling, and 20 from (3.32 - 33.25) were processed by me.

To obtain the different proxy records the following equations were used:

$$BIT = \frac{[(Ia) + (IIa) + (IIIa) + (IIa') + (IIIa')]}{[(Ia) + (IIa) + (IIIa) + (IIa') + (IIIa') + (IV)]} \quad (1)$$

$$MAT_{mr} = 7.17 + 17.1 \cdot [Ia] + 25.9 \cdot [Ib] + 34.4 \cdot [Ic] - 28.6 \cdot [IIa] \quad (2)$$

$$pH_{soil} = 7.15 + 1.59 \cdot CBT' \quad (3)$$

Where:

$$CBT' = \log\left(\frac{[Ic] + [IIa'] + [IIb'] + [IIc'] + [IIIa'] + [IIIb'] + [IIIc']}{[Ia] + [IIa] + [IIIa]}\right) \quad (4)$$

$$MAAT_{peat} = 52.18 \cdot MBT'_{5me} - 23.05 \quad (5)$$

Where:

$$MBT'_{5me} = \frac{[Ia] + [Ib] + [Ic]}{[Ia] + [Ib] + [Ic] + [(IIa) + (IIb)] + [(IIc) + (IIIa)]} \quad (6)$$

$$pH_{peat} = 2.49 \cdot CBT_{peat} + 8.07 \quad (7)$$

Where:

$$CBT_{peat} = \log\left(\frac{[Ib] + [IIa'] + [IIb] + [IIb'] + [IIIa']}{[Ia] + [IIa] + [IIIa]}\right) \quad (8)$$

The roman numerals refer to the different branched GDGTs (brGDGTs; Fig. 5). Fractional abundances were used where GDGTs are enclosed in square brackets.

The BIT (Branched Isoprenoid Tetraether) index from Hopmans et al. (2004), with the inclusion of 6-methyl brGDGTs (Sinninghe Damsté, 2016), is a proxy for the relative abundance of fluvially-transported soil organic matter (OM) relative to marine OM (Schouten et al., 2013). The pH_{soil} and MAT_{mr} (mean air temperature) calibrations were taken from De Jonge et al. (2014a), the pH_{peat} and $MAAT_{peat}$ calibrations were taken from Naafs et al., (2017b). The $MAAT_{soil5me}$ from Naafs et al., (2017a) was not used since all samples of Point Margaret had an isomerisation ratio (IR_{6me}) higher than 0.6. Since the temperature dependence is different when samples contain more 6-methyl than 5-methyl brGDGTs (Naafs et al., 2017a).

Furthermore, other ratios were used to assess changes in the distribution of the brGDGTs through time:

$$\% \text{ tetra} = \Sigma[\text{tetramethylated brGDGTs}] = [Ia] + [Ib] + [Ic] \quad (9)$$

$$\% \text{ penta} = \Sigma[\text{pentamethylated brGDGTs}] = [IIa] + [IIb] + [IIc] + [IIa'] + [IIb'] + [IIc'] \quad (10)$$

$$\% \text{ hexa} = \Sigma[\text{hexamethylated brGDGTs}] = [IIIa] + [IIIb] + [IIIc] + [IIIa'] + [IIIb'] + [IIIc'] \quad (11)$$

$$\#rings_{tetra} = \frac{[Ib] + 2 \cdot [Ic]}{[Ia] + [Ib] + [Ic]} \quad (12)$$

$$\#rings_{penta\ 5Me} = \frac{[IIb] + 2 \cdot [IIc]}{[IIa] + [IIb] + [IIc]} \quad (13)$$

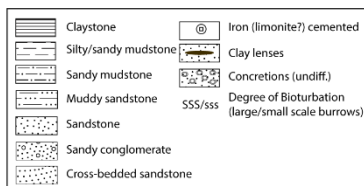
$$\#rings_{penta\ 6Me} = \frac{[IIb'] + 2 \cdot [IIc']}{[IIa'] + [IIb'] + [IIc']} \quad (14)$$

$$IR_{penta} = \frac{[IIa'] + [IIb'] + [IIc']}{\Sigma[\text{pentamethylated brGDGTs}]} \quad (15)$$

$$IR_{hexa} = \frac{[IIIa'] + [IIIb'] + [IIIc']}{\Sigma[\text{hexamethylated brGDGTs}]} \quad (16)$$

The ratios and formulas are selected from Sinninghe Damsté (2016). The #rings (see Eqs. 12,13 and 14) calculate the weighted average number of cyclopentane moieties for the tetra- and pentamethylated brGDGTs, whereas the isomer ratio (IR, Eqs 15 and 16) calculates the 6-Me share of penta- and hexamethylated brGDGTs over the total penta- and hexamethylated brGDGTs.

To identify the sources and evaluate distributional changes of brGDGTs at Point Margaret the data was compared to the global soil data set comprised by De Jonge et al. (2014a) and to the global peat dataset comprised by Naafs et al. (2017b). The global soil dataset consists of 239 soils, from which 21 soils were left out due to insufficient amounts of brGDGT to calculate the indices. From 2 samples, Egypt-2 and France-TES033, the data was not available. The list of global soils used here is shown in Appendix C, table 1. The global peat dataset contains 470 samples from 96 different peatlands. The average values per peat were used to derive the different distribution indices as multiple samples were taken per peatland. From these 96 averages, 18 samples were excluded because of insufficient amounts of brGDGTs. The list of the global peat dataset is shown in Appendix C, table 2.



3.5 Statistical analyses

Principal component analysis (PCA) was performed on the dinocysts assemblages to show the behaviour of the dinocyst species compared to each other. It was performed by the program C2

4. Results

4.1 Lithology

The Pebble Point Formation at Point Margaret is mainly composed of (muddy, and sometimes conglomeritic) sandstone beds with varying grainsizes (ϕ between 0 and 3) and changes in relief containing large burrows and pebbles (Fig. 6). Some (sandy) mudstones are also present in the first ~23 m, where the larger beds show fining or coarsening upward sequences. From ~23 m onwards the lithology becomes dominated by sandy mudstones which marks the beginning of the Pember Mudstone member of the Dilwyn Formation. The sandy mudstone is very dark brown to black when freshly exposed and contains elemental sulphur in filling cracks, higher up small burrows are present. There are only four beds which are of a different lithology in the Pember Mudstone, these are two sandier intervals at ~30.5 and ~42 m and two iron concretionary zones at ~37.5 and ~46 m. Just before the second concretionary zone the clay content increases, and after this zone the lithology becomes silty claystone with a slightly higher relief than the sandy mudstone. The silty claystone is dark brown to black when freshly exposed, contains elemental sulphur in filling cracks and contains abundant burrows. Between ~49 and ~51 m, the silty claystone becomes very dark and after this interval the Pember Mudstone is no longer pyritic.

4.2 Elemental and isotopic changes

$\delta^{13}\text{C}$ values vary between -24.19 and -29.94 ‰, where a sharp decline is visible at the top of the section from 50.92 to 52.23 m (Fig. 7). The drop in $\delta^{13}\text{C}$ goes from -26.69 to -29.94 ‰, which is a difference of ~3-4‰. A negative carbon isotope excursion (CIE) of this magnitude is linked to and characteristic of the PETM (Kennett and Stott, 1991; Koch et al., 1992; Schouten et al., 2007). As the Pember Mudstone in which this CIE is found is of Late Paleocene age, it is certain that the negative CIE found at Point Margaret represents the PETM.

For each sample, the measured $\delta^{13}\text{C}$ values were compared to other measured environmental variables from Point Margaret

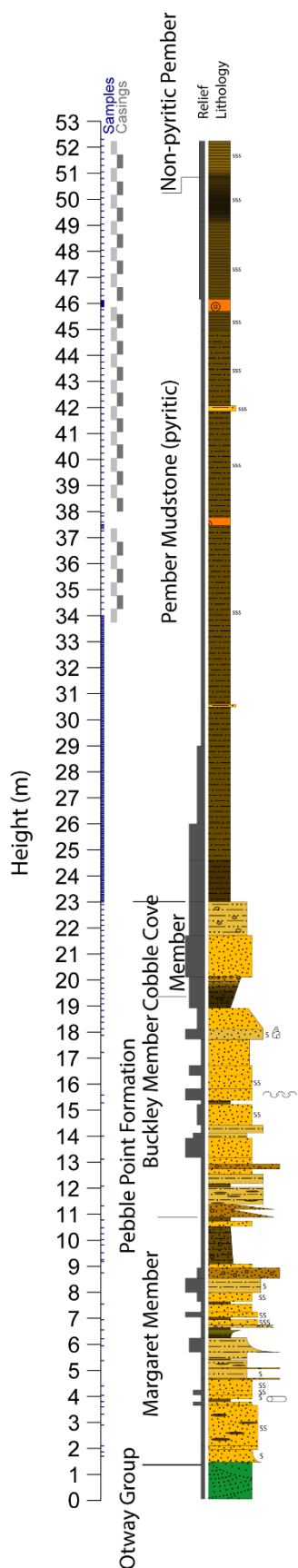


Figure 6: Point Margaret lithology

(Appendix C; Fig. 1). As no correlation was visible between $\delta^{13}\text{C}$ and the C:N ratio, TOC, grainsize (a value for ϕ , ranging between -3, conglomerate, and 7, claystone) or the marine percentage per sample, I assume that the global signal of $\delta^{13}\text{C}$ was captured at Point Margaret.

The TOC values of Point Margaret range between 0.11 and 2.4 wt%, where values during the PETM (> 51.16 m) are lower than 1.0 wt%. TOC values are only higher than 0.83 when the grainsize of the samples is 5 or higher, which represents mud- or claystone.

4.3 Age model

Since it has been determined that the PETM is present at Point Margaret, the onset at 50.92 m can be dated as 56 Ma (Gradstein et al., 2012). Furthermore, when applying the new geologic time scale (Gradstein et al., 2012), *Globalomalina australiformis* has a FAD at 56.56 Ma. This foram was found in the Pebblestone Formation close to Point Margaret in a bed containing shells and gastropods (McGowran, 1965). At the outcrop itself this can either be a medium sandstone containing red iron staining, 50% pebbles (2-10mm) and ~10% shell hash with bivalves and gastropods moderately cemented, which is situated between 15.31 and 15.76 m in the section. Or, less likely, a fine to coarse, poorly sorted, sandstone with iron oxide (and chert), ~5% pebbles (2-5 mm) and well cemented gastropod casts, which is situated between 17.66 and 18.06 m in the section. The bioevent containing *Morozovella Acuta* has an age 0.7 Ma younger than *Globanomalina australiformis* (Wade et al. 2011; table 4). Which means the Rivernook-A bed has an age of ± 55.69 Ma or younger so the outcrop is younger than ± 55.69 Ma. Which is in agreement with the age determined at the top of the section related to the onset of the PETM.

Dinocysts can also be used as biostratigraphic markers and placed in regional zonations. For the Southern Ocean the most recent zonations have been made for the early Paleogene South Pacific Ocean by Bijl et al., (2013b) and eastern New Zealand by Crouch et al. (2014). Although these regions are from a different oceanographic setting (Fig. 3), Point Margaret can be correlated to zones SPDZ1 and SPDZ2 from Bijl et al. (2013b) and to zones NZDP7 and NZDP8 from Crouch et al., (2014). The zones from both zonations are mainly based on the First Common Occurrence (FCO) of *Apectodinium homomorphum* (SPDZ1 to SPDZ2) or Lowest Common Occurrence (LCO) of the *Apectodinium* genus (end of NZDP8) which is the same event at Point Margaret. This FCO or LCO of *Apectodinium* occurs just before or at the onset of the PETM at the studied site for the zonations whereas it occurs more than 17 m before the PETM at Point Margaret. This means that although Point Margaret can be correlated to these zonations it is more logical to correlate with (SE) Australian zonations. However, the comparisons between Point Margaret and the zonations from Wilson (1988) and Arditto (1995) do not improve the age constraints delimited in the paragraph above and so are not discussed here.

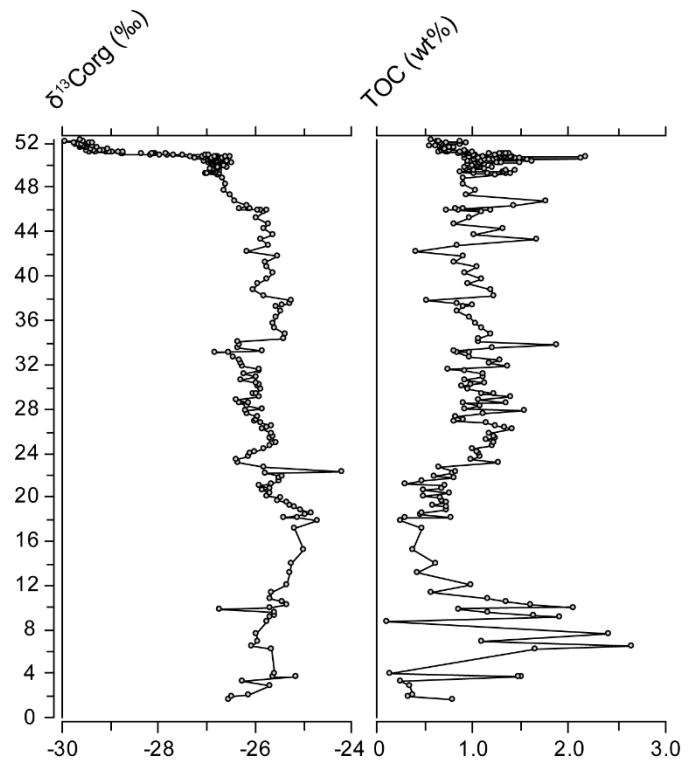


Figure 7: The $\delta^{13}\text{C}$ and TOC records plotted against depth (m)

When it is assumed that there was a constant sedimentation rate, the age range of this section can be determined with the two age tie points. Namely the negative CIE at 50.92 m and the presence of *Globanomalina australiformis* in the Pebble Point formation. When the more likely tie point of *Globanomalina australiformis* is used the age range of this section, from the Pebble Point formation onwards, lies between 56.80 and 55.98 Ma. When you choose the less likely tie point of *Globanomalina* you get an age between 56.86 and 55.97 Ma (Fig. 8). This indicates that this section is less than a million years old. From which it can be calculated that the average sedimentation rate was around 6,38 cm/kyr.

However, the assumption that there was a constant sedimentation rate is unlikely as especially the lower part of the section (<23 m) shows many changes in lithology and the lithology changes drastically from mainly sandstone to sandy mudstone at 23 m and from sandy mudstone to claystone at 45 m (Fig. 6).

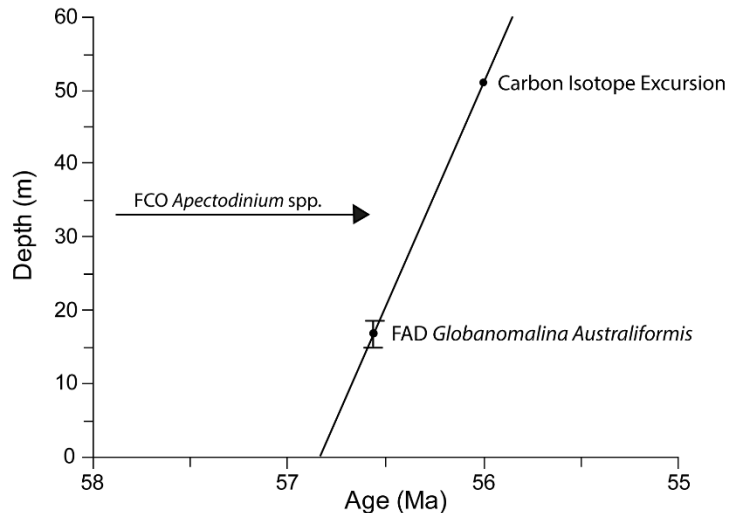


Figure 8: Age model of the Point Margaret outcrop with the indication at what depth the FCO of *Apectodinium* spp. (or homomorphum) is present

4.4 Marine palynomorphs

The first ± 20 meters of the section is dominated by *Senegalinium*, in this interval *Cerodinium* is abundant too and there are some abundant occurrences of *Spinidinium*, *Operculodinium* and *Hafniasphaera* (Fig. 9). The absolute and relative abundances of marine palynomorphs is low. This changes between 19.88 and 21.03 m, when the percentage of marine palynomorphs increases to 65% due to the appearance of *?Goniodomid* sp. 1. This species reaches abundances of up to 78 % of the assemblage but adds to the community rather than replacing other species, since the absolute abundance of *Senegalinium* is not significantly affected by the appearance (Fig. 7). At 22.1 m, *?Goniodomid* sp. 1 is not abundant anymore and *Spinidinium*, *Areoligera* and *Cordosphaeridium* fill this gap. The assemblage up to 45.75 m, is dominated by *Diphyes* and *Senegalinium* where first *Cerodinium* and *Spiniferites* and then *Spinidinium*, *Phthanoperidinium*, *Deflandrea* and *Spiniferites* are moderately abundant. During this interval there are many fluctuations in the absolute and relative abundance of marine palynomorphs, which seem to covary the most with the absolute abundances of *Diphyes* and *Senegalinium*. At 33.25 m, the first common occurrence (35%) of *Apectodinium* is observed. The next *Apectodinium* acme (>55 %) occurs between 45.75 and 46 m, as a result the relative abundance of marine palynomorphs reaches abundances up to 46% (Fig. 9). During the interval with increased *Apectodinium*, between 45.75 and 46.07, first *Glaphyrocysta* then *Enneadocysta* and finally *Muratodinium* show increased abundance.

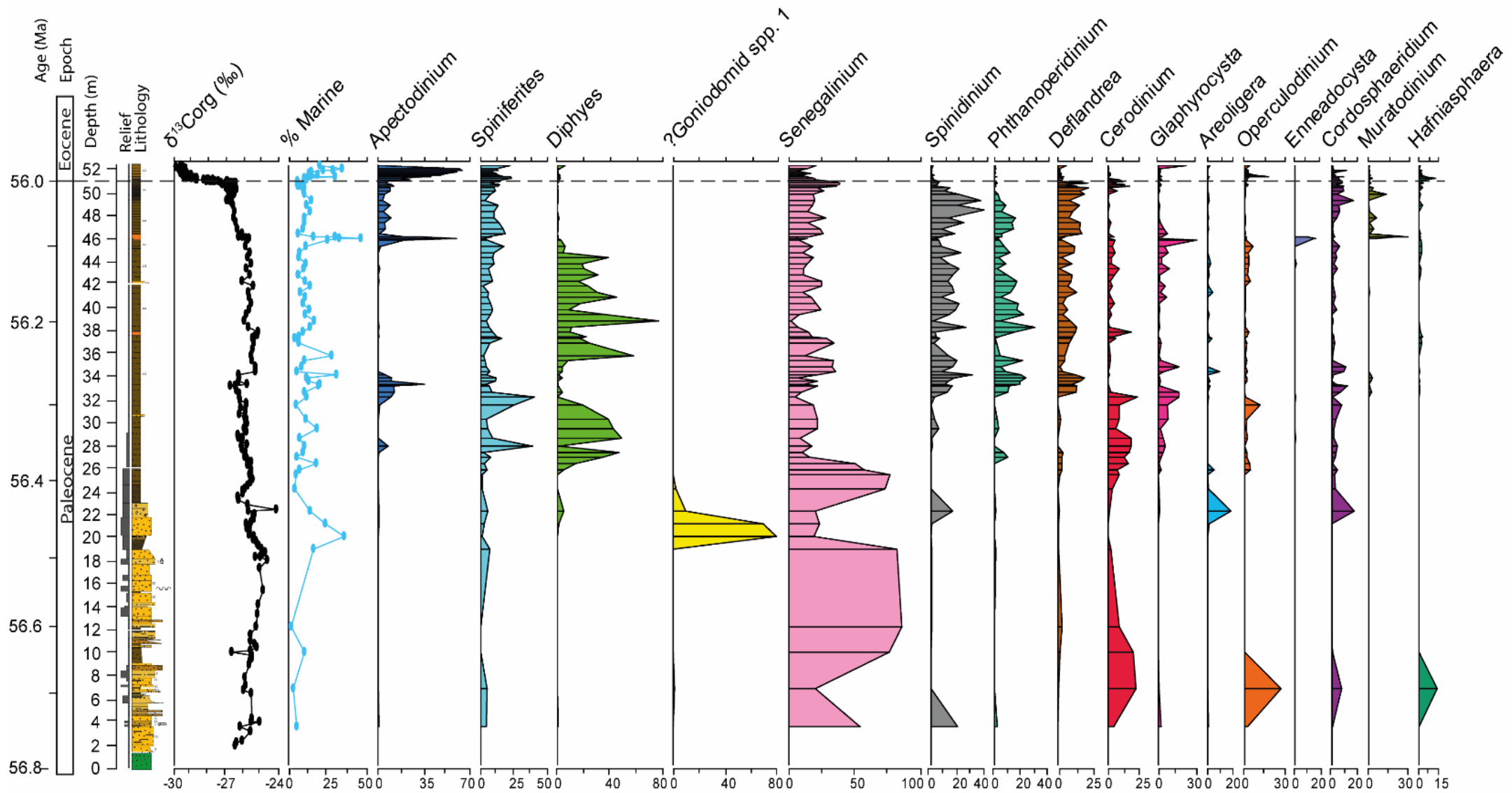


Figure 9: Relative dinocysts abundances plotted against depth and age of the section. All species with more 15% contribution somewhere in the section was selected. The lithology, $\delta^{13}\text{C}$ and the marine %, the part of the sample that has a marine origin, are also displayed. The dashed line indicates the onset of the PETM.

The final *Apectodinium* acme occurs between 51.275 and 52.03 m, during this period *Spiniferites* and *Senegalinium* are also moderately present. The section ends with an increased abundance of *Glaphyrocysta*.

There is a lot of variability between gonyaulacoid and peridinioid dinocysts at Point Margaret (P/G ratio, Fig. 12). Peridinioid dinocysts are present somewhat more abundantly over the section and show a gradual increase from ±38 m till the onset of the PETM, where the percentage of peridinoids decreases from 75 to 46% and then recovers to 75% again. Since peridinioid dinocysts are considered to be mostly heterotrophic dinoflagellates thriving on e.g. diatoms (Pross and Brinkhuis, 2005; and references therein), the gradual increase at the top of the section indicates an increase in nutrient availability. Whereas the change to gonyaulacoid dinocysts at the onset of the PETM can be explained by a decrease in nutrients.

Finally, PCA was performed on the dinocyst assemblage to reveal which dinocysts show similar or opposite behaviour compared to other dinocysts. It was performed on the entire dinocysts abundance (Fig. 10), but also on only the lower and only the upper part of the section (Appendix C - Fig. 2). The PCA indicates that there are five main dinocyst groups. *Diphyes* and *Apectodinium* behave almost opposite to each other but also behave different from the rest of the dinocysts. Although *Spiniferites* seems to have a slight correlation with *Apectodinium*. *Phthanoperidinium*, *Spinidinium* and *Deflandrea* (and *Glaphyrocysta*) plot together and behave opposite from *Senegalinium*, *Cerodinium* and *?Goniodomid sp. 1* (and *Morkallacysta*). The other species, *Operculodinium*, *Areoligera*, *Hafnispheera* and *Cordosphaeridium*, do not correlate to the other groups.

4.5 Terrestrial palynomorphs

Terrestrial palynomorphs dominate at Point Margaret (Fig. 12), with an average of 85.95 percent of the samples being from terrestrial origin. The percentage of terrestrial palynomorphs only drops under 70% at 4 intervals in the section: 19.88 (64.8%), 34 (69.9%), 45.93 - 45.97 (67.9-54.4%) and 52.03 m (66.2%). Also high absolute abundances of terrestrial palynomorphs were recorded (Fig. 11), especially at 6.65, 19.88 - 21.03, 50.7 and 51.83 m where more than 68000 specimen/gram dried sediment were found.

Of the terrestrial palynomorphs, gymnosperms are mainly present with abundances between 60.6 and 80.0 %. The pteridophytes are present in percentages between 12.7 and 32, whereas angiosperms only reach values between 3.5

Figure 11: The absolute abundance of terrestrial palynomorphs plotted next to the major terrestrial groups of the lower part of the Point Margaret section. Gymnosperms (green), pteridophytes (brown) and angiosperms (olive). Circles in all the graphs represent the location of the used samples.

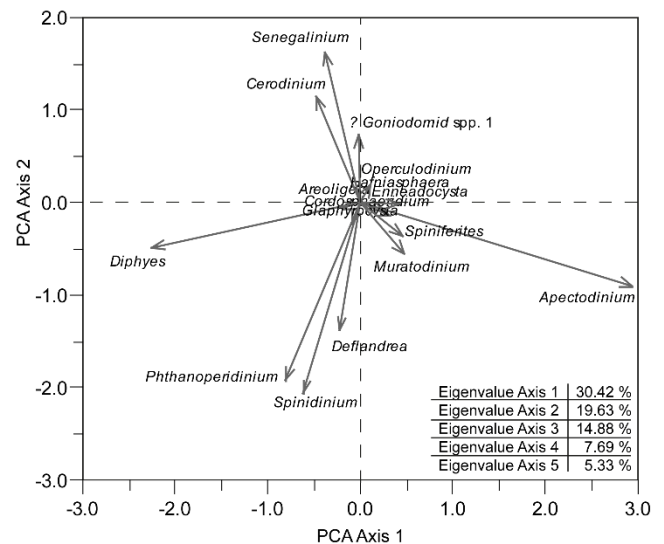
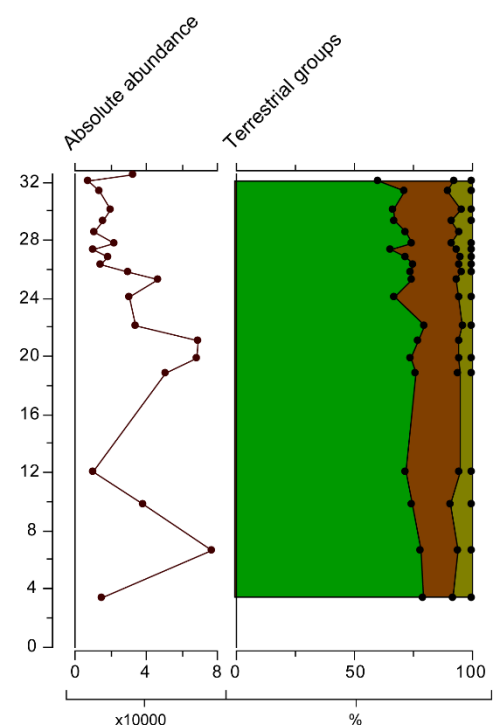


Figure 10: Principal component analyses with square root transformation performed on the entire dinocyst assemblage.



and 9.9%. The gymnosperms show a decreasing trend towards 32 m whereas the pteridophytes show an increase in abundance. The angiosperms are present more abundantly at the bottom and top of the investigated interval.

Finally, *sphagnum* spores were counted in small abundances, up to 0.75% of the terrestrial components, in most of the lower 33 m of the outcrop. Also in the rest of the section sphagnum spores were found although they were not counted.

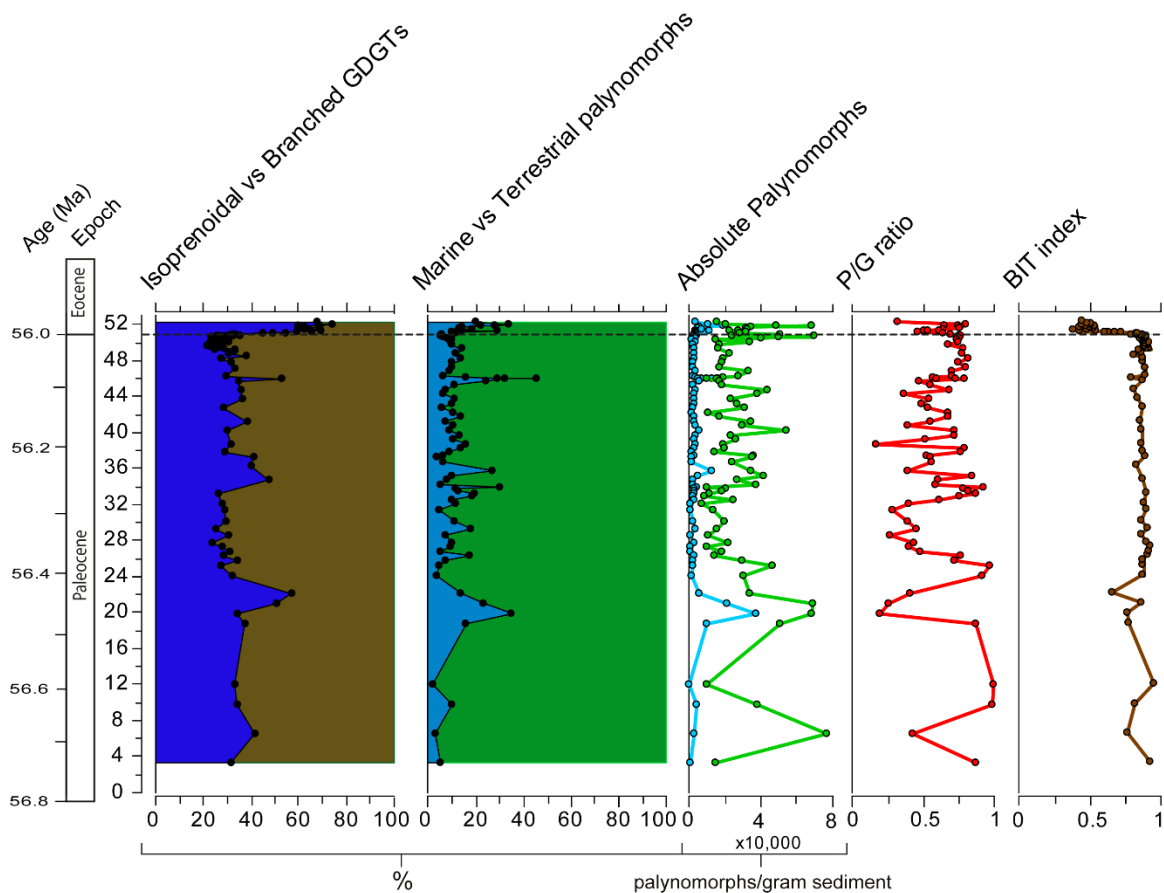


Figure 12: Proxies indicating changes in the terrestrial or nutrient input at Point Margaret. Isoprenoidal GDGT percentage, marine palynomorph percentage and the absolute abundance of the marine palynomorphs are indicated in blue, the branched GDGT percentage in brown and the percentage and absolute number of terrestrial palynomorphs in green.

4.6 GDGTs

Point Margaret samples contain a higher percentage of branched compared to isoprenoidal GDGTs, with an average of 62 % branched GDGTs with values ranging between 79 and 26% (Fig. 12). Samples from the PETM, in this case ≥ 50.94 m, contain more isoprenoidal GDGTs (average: 61%) than the samples below this interval (average: 31.5 %).

Crenarchaeol is the most abundant isoprenoidal GDGT, with an average concentration of $5.86 \cdot 10^5$ ng/g sediment dry wt, closely followed by GDGT-0 ($4.68 \cdot 10^5$ on average). GDGTs 1-3 range between $1 \cdot 10^5$ and $1.2 \cdot 10^5$ and the crenarchaeol regio isomer has the lowest average concentration ($4.9 \cdot 10^4$). The increase in iGDGTs during the PETM (> 50.92 m) is not uniform. The concentration of Cren' is 4.9 times higher during the PETM than in the entire period before, whereas the concentration of GDGT-1 only increases by 6%. Furthermore, Cren shows a 263% increase in concentration during the PETM, whereas GDGTs 0, 2 and 3 change moderately with 32, 51 and 15% respectively.

Of the branched GDGTs, brGDGT-Ia (m/z 1022) dominates with fractional abundances between 0.86 and 0.72. This compound is followed by brGDGT-IIa (m/z 1036), contributing 0.13-0.024. Also, brGDGT-IIIa (0.023-0.004), IIa' (0.031-0.012), Ib (0.089-0.040) and Ic (0.032-0.016, except at 25.3 m) are always present. Where Ib and Ic show higher, and IIa lower, values from 51 m onwards. The other brGDGTs, IIIa', IIIb, IIIb', IIIc, IIIc', IIb, IIb', IIc and IIc', have only limited abundance, with maxima of 0.015, 0.001, 0.003, 0.0003, 0.001, 0.012, 0.006, 0.005 and 0.002, and are not always present. There are also many higher peaks at the start of this section. IIIa shows an increased contribution between 3.32 and 25.3 m and IIIa' at 3.2, 6.5 and 12.08 m. At 6.5 m, there is also the only appearance of the IIb, IIb', IIc and IIc' peaks.

The BIT index ranges between 0.39 and 0.95 (Fig. 12), which indicates a large contribution of (fluviially-transported) soil OM at Point Margaret. During the PETM (>0.51) only BIT values between 0.39 and 0.64 are present. This indicates that there was a significant change in the origin of OM during the PETM. High input of soil-derived OM causes a major bias for the use of TEX₈₆ (Weijers et al., 2006b). Since OM from soils and peats contains GDGTs 1-3 and the crenarchaeol regio isomer, this transported signal alters the GDGT distribution produced in the water column and so changes the temperature signal recorded from the sediment (Weijers et al., 2006b). Looking at the relationship between brGDGT-Ia and GDGTs 1-3, the strong correlation with especially GDGT-1 ($r^2 = 0.43$) indicates this influence (Fig. 13). Therefore, Point Margaret cannot provide a reliable marine temperature signal using TEX₈₆.

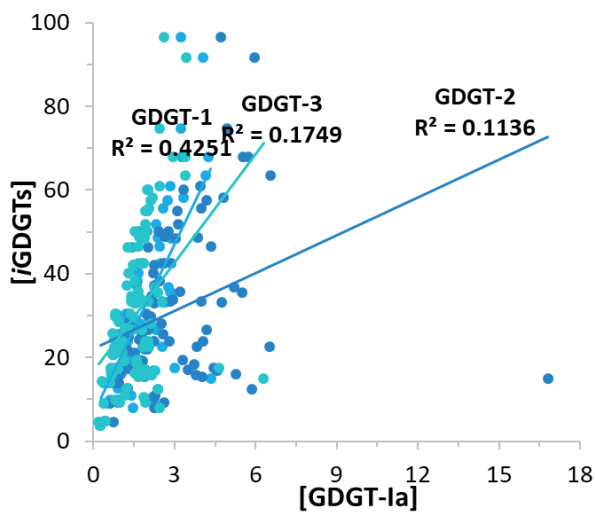


Figure 13: The relationship between br-GDGT-Ia and GDGT-1, GDGT-2 and GDGT-3 and the linear regressions

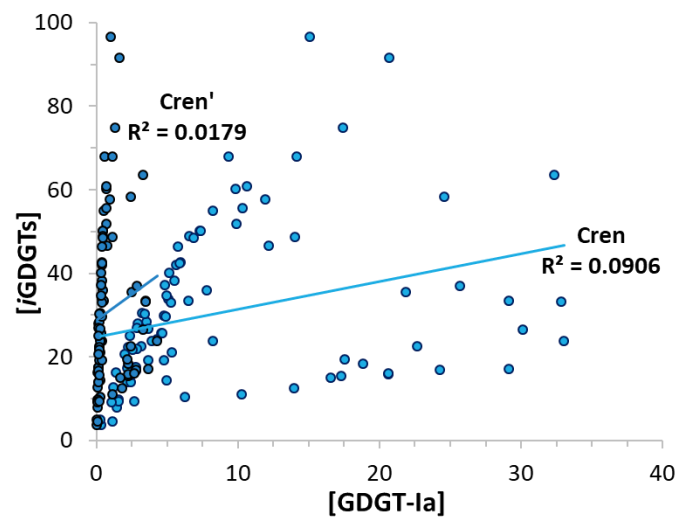


Figure 14: The relationship between br-GDGT-Ia and Crenarchaeol (Cren) and the Crenarchaeol regio isomer and the linear regressions

However, crenarchaeol and the crenarchaeol regio isomer show only a weak correlation with branched GDGT, brGDGT-Ia; r^2 of 0.091 and 0.018 respectively (Fig. 14). A different proxy was therefore used to determine a SST record for Point Margaret. This is the $Cren'/(Cren+Cren')$ proxy where SST can be calculated with the two iGDGTs that show the least influence of the transported terrestrial signal (J. Frieling, personal contact).

$$SST = \log \frac{Cren'}{(Cren + Cren')} \cdot 16.548 + 43.387 \quad R^2 = 0.69$$

With this proxy the recorded SSTs of Point Margaret range from 20.4 to 27.9 °C, where a clear trend towards higher temperatures is visible (Fig. 15). During the PETM the SSTs of Point Margaret increase rapidly, at 51 m temperatures above 25 °C are reached but 0.2 m later temperatures of 27.8 °C are recorded. The mean SST during the PETM is 27.2 °C whereas the mean SST for the Late Paleocene is 23.1 °C.

From brGDGT concentrations also temperatures can be reconstructed, since brGDGTs are from soil or peat origin this means that (mean annual) air temperatures are recorded instead of sea surface temperatures. MAT_{mr} gives air temperatures ranging between 17.6 and 24 °C with a mean value of 21 °C, whereas MAAT_{peat} shows air temperatures ranging between 20 and 27.6 °C with a mean value of 24.6 °C (Fig. 15). The two land temperature proxies show a similar trend, which is also similar to the SST reconstructed by the Cren'/(Cren+Cren') proxy (Fig. 15). All proxies indicate a rapid increase in temperature during the PETM, however the relative increase of the SST proxy is larger than that of the MAT records (4.1 vs 2.4 and 1.7 °C; Table 1 and 2).

By calculating certain ratios we can assess the origin of GDGTs. The division between tetra-, penta- and hexamethylated brGDGTs (Eqs. 9 - 11) reveals a distinct location within the ternary diagram for the Point Margaret samples (Fig. 16). The brGDGTs mainly occur as tetramethylated with values ranging between 95.97 and 78.41 %. The pentamethylated brGDGTs show abundances between 18.10 and 3.6 % and the hexamethylated between 3.49 and 0.37 %. Samples from Point Margaret plot similar to tropical soils from the global soil and peats with ≤ 1.7 % hexamethylated brGDGTs from the peat dataset (Fig. 16). However, some of the Point Margaret samples contain more hexamethylated brGDGTs and therefore plot somewhat to the left of the pattern visible from the global soil and peat datasets.

Also, the weighted average number of cyclopentane moieties (i.e. #rings) was calculated for tetra- and pentamethylated brGDGTs. For pentamethylated brGDGTs this was done for both the 5 and 6-Me (Eqs 13 - 14). The #ringstetra increases towards the

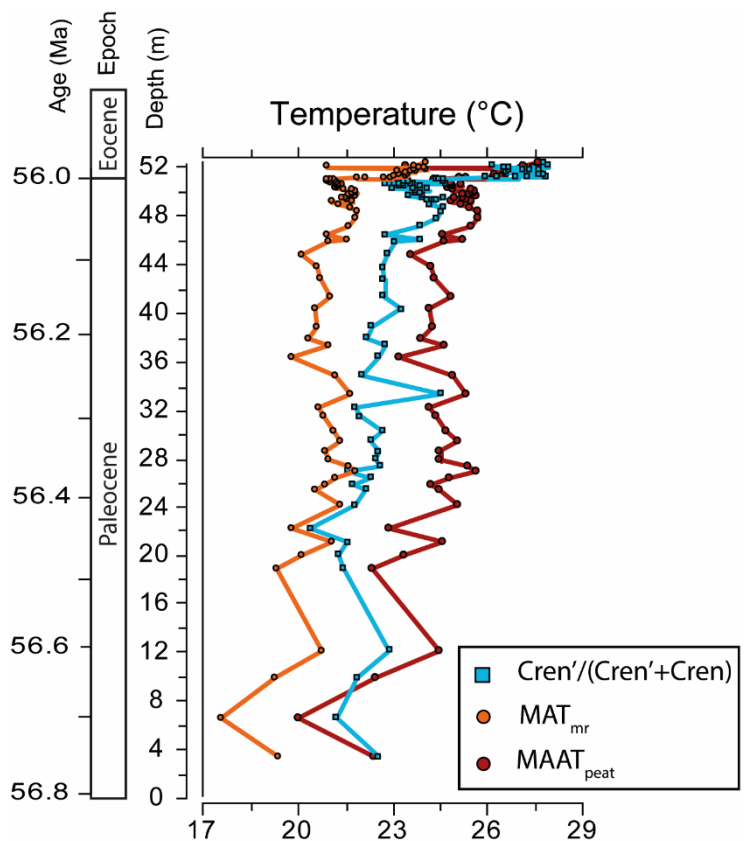


Figure 15: The different temperature proxy records of Point Margaret.

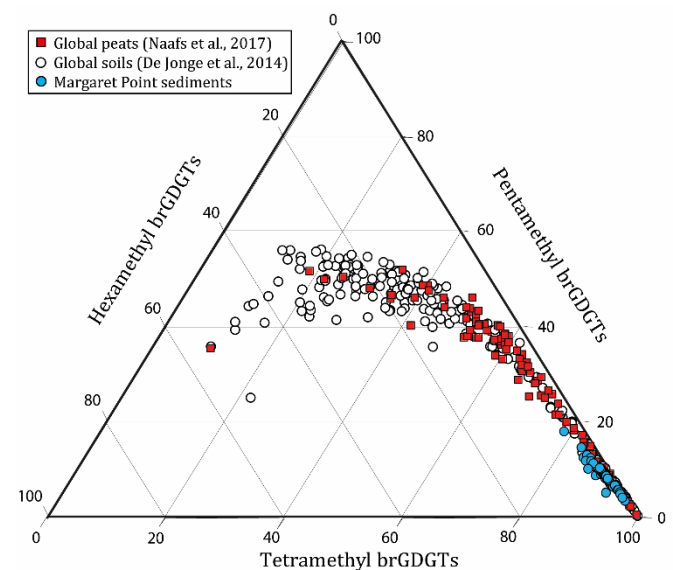


Figure 16: Ternary diagram comprising the different brGDGT groups: tetra-, penta- and hexamethylated brGDGTs. The Point Margaret samples (blue) are compared to the global soil dataset of De Jonge et al. (2014a) and the global peat dataset of Naafs et al. (2017b).

top of the section, and has values ranging from 0.06 to 0.16. Because peaks of I1b, I1b', I1c and I1c', are not always detected, #ringspenta5Me and #ringspenta6Me are often zero. This means that #ringspenta5Me has 48 and #ringspenta6Me 28 remaining samples which have a value. The remaining values range between 0.05 – 0.43 and 0.12 – 0.31, respectively.

Furthermore, the #ringstetra were plotted against #ringspenta5Me and #ringspenta6Me (Fig. 17), as #ringstetra has less variation in values compared to the #ringspenta indices this results in a line of samples instead of a cluster. For #ringstetra (x-axis) plotted against #ringspenta5Me this line is between 0.08 and 0.16 wide and between 0.05 and 0.43 high (Fig. 17, upper graph), where the higher values (>0.2) are only present from 51 m onwards. For #ringstetra plotted against #ringspenta6Me this line is even more expressed, between 0.08 and 0.11 wide and between 0.12 and 0.31 high (Fig. 17, lower graph). Compared to the global soil and peat datasets, there is no 1:1 correlation between #ringstetra and #ringspenta at Point Margaret since the values for #ringstetra remain relatively low. Especially, for the #ringspenta5Me the Point Margaret samples plot differently from the global trend.

Finally, the isomer ratio (IR, Eqs 15 - 16) was calculated to look at the origin of brGDGTs since soils and aquatic environments give a different response regarding IR values (Sinninghe Damsté, 2016). The IRhexa of this section ranges between 0.56, at 12.08 m, to 0. The part of the section with no value for IRhexa occurs from 51.1 m to the top of the section except at 51.55 and 52.03 m where an IRhexa of 0.48 and 0.30 are calculated, respectively. The IRpenta ranges between 0.44 and 0.16, generally the lower values are present at the bottom and higher values at the top of the section. In Figure 18, you can see that this results in a cluster between 0.3-0.13 IRpenta and 0.4-0.2 IRhexa. There are two outliers from this cluster, which are the two samples with a high IRhexa value of 0.56 and 0.48 at 12.08 and 51.55 m, respectively.

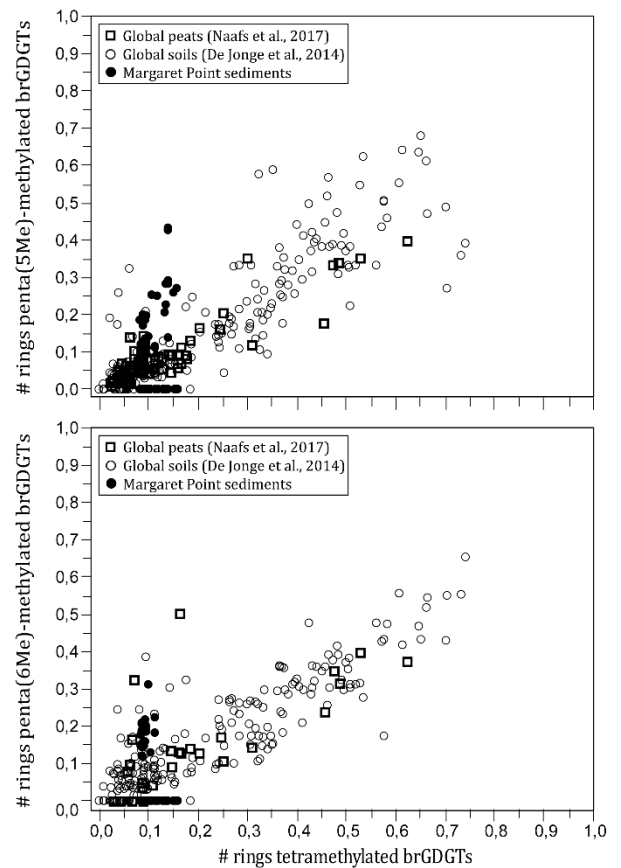


Figure 17: #rings tetramethylated brGDGTs plotted against #rings penta(5Me)methylated brGDGTs (upper graph) and #rings penta(6Me)methylated brGDGTs (lower graph) for both the Margaret Point section and the global soil and peat datasets comprised by De Jonge et al. (2014a) and Naafs et al. (2017b)

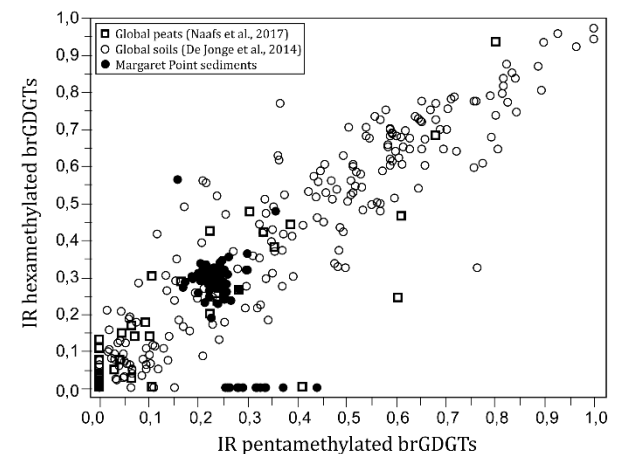


Figure 18: The isomer ratios of penta- and hexamethylated brGDGTs plotted against each other for both the Margaret Point section and the global soil and peat datasets comprised by De Jonge et al. (2014a) and Naafs et al. (2017b)

5. Discussion

5.1 Environmental changes

Senegalinium and other closely related genera (i.e. *Phthanoperidinium*, *Spinidinium*, *Cerodinium* and *Deflandrea*) have been shown to tolerate very low salinities (Sluijs & Brinkhuis, 2009; and references therein) and to thrive during stages with abundant nutrients/food (Dale & Fjellså, 1994; Firth, 1996; overview in Sluijs et al., 2005). Since these genera are dominating the section, Point Margaret was likely located near-shore with high nutrient availability and close to a river which provided fresh-water runoff. This is supported by high absolute and relative abundances of terrestrial palynomorphs, BIT index values higher than 0.4 and a larger contribution of brGDGTs than iGDGTs before the PETM (Fig. 12). This reconstructed environment for Point Margaret is similar to the environment of the eastern end of the AAG during the Late Cretaceous and Paleocene (Exon et al., 2001). However, at Point Margaret these morphologically similar peridinoid cysts are not all showing the same signal since especially the PCA of the entire section shows that *Senegalinium* and *Cerodinium* behave differently than *Phthanoperidinium*, *Spinidinium* and *Deflandrea* (Fig. 10). This means that since the conditions at Point Margaret were highly favourable for these type of dinocysts, they do not show the same response anymore. Also, different morphotypes of *Senegalinium* occur at Point Margaret (Plate I, Appendix A) confirming that the conditions at this site were very favourable for these type of genera.

The abrupt *?Goniodomid* sp. 1 peak (Fig. 9) possibly indicates the creation of a lagoon, since this species belongs in the Goniodomid group, which is characteristic of containing species representative of mainly polysaline, lagoonal environments (Wall et al., 1977). However, since *Senegalinium* does not show a decrease in absolute abundance (Appendix C, Fig. 3) the conditions were possibly saline rather than polysaline. Another explanation for the increased abundance of *?Goniodomid* sp. 1, is a (tropical) storm, as increased river run-off decreases the salinity and reduced turbulence after the storm can create surface stratification (Dale, 2001; Siringan et al., 2008). This phenomenon is caused by the resuspension of dormant cysts into the water column, which can subsequently hatch and continue living (Villanoy et al., 1996; Villanoy et al., 2006). Both causes are explained by increased river run-off which is consistent with the increased absolute abundance of terrestrial palynomorphs during this interval (Fig. 12). However, during and just after this interval there is a relative increase in isoprenoidal GDGTs (51 and 57 %; Fig. 12). A (tropical) storm could transport both terrestrial palynomorphs and isoGDGTs to Point Margaret, which suggests that a storm caused the *?Goniodomid* sp. 1 bloom rather than the formation of a lagoon.

The fluctuations of *Diphyes*, *Spiniferites* and *Glaphyrocysta*, between 27.75 and 44.25 m (Fig. 9), indicate that there were changes in relative sea level as large relative abundances of *Spiniferites* indicate an outer neritic environment (Brinkhuis, 1994; Pross and Brinkhuis, 2005), intervals with more *Diphyes* contain less *Spiniferites* and peaks in the abundance of *Glaphyrocysta* are correlated to (relative) sea level rise (Iakovleva et al., 2001; Pross and Brinkhuis, 2005).

The first *Apectodinium* acme (35%) occurs at 33.25 m into the section (Fig. 9), almost 300 kyr before the onset of the PETM. There is a sharp increase in SST during the acme, from 21.8 °C at 32.1m to 24.5 °C at 33.25 m (Fig. 15). The occurrence of an *Apectodinium* acme at higher SSTs is coherent with the fact that the *Apectodinium* genus only occurs at temperatures ≥ 20 °C (Frieling et al., 2014). The appearance of an

Apectodinium acme this far from the PETM has not been found before and so the acme is probably unrelated to the PETM. This must mean that either waters transported into the AAG or local conditions at Point Margaret were temporarily suitable for the tropical *Apectodinium* species to appear. In the period before the acme, 26.3 to 33.25 m, conditions already changed at Point Margaret, with more *Spiniferites* present and a decrease in the absolute abundance of terrestrial palynomorphs (Fig. 9 and 12). Just before the acme *Spiniferites* (40%), *Glaphyrocysta* (16%) and *Cordosphaeridium* (11%) show increased abundance, this indicates that there was a relative sea level rise leading up to the early acme. Sea level rise is globally recorded around the PETM (Sluijs et al., 2008) and so could be connected to the appearance of *Apectodinium* acmes. However, decreased river run-off as a result of a migration away from the coast likely results in less nutrient availability, whereas a strong increase in nutrient availability is associated with *Apectodinium* acmes at marginal marine settings since *Apectodinium* is believed to be heterotrophic (Sluijs et al., 2007a; and references therein). But the P/G ratio increases around the early *Apectodinium* acme with a value of 0.87 during the acme (Fig. 12). This suggests that there might have been increased nutrient availability even though there was less transport of terrestrial material to Point Margaret. It seems that these observations do not necessarily explain the occurrence of an *Apectodinium* acme due to local changes. Also, the critical environmental factor(s) that causes the *Apectodinium* acme has not yet been identified (Sluijs and Brinkhuis, 2009). If the early *Apectodinium* acme was caused by regional changes, the La-Trobe core would have been influenced by changed conditions in the AAG too, but the early acme was not recorded there. However, only 3 samples were used to describe the Late Paleocene and so the early *Apectodinium* acme could have been missed at La-Trobe (Hurdeman, 2017). Indian Ocean conditions must have been favourable for *Apectodinium* to occur in such abundances if changed PLC conditions brought the *Apectodinium* genus to Point Margaret. But hardly any sites from the Indian Ocean record sediments from the Late Paleocene and the remaining sites do not discuss (sea surface) temperature changes (e.g. Slotnick et al., 2015). Only Zachos et al. (1992) found that intermediate and deep waters of the Indian Ocean warmed uniformly by 4 °C between 60 and 56 Ma. However, in the early Eocene the *Apectodinium* genus is abundantly (50-80%) present along the Wilkes Land margin which is also located in the AAG (Bijl et al., 2013a). This means that conditions in the AAG were favourable for *Apectodinium* to thrive while being unrelated to the changing conditions during the PETM. This indicates that changes in the AAG or in the PLC, or both, could have caused the early acme at Point Margaret. The upcoming IODP expedition 369 at Mentelle Basin and Naturaliste Plateau, SW Australia, could indicate whether there were changes in the proto-Leeuwin current or the AAG during the Late Paleocene (Hobbs et al., 2016).

The second *Apectodinium* acme occurred at 45.75 m with more relative (>50%) and absolute abundance than the first acme (Fig. 9; Appendix C Fig. 3). The *Apectodinium* species remained present at Point Margaret from the second acme onwards. This indicates that the ocean temperature at Point Margaret was higher than 20 °C the last ±100 kyr of the section, which is supported by the SST results (Frieling et al., 2017; Fig. 15).

The final *Apectodinium* acme occurs at the onset of the PETM and was accompanied by moderate abundances of *Spiniferites* and *Senegalinium* (Fig. 9) indicating that there was a relative sea level rise but not big enough to remove the freshwater influence, this is confirmed by the increase in *Glaphyrocysta* at the top of the section. Sea level rise is globally recorded around the PETM (Sluijs et al., 2008).

5.2 Regional and global variability before and during the PETM

Both Point Margaret and La-Trobe show a dinocyst assemblage dominated by *Diphyes*, *Senegalinium*, *Cerodinium/Deflandrea* and *Spiniferites* during the Late Paleocene (Hurdeman, 2017). ODP Site 1172 also shows similarities with Point Margaret regarding the dinocyst assemblage during this interval. Both sites are almost completely dominated by *Senegalinium* followed by an increase in *Spiniferites* and *Glaphyrocysta* and an *Apectodinium* acme before the PETM (Sluijs et al., 2011). The acme is accompanied by a small step ($\sim 0.6\%$) towards more negative $\delta^{13}\text{C}$ values at both sites. This is also the case at La-Trobe, however Hurdeman (2017) determined that the onset of the PETM at La-Trobe occurred at the first *Apectodinium* peak during this small (somewhat less expressed) negative $\delta^{13}\text{C}$ step. Since he believed that the CIE onset was relatively expanded when looking at the chemostratigraphy of Point Margaret. However, I have determined that the onset of the negative CIE occurred at the larger shift in $\delta^{13}\text{C}$ values for Point Margaret since the onset of the PETM is characterized by at least a 3-4% shift in $\delta^{13}\text{C}$ (Kennett and Stott, 1991; Koch et al., 1992; Schouten et al., 2007) and a consistent determination of the onset simplifies intra-site comparison of the PETM. A negative shift before the actual excursion is also found in other sites, namely at Talbot County, Maryland USA, and the Bighorn Basin, Wyoming USA (Self-Trail et al., 2012; Bowen et al., 2014). At Bighorn Basin the pre-onset excursion (POE) is $\sim 3\%$ in magnitude whereas the main CIE shows a 5.7% $\delta^{13}\text{C}$ decline and occurs between 2 and 5.5 kyr after the POE (Bowen et al., 2014). The South Dover Bridge core shows a $\sim 2\%$ $\delta^{13}\text{C}$ POE, where the actual CIE shows a $\sim 4\%$ $\delta^{13}\text{C}$ decline (read from Fig. 5 of Self-Trail et al., 2012). Bowen et al. (2014) conclude that there must have been a discrete pulse of carbon released into the atmosphere before the onset of the PETM to cause the POE at Bighorn Basin. Since the POEs at the Southern Ocean sites are smaller than the one at Bighorn Basin this must have been either a smaller release of carbon or the shift in $\delta^{13}\text{C}$ values was a result of other processes. One possible explanation could be a decrease in sedimentation rate, supported by a condensed iron cemented zone during the interval (Fig. 6), which would make the change seem more abrupt. Another explanation could be related to the origin of the $\delta^{13}\text{C}$ value, since the value of $\delta^{13}\text{C}$ from bulk sediment can become more negative when there is more marine than terrestrial influence (Sluijs and Dickens, 2012). Most notably, at this interval the absolute abundance of terrestrial and marine palynomorphs is almost equal whereas in the rest of the samples the terrestrial palynomorphs are more abundant (Fig. 12). Also the calculated marine and terrestrial end-members of Point Margaret form a smaller band at the interval of the small step in $\delta^{13}\text{C}$ values (Fig. 19). These two explanations, possibly combined, are more plausible than a release of carbon causing the small POE at Point Margaret. However, at Site 1172 the small $\delta^{13}\text{C}$ excursion is probably not explained by these factors since the percentage of terrestrial palynomorphs increases whereas the absolute abundance of dinocysts decreases during this interval (Fig. 4 of Sluijs et al., 2011).

The presence of an *Apectodinium* acme before the onset of the CIE does not only occur in the Southern Ocean (at Tawanui (New Zealand), Site 1172 and Point Margaret; Crouch et al., 2001; Crouch et al., 2003; Sluijs et al., 2011), sites on the New Jersey Shelf and the Central North Sea also record this phenomenon (Sluijs et al., 2007a). However, at Tawanui, Bass River, Wilson Lake and Fina Well 30 14/1 the *Apectodinium* acme only occurs ~ 4 kyr before the onset of the PETM (Sluijs et al., 2007a), whereas it occurs ~ 80 kyr and ~ 100 kyr before the onset at Point Margaret and ODP Site 1172, respectively. Sluijs et al. (2011) interpret the early acme in two ways, a significantly higher sedimentation rate

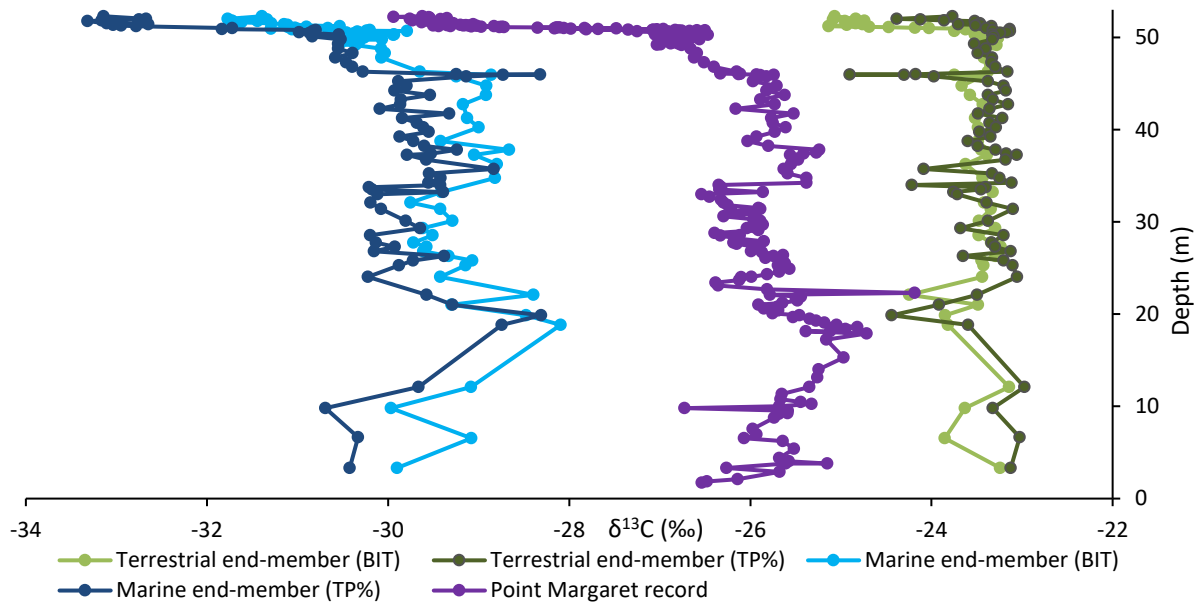


Figure 19: The terrestrial and marine $\delta^{13}\text{C}$ end-member, calculated with the equations of Sluijs & Dickens (2012) using both the BIT index and terrestrial percentage per sample (TP%), plotted together with the actual $\delta^{13}\text{C}$ record of Point Margaret

during the interval causing the time between the onset and the acme to be much less or that the conditions were locally similar to low latitude equatorial environments already ~ 100 kyr before the PETM. At Point Margaret it seems unlikely that higher sedimentation rates occurred as an already high average sedimentation rate of 6,38 cm/kyr was recorded. This suggests that the conditions were similar to low latitude equatorial environments and that regional changes could have caused the *Apectodinium* acme just like the early acme. The conditions during the second acme are similar to conditions during the early acme, although there are higher absolute and relative abundances of marine palynomorphs and isoGDGTs during the acme (Fig. 12). This could mean that low latitude equatorial environments did occur at Point Margaret ~ 80 kyr before and unrelated to the PETM, possibly with a similar cause as the early *Apectodinium* acme.

The similarities between Point Margaret and ODP Site 1172 are remarkable, where both show a small step in $\delta^{13}\text{C}$ values during an *Apectodinium* acme with an increasing SST trend, followed by an interval with decreasing temperatures, then SSTs increase again at the CIE where another *Apectodinium* acme occurs (Fig. 20). There is also a strong similarity between the mean Cren'/Cren'+Cren proxy SST differences between the Late Paleocene and PETM for Point Margaret (4.1 °C; Table 1) and Site 1172 (3.9 °C; Table 1). This suggests that the two sites were more connected than possible with a closed Tasmanian Gateway and the difference in ocean temperatures between the Proto-Leeuwin Current and Tasman Current during the Paleocene (Huber et al., 2004; Sluijs et al., 2011; Bijl et al., 2013a). Since both sites experience a sea level rise starting before and lasting up to the PETM, it might be that water locally passed over the Tasmanian Gateway during this interval. There must have only been a small amount of throughflow since none of the many studied sites in New Zealand show similar behaviour (Crouch et al., 2001, 2003; Hollis et al., 2012, 2014, 2015).

There are a number of environmental changes that occur globally during the PETM, examples of this are changes in sea level, sediment supply and productivity (Sluijs et al., 2011). Comparing Point Margaret with these global and regional (at site 1172) changes might indicate how the AAG reacts to changing conditions during the PETM.

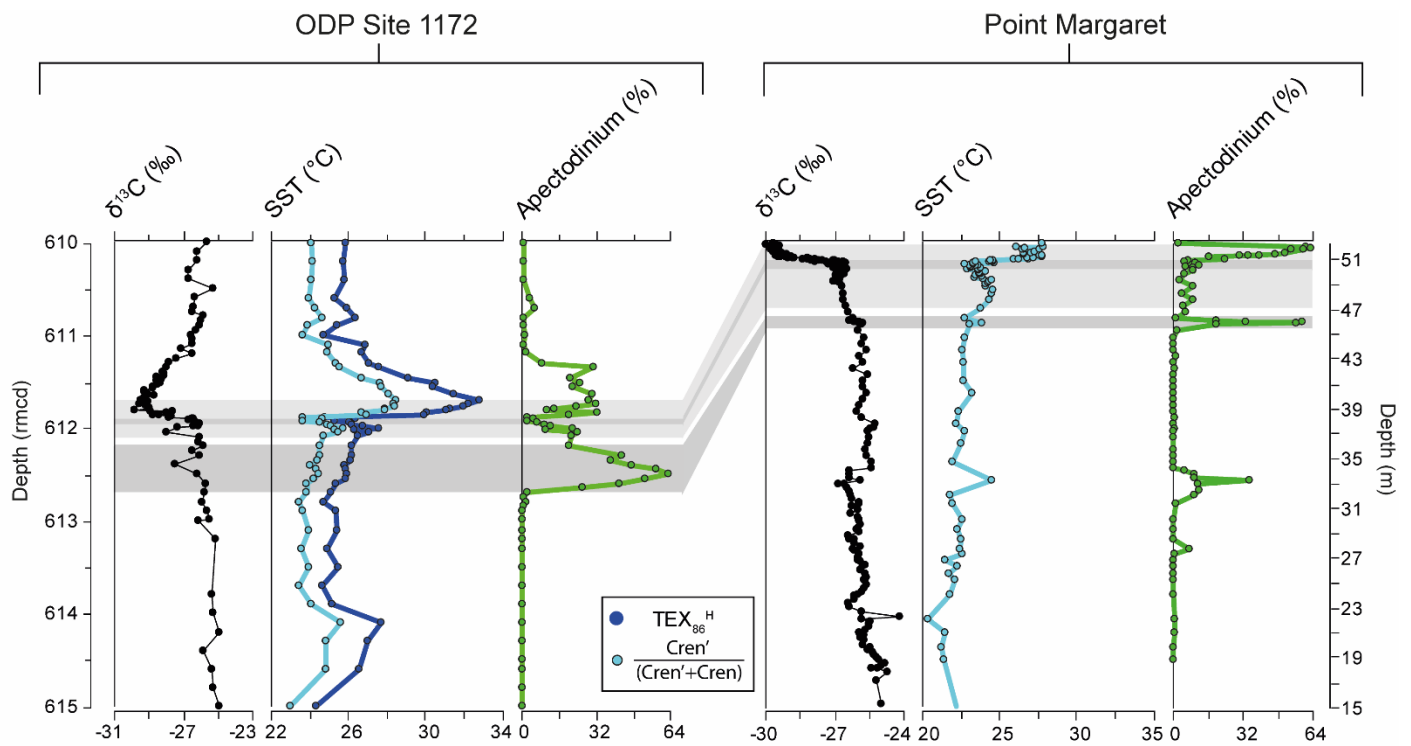


Figure 20: The comparison between the behaviour of Apectodinium genus, $\delta^{13}\text{C}$ and SST regarding ODP Site 1172 (data from Sluijs et al., 2011) and Point Margaret. The alternating grey bands are showing the different phases of similarity between the sites.

Most of the marginal marine sites studied for the PETM show a large increase in sediment supply from the continent (Sluijs et al., 2008). Generally, it is thought to indicate increased terrestrial weathering causing the supply of siliciclastic materials to the shelf by rivers to increase (Sluijs et al., 2011). At Site 1172, the global sea level rise is recorded but the increase in siliciclastics is not, which they support by the decline in the low salinity tolerant dinocysts (Sluijs et al., 2011). At Point Margaret, the sediment deposition changed to clay at 45 m (Fig. 6), just before the start of the second Apectodinium acme, which indicates a migration further off shore. The absolute abundances of terrestrial palynomorphs do not follow the same trend as the BIT index and TOC content (Fig. 7 and 9) but seem to increase towards and during the PETM at Point Margaret. This indicates that, even as the section migrated further off shore, the river run-off increased, which supports the global increase in terrestrial weathering. However, it might also be related to the appearance of tropical storms as the Goniodomid species *Florentinia* and *Eocladopyxis* peak in absolute abundances during the PETM (Appendix C, Fig. 3; Sluijs et al., 2011, and references therein). Another conclusion that can be drawn from this is that the record of ODP Site 1172 probably did not catch the increased siliciclastic signal as the Tasmanian Plateau lacks a large hinterland and so can only receive limited amounts of terrestrial material. This shows that although there might be a small throughflow over the Tasmanian Gateway, there are still differences between the two sites due to local effects like sediment transport by rivers.

Sluijs & Brinkhuis (2009) and Sluijs et al., (2011) found that there was increased variability within the dinocyst community during the PETM compared to before the onset. This change in variability is not reflected at Point Margaret as the variability is already high even before the oldest Apectodinium acme ± 300 kyr before the onset of the PETM (Fig. 9).

Finally, Contreras et al. (2014) described that gymnosperm-rich forests dominated the middle and late Paleocene at Site 1172. Which is probably also the case at Point Margaret (Fig. 11). Angiosperms are known to increase at the onset of the PETM at high-latitude locations in the Southern hemisphere (Crouch and Brinkhuis, 2005; Contreras et al., 2014). The change towards increased angiosperm abundance is not yet visible after

32 m into the section (Fig. 11), but also the relatively small CIE of $\pm 3\%$ indicates that angiosperms might not have been as dominant during the PETM as described in other records (Schouten et al., 2007).

5.3 Origin of brGDGTs

Although brGDGTs are assumed to be primarily produced in soils, recent studies indicate that brGDGTs can also be produced in the aquatic environment, both in fresh water (lakes; Tierney and Russell, 2009; Weber et al., 2015; and rivers; De Jonge et al., 2014b; Zell et al., 2014; Sinninghe Damsté, 2016) and in the marine realm (water column; Zell et al., 2014; De Jonge et al., 2015; and sediment; Peterse et al., 2009; Zhu et al., 2011; Sinninghe Damsté, 2016). Since there is an influx of OM from a terrestrial or fresh water source at Point Margaret, indicated by the large amounts of terrestrial palynomorphs, high BIT index and abundant brGDGTs (Fig. 12), the origin of the brGDGTs must be determined to be able to rely on the MAT proxies and to use the brGDGTs as a tracer for soil OM. In order to derive the origin of the brGDGTs three different methods were used, defined by Sinninghe Damsté (2016), to compare the brGDGTs in river-influenced shelf environments to those in soils. These methods involve looking at the methylation, average number of rings and isomer ratio of brGDGTs.

Firstly, the brGDGTs from Point Margaret are mainly tetramethylated ($>83\%$; Fig. 16), this high contribution of tetramethylated brGDGTs is indicative of tropical soils since temperature changes have an effect on the degree of methyl branching of GDGTs in soils (Sinninghe Damsté, 2016). Secondly, when the average number of rings tetra exceeds 0.7, the brGDGTs cannot only be derived from soil erosion but also have a marine origin. All the samples of Point Margaret have brGDGTs with an #ringtetra well below 0.7 (Fig. 17). Thirdly, rivers are more likely to show higher average IR values compared to brGDGTs derived from soils (De Jonge et al., 2014b). This occurs as fresh water mainly has a higher pH compared to soils and the change to 6Me-brGDGTs depends on pH, so more 6Me is expected when the pH is higher (De Jonge et al., 2014b; Freymond et al., 2017). Since the brGDGTs show IRhexa and IRpenta values of less than 0.7 (Fig. 18), it is more likely that soil erosion is the origin rather than in situ river production. From this it can be concluded that the brGDGTs from Point Margaret record a tropical soil signal and are not in situ produced in rivers or the marine environment. Meaning that the two air temperature proxies and the BIT index are recording the right signal.

5.4 Temperature

Mean annual air temperatures at Point Margaret change from 21-25 °C at the Late Paleocene to 23.4-26.7 °C at the PETM (Table 1). Since the calibration range of the MAT_{mr} proxy is ~ 26 °C (De Jonge et al., 2014a), the actual temperatures over the entire interval might be higher. The MAAT_{peat} proxy has just been developed by Naafs et al. (2017b) and so the calibration range of this proxy is unknown although it seems that the proxy does reconstruct temperatures consistent with other temperature proxies during longer-term shifts in climate (Naafs et al., 2017b). Pollen of the mangrove palm *Nyssa* were only found during the PETM at Point Margaret, this species occurs only when the air temperature ranges between 21.7 and 28 °C (Utescher and Mosbrugger, 2015). It is strange that *Nyssa* pollen are not present before the PETM at Point Margaret since all the other proxies indicate that it is already warmer than 21.7 °C well before the PETM. This suggests that other conditions at Point Margaret prohibit the species from occurring.

Table 1: Sea surface temperatures compilation for the Southern Ocean, reconstructed vs modelled temperatures. The mean SSTs of the Late Paleocene were determined for the entire interval up to the PETM, for the PETM only the samples from the plateau phase of the CIE were used.

Area	Site	Proxy type	Late Paleocene (58-56) SST (°C)	Modelled SST (°C) for 2240 ppm scenario (Hollis et al., 2012)	PETM mean SST (°C)	Modelled SST (°C) for 4480 ppm scenario (Hollis et al., 2012)	Data available from:
New Zealand	ODP 1172	TEX ₈₆ ^H	25.9	±12	31.8	±16	(Sluijs et al., 2011)
	ODP 1172	Cren'/(Cren'+Cren)	24.3	±12	28.2	±16	(Sluijs et al., 2011)
	DSDP 277	Mg/Ca (<i>Acarinina</i>)	29.9	±14	32.2	±18	(Hollis et al., 2015)
	Mid-Waipara	TEX ₈₆ ^H	-	±16	33.3	±20	(Hollis et al., 2012)
SE Australia	La-Trobe	Cren'/(Cren'+Cren)	24.3	±17	25.8	±21	(Huurdeeman, 2017)
	Point Margaret	Cren'/(Cren'+Cren)	23.1	±17	27.2	±21	This study
Weddell Sea	ODP 690	δ ¹⁸ O (<i>Acarinina</i>)	10.8	±11	21.2	±15	(Thomas et al., 2002)

Table 2: Reconstructed mean annual air temperatures for the Southern Ocean. The Australian and SE Asian Calibration are described in Greenwood et al. (2004). The LMA, Clamp and Bioclimatic analyses already give a mean MAAT value whereas for the MBT/CBT', MAT_{mr} and MAAT_{peat} the average value over the time interval was taken. For the Late Paleocene this was determined for the entire interval up to the PETM, for the PETM only the samples from the plateau phase of the CIE were used.

Area	Site	Proxy type	Late Paleocene (58-56) mean MAAT (°C)	PETM mean MAAT (°C)	Data available from:	Error (°C)
New Zealand	Otaio Gorge	LMA (Australian Calibration)	-	16	(Pancost et al., 2013)	±3.0
	Otaio Gorge	Clamp	-	20	(Huber & Caballero 2011; Pancost et al., 2013)	±2.4
	Otaio Gorge	LMA (SE Asian Calibration)	-	21.6	(Pancost et al., 2013)	±3.4
	Mid-Waipara	MBT/CBT' (Peterse et al., 2012)	-	21.2	(Pancost et al., 2013)	
SE Australia	SE Australia (7 sites)	Bioclimatic analyses	22-23	-	(Greenwood et al. 2003)	±2.0
	Point Margaret	MAT _{mr}	21	23.4	This study	
	Point Margaret	MAAT _{peat}	25	26.7	This study	

Sea surface and mean air temperatures show almost the same absolute values at Point Margaret, where sea surface temperatures are even higher during the PETM. There are different reasons why comparing MAT and SST is complex, changes in the source of brGDGTs, a summer bias and changes in the depth of GDGT production and export are some of them (Pancost et al. 2013; and references therein). However, the difference between a maximum MAT of 26.7 °C at Point Margaret and SST of 31.8 °C at ODP Site 1172 during the PETM is more than 5 °C and the reconstructed difference between MAT and SST at Mid-Waipara is more than 12 °C during the PETM (Tables 1 and 2). This means that more research needs to be done to be able to reconstruct MAT records that can be used at warmer climate conditions. But also to compare absolute mean annual air and sea surface temperatures with more precision.

The two MAT proxies at Point Margaret show a ± 2 °C in warming from the Late Paleocene to the PETM (Fig. 15). Unfortunately there are no other sites in the Southern Ocean that reconstruct both the MAT of the Late Paleocene and of the PETM (Table 2), which makes further regional comparison regarding the magnitude of warming impossible. Global MAT records which contain both the Late Paleocene and PETM are far less abundant than SST records for the same interval (e.g. Weijers et al., 2007a). So only the MAT records at the central Arctic Lomonosov Ridge and Bighorn Basin Wyoming, USA, can be used to compare the MAT change during the PETM. For the Arctic the temperature difference between the Late Paleocene and PETM was ~ 6 °C using the MBT'-CBT proxy (Peterse et al., 2012), for the Bighorn Basin ~ 5 °C using leaf margin analyses (Wing et al., 2005). This suggests that either the calibration range of the MAT proxies prohibit the reconstruction of the full warming of the PETM at Point Margaret, or warming at the Southern Ocean was much less expressed than at other locations across the globe during the PETM. However, there was almost no temperature gradient between the tropics and polar regions during the early Paleogene (Bijl et al., 2009; Pross et al., 2012) and so you would expect Point Margaret to show a larger temperature change during the PETM. This indicates that MAT reconstructions are underestimating the temperature increase during the PETM at Point Margaret.

Since the $\text{Cren}'/(\text{Cren}' + \text{Cren})$ proxy has not been used before, first the validity of the proxy must be confirmed. Since this SST proxy captures almost the same trend as the MAT_{mr} and MAAT_{peat} proxies, it is likely that the recorded trend is correct. To test the correctness of the SST values, the SST calculated with the $\text{Cren}'/(\text{Cren}' + \text{Cren})$ proxy were compared to dinocysts which show a relation to temperature. The dinocysts which correlate to relatively high temperatures are: *Hafniasphaera* (does not occur in great abundance below 25 °C), epicystal *Goniodomids* (does not occur below 25 °C) and *Florentinia Reichartii* (does not occur below 30 °C) (Frieling, 2016). If these dinocyst relations to temperature are correct the SST at 6.65 m into the section would have to be ≥ 25 °C and above 25 °C at 19.88 m (Fig. 9). Also, the temperatures during the PETM might be much higher than observed with the $\text{Cren}'/(\text{Cren}' + \text{Cren})$ proxy since *Florentinia Reichartii* occurs from 51.2 m onwards whereas the recorded SST do not reach above 28 °C. The $\text{Cren}'/(\text{Cren}' + \text{Cren})$ proxy also reconstructs lower SSTs compared to TEX₈₆^H when looking at Site 1172 and La-Trobe (Table 1; Sluijs et al., 2011; Hurdeman, 2017). This suggests that sea surface temperatures at Point Margaret are about 3 °C higher than the temperatures established by the $\text{Cren}'/(\text{Cren}' + \text{Cren})$ proxy. And would therefore be in the same range as SST recorded at Site 1172.

Even though the $\text{Cren}'/(\text{Cren}' + \text{Cren})$ proxy probably underestimates the SST, the mean SSTs at Point Margaret for the Late Paleocene and PETM are in the same range as those reconstructed at other sites from the Southern Ocean (Table 1). Care must be taken

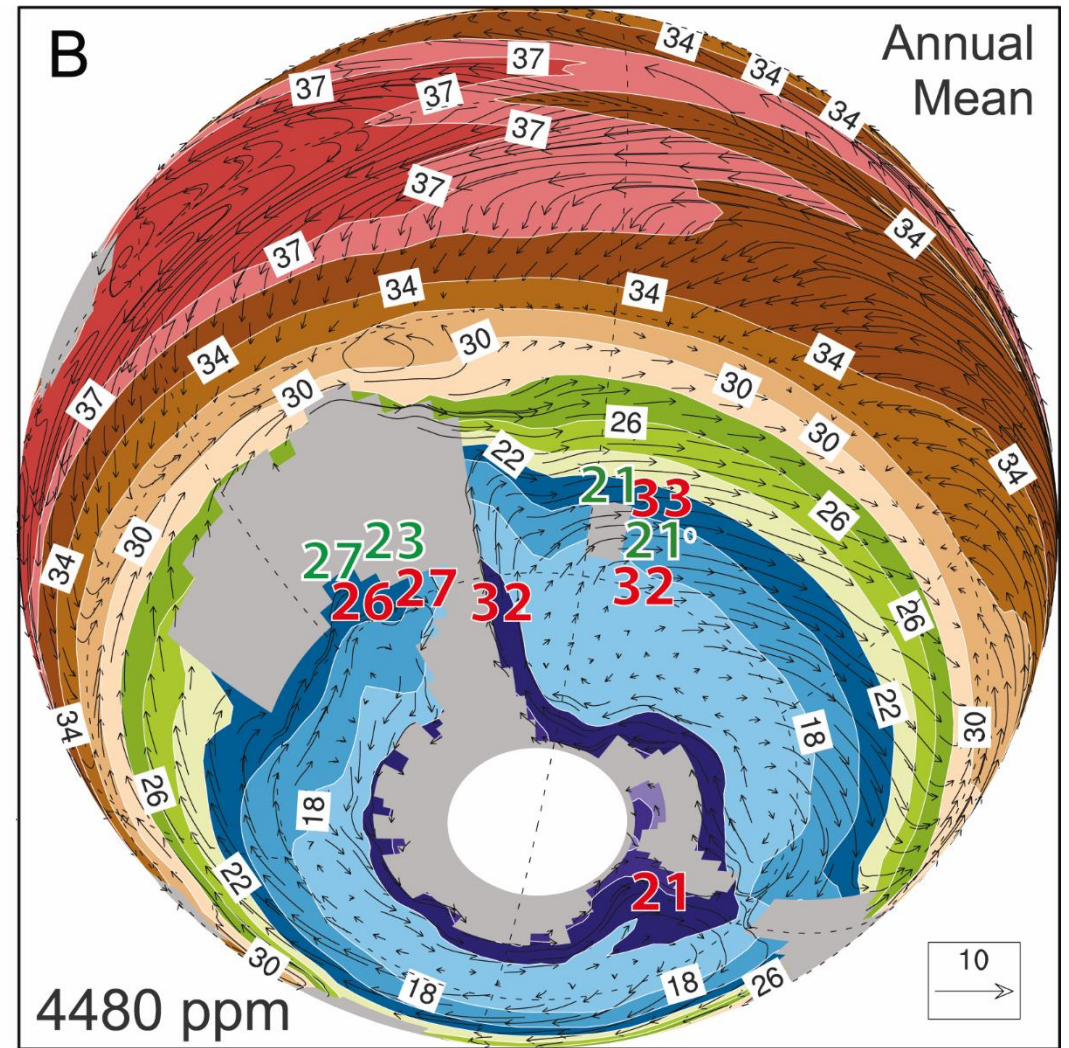
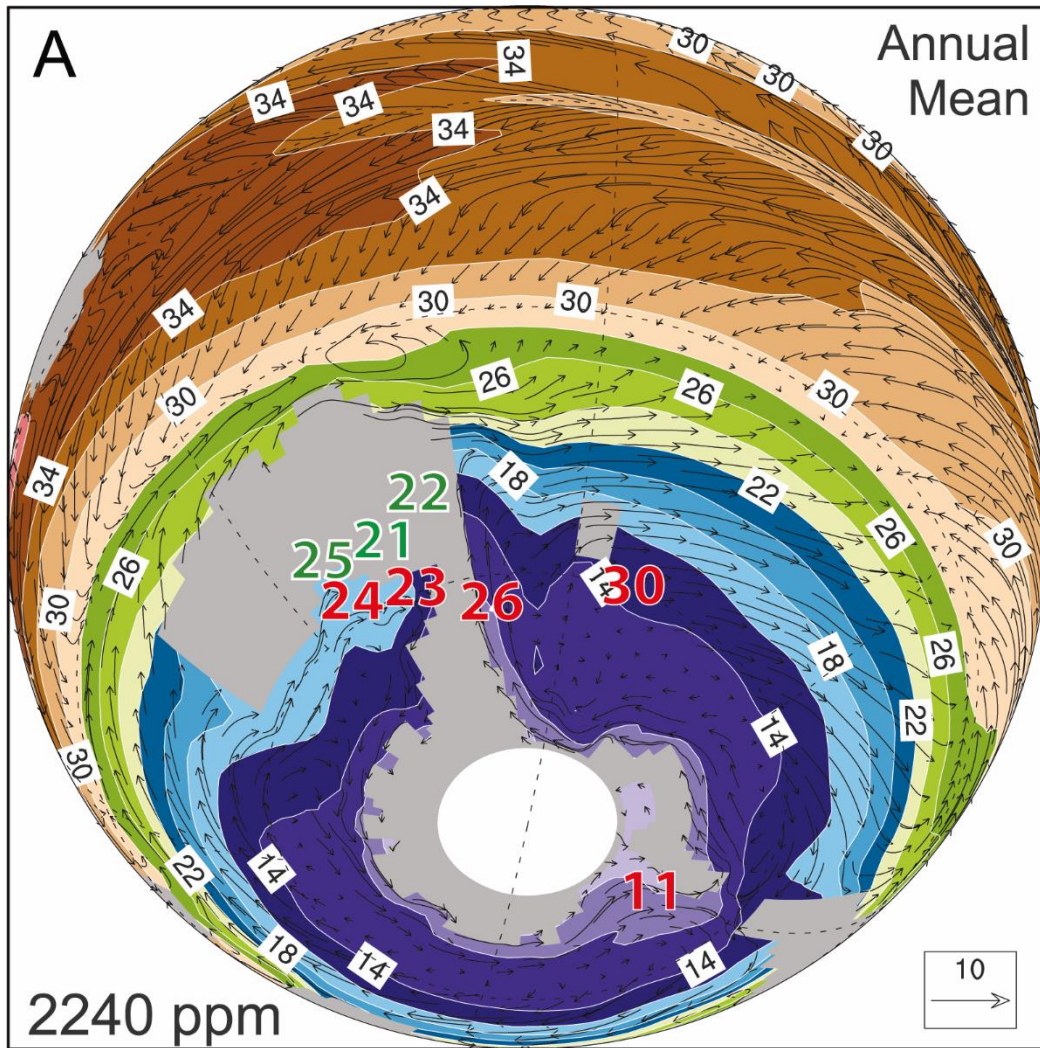


Figure 21: A. Late Paleocene SST Model from Hollis et al., 2012, B. PETM SST Model from Hollis et al., 2012. Reconstructed SST values are shown in red (Table 1) and reconstructed MAAT values are shown in green (Table 2). For Otaio Gorge the average value of the MAAT reconstructed by LMA (SE Asian Calibration) and MBT/CBT' was taken.

when looking at and comparing the absolute temperatures collected in Table 1, due to the use of different proxies, increased importance of seasonal changes in the Southern Ocean and high PETM temperatures being out of the range of modern SST (e.g. Dunkley Jones et al., 2013 and references therein). However, the relative differences between the Late Paleocene and PETM between each site can be compared with more certainty. The difference in SST between the Late Paleocene and the PETM at Point Margaret was 4.1 °C whereas the warming trend at La-Trobe was less expressed which resulted in a 1.5 °C difference. For New Zealand, DSDP Site 277 shows an increase of 2.3 °C whereas for ODP Site 1172 SST differences of 5.9 °C ($\text{TEX}_{86}^{\text{H}}$) and 3.9 °C ($\text{Cren}'/(\text{Cren}' + \text{Cren})$) are recorded between the Late Paleocene and PETM. According to the model by Hollis et al. (2012) the temperature difference between the Late Paleocene and PETM is 4 °C at every location in the Southern Ocean. Furthermore, Dunkley Jones et al., (2013) indicate that it is unlikely that the global mean surface temperature anomaly is in excess of 5 °C across the PETM. Both SST differences derived from proxies and models between the Late Paleocene and PETM for the Southern Ocean seem to agree with this amount of warming (Hollis et al., 2012; Table 1). Although, the Weddell Sea experiences a temperature difference of more than 10 °C (Thomas et al., 2002), whereas the model shows a similar warming as the rest of the Southern Ocean. The difference between model and proxy data regarding the absolute SST change, between the Late Paleocene and the PETM, reveal that the model is not equipped with a detailed description of the oceanography in the Southern Ocean. This is especially visible in the Pacific Ocean, where the model underestimates both Late Paleocene and PETM temperatures sometimes by more than 14 °C (Fig. 21). The SST differences in the AAG are less expressed than those from the Pacific Ocean, which might be attributed to the underestimation of temperature, but occur nevertheless. These temperature differences between model and proxy records cannot only be explained by uncertainties in proxy temperature estimations.

The fact that such large temperature differences between model and proxy data also occur at the transition towards the EECO (e.g. Bijl et al., 2009; Hollis et al., 2012) indicate that models have problems defining early Paleogene hothouse conditions. Reasons that might explain these problems are related to climate sensitivity and feedback mechanisms (Caballero and Huber, 2013; Royer, 2016). Also, low latitudinal SST gradient (Bijl et al., 2009) and a greater polar amplification of temperature at more acceptable CO₂ conditions (Hollis et al., 2012) have to be applied when modelling the Southern Ocean during the early Paleogene. If these issues are resolved and model and reconstructed data are in better understanding, models could be applied to the current warming of the Earth and its consequences.

Conclusion

The paleoenvironmental reconstructions of the Point Margaret outcrop have given new insights in the conditions of the AAG during the Late Paleocene and PETM. Especially the early *Apectodinium* acme and the similarity in response to Site 1172 show that the conditions at the AAG are specific and that the Tasmanian Gateway and the related oceanography do not necessarily prohibit the exchange of water between the AAG and the South Pacific Ocean. SST reconstruction at Point Margaret and a compilation of SST data of the Southern Ocean indicates that the mismatch between models and reconstructed data also occur at the AAG. Also the compilation of SST data from the Southern Ocean shows that especially a low latitudinal gradient and polar amplification at lower CO₂ values must to be taken into account when modelling the Southern Ocean during the early

Paleogene. The difference between MAT and SST reconstructions indicate that the calibration range of current MAT proxies is complicating the reconstruction of valid MAT records during hothouse conditions. This also makes the comparison between MAT and SST more difficult. Nevertheless, the relative SST increase during the PETM at almost all Southern Ocean sites is in accordance with the increase obtained from models and the maximal global mean surface temperature anomaly.

Acknowledgements

I would like to thank my supervisors Peter Bijl, Francien Peterse and Joost Frieling for especially helping me to determine the many peridinoid dinocysts and discussing the strange behaviour of GDGTs. But I would not have been able to make it through this Thesis without the help and support of my friends from room 5.17!

Appendix A: list of encountered dinocysts

Below all the dinocyst genera are listed that were present at the Point Margaret. The lower part of this section (up to and including PP237 (32.1 m) was counted by me while the upper part of this section was counted by Joost Frieling. The dinocysts that were found only in the lower part of the section are marked by an asterisk while the dinocysts which were only found in the upper part are marked by a degree sign. No information is yet available on the exact description of the dinocysts counted by Joost Frieling. Genera which are not marked occur in both parts of the section.

*Achomosphaera alcicorna**
*Achomosphaera andalouisiensis**
Achomosphaera sp.°
Achomosphaera spp*
Adnatosphaeridium multispinosum°
Adnatosphaeridium sp.°
*Aireiana verrucosa**
Apectodinium augustum
Apectodinium cf. *Wetzeliella*°
Apectodinium homomorphum – Plate II, 6
Apectodinium homomorphum B°
Apectodinium hyperacantus
Apectodinium kaal°
Apectodinium paniculatum°
*Apectodinium parvum**
Apectodinium quinquelatum
Apectodinium spp
Apectodinium/Wetzeliella indet*. This indet refers to the dinocyst specimen which are indistinguishable between *Apectodinium* and *Wetzeliella*.
Areoligera coronate
Areoligera senonensis°
Areoligera spp*
Areoligera tauloma°
*Batiacasphaera compta**
Batiacasphaera spp°

Brigantedinium spp*
Cerebrocysta magna*
Cerodinium albertii* Plate I, 14-15
Cerodinium depressum°
Cerodinium angulatum*
Cerodinium dartmoorium Plate I, 13
Cerodinium pachyceros
Cerodinium speciosum*
Cerodinium sp.°
Cerodinium spp*
Cerodinium striatum*
Cerodinium/Deflandrea indet*. This indet refers to the dinocyst specimen which were indistinguishable between Cerodinium and Deflandrea.
Cleistosphaeridium sp.°
Cribroperidinium sp.°
Cordosphaeridium cantharellus*
Cordosphaeridium cf. exilimurum?°
Cordosphaeridium fibrospinosum
Cordosphaeridium gracile*
Cordosphaeridium inodes*
Cordosphaeridium multispinosum
Cordosphaeridium sp.°
Cordosphaeridium spp*. As species of this genus tend to differ from described specimen, many were assigned here.
Dapsulodinium pseudocolligerum*.
Deflandrea antarctica°
Deflandrea "bol" (convexa?)°
Deflandrea obliquipes°
Deflandrea oebisfeldensis
Deflandrea spp
Diphyes spp. A. A different archeopyle type, precingular instead of apical, was found in some of the Diphyes specimen. Plate II, 13-14
Diphyes colligerum. Plate II, 11-12
Diphyes/Dapsilidinium/Lingulodinium indet* This indet refers to the dinocyst specimen which were indistinguishable between Diphyes, Dapsilidinium and Lingulodinium.
Diphyes sp.°
Diphyes spp*
Eisenackia circumtabulata°
Eisenackia reticulata°
Elytrocysta brevis*
Elytrocysta sp.°
Enneadocysta arcuate*
Enneadocysta multicornita*
Enneadocysta spp*
Eocladopyxis spp.*
Enneadocysta? sp.°
Eocladopyxis tessellata°
Florentinia ferox*

Florentinia reichartii°
Florentinia sp.°
Glaphyrocysta delicata°
Glaphyrocysta divaricate*
Glaphyrocysta exuberans*
Glaphyrocysta ordinata
Glaphyrocysta pastielsii
Glaphyrocysta preordinata*
Glaphyrocysta retiintexta*
Glaphyrocysta sp.°
Glaphyrocysta spp*
Goniodomids. This includes all species representative of Eocladopyxis, Homotryblium,
Goniodomids? spp and Pyxidinopsis.
Hafniasphaera cryptovesiculata
Hafniasphaera septata
Hafniasphaera spp*
Heteraulacysta pustulata°
Homotryblium abbreviatum°
Homotryblium spp
Homotryblium tenuispinosum°
Hystrichokolpoma rigaudiae°
Hystrichokolpoma truncata*
Hystricosphaeridium sp.°
Isabelidium cingulatum*
Ifecysta lappacea°
Kallosphaeridium breviparbatum°
Kallosphaeridium nigeriaense °
Kallosphaeridium spp.°
Kallosphaeridium yorubaense°
Kenleyia cpx.°
Lanternosphaeridium lanosum°
Lejeunecysta beninensis°
Lejeunecysta cf. lata°
Lejeunecysta hyaline*
Lentinia serrata°
Lingulodinium machareophorum*
Lingulodinium spp
Melitasphaeridium pseudorecurvatum*
Membranosphaera spp*
Morkallacysta sp. This genus has been described by Guler et al., (2014), but the
specimen found in this section differ from the description as a.o. the archeopyle cannot
be distinguished. Plate I, 9-10
Muratodinium fimbriatum°
Operculodinium centrocarpum
Operculodinium piaseckii* Plate II, 10
Operculodinium sp.°
Operculodinium spp* Plate II, 9
Operculodinium tiara
Palaeocystodinium golzowense*

Palaeocystodinium sp.^o
Palaeocystodinium spp*
Paucisphaeridium spp
Phelodinium magnificum*
Phelodinium spp.^o
Phthanoperidinium alectrolophum*
Phthanoperidinium cf. crenulatum^o
Phthanoperidinium crenulatum*
Phthanoperidinium echinatum*
Phthanoperidinium sp.^o
Phthanoperidinium spp*
Polysphaeridium subtile
Polysphaeridium zohayi*
Pterodinium cingulatum^o
Pterodinium striatum*
Pyxidiniopsis sp.^o
Pyxidiniopsis spp*
Pyxidiniopsis tuberculata*
Rottnestia borussica^o
Round Browns*
Selenopemphix nephroides^o
Senegalinium asymmetricum*
Senegalinium BIG^o
Senegalinium dilwynense Plate I, 3-4
Senegalinium laevigatum*
Senegalinium obscurum. These specimen are small, ±50 µm, transparent cysts with a triangular precingular archeopyle. Plate I, 5
Senegalinium sp.^o
Senegalinium spp*
Senegalinium striatum* Plate I, 1-2
Senegalinium tabulated. These specimens are peridinioid cysts with tabulation but without spines. Plate I, 6-8
Spiny indet*. This indet refers to the dinocyst specimen that were indistinguishable between Spinidinium, Phthanoperidinium and Vozzhennikovia.
Spinidinium "bruin"^o
Spinidinium clavus*
Spinidinium densispinatum* Plate I, 11
Spinidinium macmurdoense Plate I, 12
Spinidinium schellenbergii
Spinidinium spp
Spiniferites cornutus^o
Spiniferites mirabilis
Spiniferites pseudofurcatus
Spiniferites ramoses*
Spiniferites spp
Thanyiosphaeridium xanthypoxyds
Thalassiphora sp.^o
Vozzhennikovia roehlia* Plate II, 8
Vozzhennikovia rotunda*

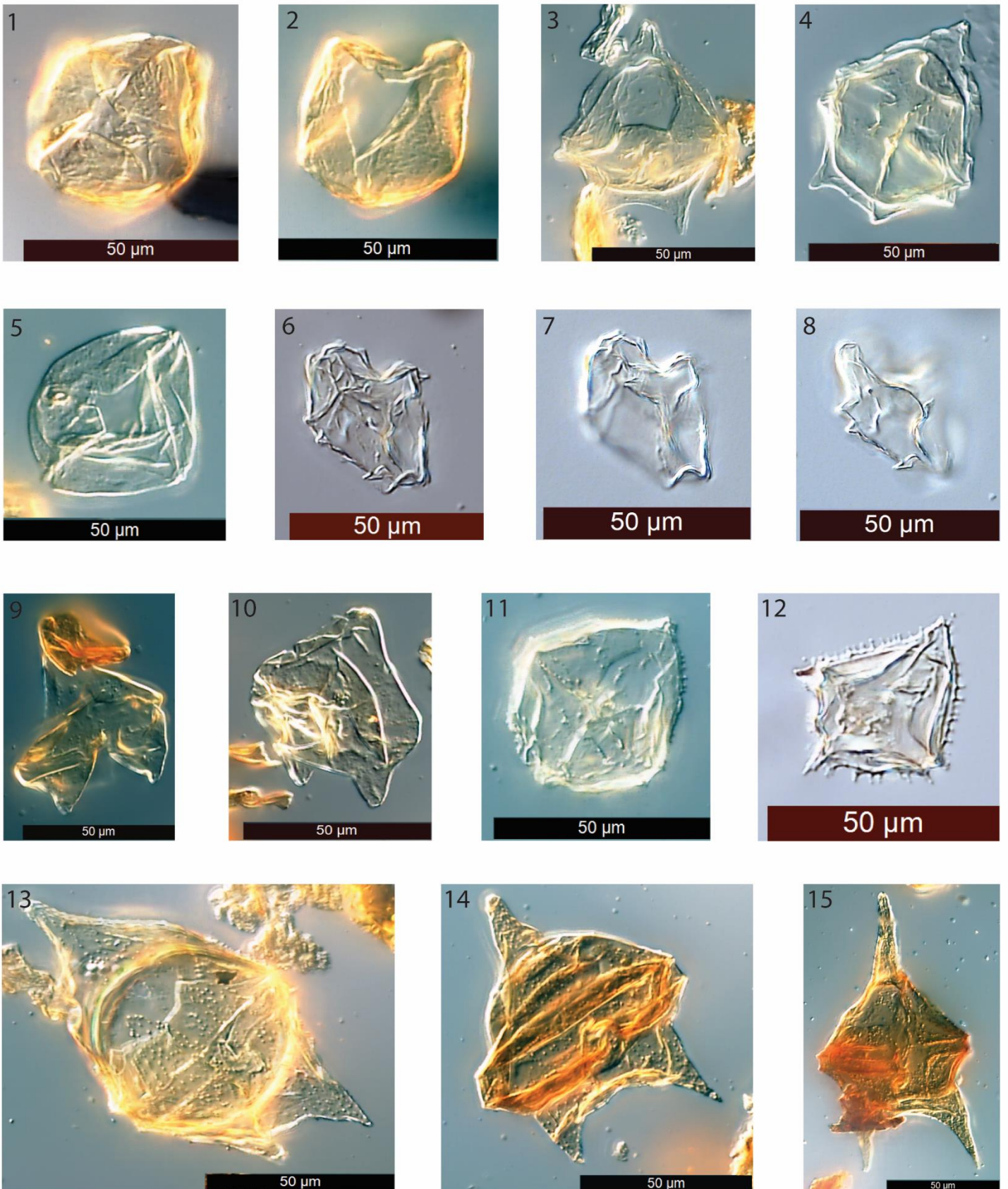
Vozzhennikovia spp

*Vozzhennikovia stickleyae**

Vozzhennikovia tawanuiensis. The description of this species can be found in Crouch et al., (2014). Plate II, 7

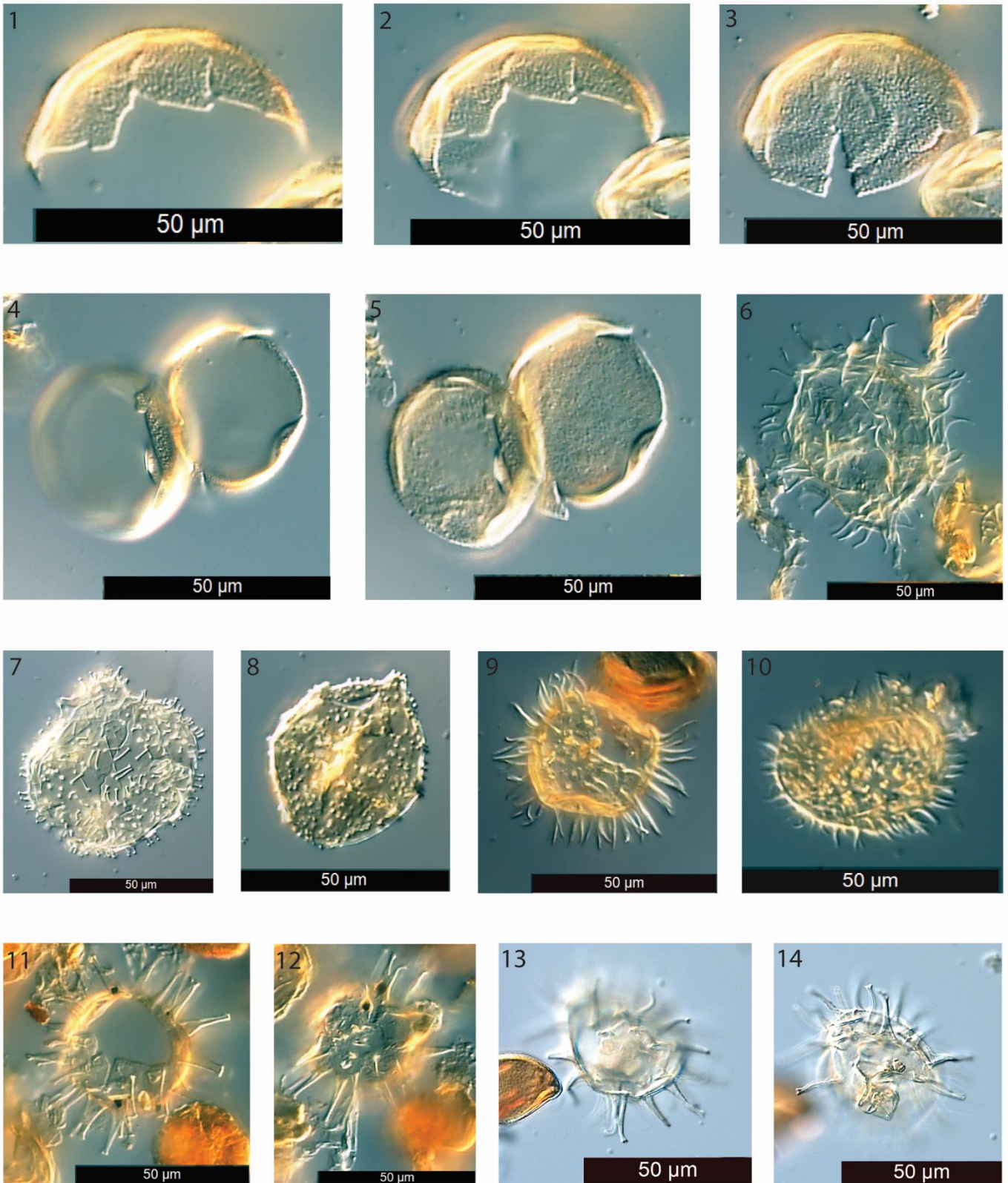
?Goniodomids sp. 1.* An epicystal dinoflagellate with granular wall texture, tabulation only visible on the parasulcal notch or tongue, sometimes containing longer spines, the archeopyle consist of 3 apical plates which are often found together. Plate II, 1-5

Plate I



1, 2. *Senegalinium striatum* (PP76.1, F33.left) 3. *Senegalinium dilwynense* (PP40.1, E34.2) 4. *Senegalinium dilwynense* (PP4.1, E36.1) 5. *Senegalinium obscurum* (PP76.1, G33.1/F33.3) 6, 7, 8. *Senegalinium tabulated* (PP4.1, F30.2) 9. *Morkallacysta* (PP101.1, H38.4) 10. *Morkallacysta* (PP101.1, N20.1) 11. *Spinidium densispinatum* (PP181.1, E20.right) 12. *Spinidium macmurdoense* (PP4.1, G33.up) 13. *Cerodinium dartmoorium* (PP121.1, E27.up) 14. *Cerodinium albertii* (PP12.1, M37.1/L37.3) 15. *Cerodinium albertii* (PP12.1, X38.2)

Plate II



1, 2, 3. *Goniodomid? spp.* (PP40.1, F31.2/F32.1) 4, 5. *Goniodomid? spp.* (PP40.1, D37.4) 6. *Apectodinium homomorphum* (PP45.1, J25.3) 7. *Vozzhennikovia tawanuiensis* (PP40.1, E30) 8. *Vozzhennikovia roehlia* (PP111.1, E20.1) 9. *Operculodinium spp.* (PP12.1, K34.4) 10. *Operculodinium piaseckii* (PP12.1, N31) 11, 12. *Diphyes colligerum* (PP50.2, F39) 13, 14. *Diphyes spp. A* (PP161.1, D30.4)

Appendix B: list of encountered pollen and spores

Pollen and spores were only counted in major groups in the lower part of Point Margaret. A distinction has been made between Gymnosperms, Angiosperms and Pterodiphytes or Spores.

Gymnosperms:

Bisaccate Pollen

Trisaccate Pollen

Lygestipollenites? sp. Questionably designed to this species.

Crassopollis

Other Pollen. All other specimen recognised as pollen but not counted in a particular species group.

Angiosperms:

Proteacidites/Propylipollis

Beaupreaidites

Nothofagidites/nothofagus

Tetrads

Peripollenites? spp. Questioningly designed to this genus.

Tricolpites

Gambierina

Anacolosidites

Pterodiphytes/Spores:

Ischyosporites/Polypodiisporites

Ceratospores/Neoraitrickia/Peromonolites

Tripunctisporis/Sphagnumsporites

Retitriletes? spp. Questioningly designed to this genus.

Other Spores. All other specimen recognised as spores but not counted in a particular species group.

References

- Arditto, P A. 1995. "The Eastern Otway Basin Wangerrip Group Revisited Using an Integrated Sequence Methodology." *Apea Journal*, no. 35: 372–84.
- Beerling, David J, and Dana L Royer. 2011. "Convergent Cenozoic CO₂ History." *Nature Geoscience* 4: 418–20.
- Bijl, P. K., J. A. P. Bendle, S. M. Bohaty, J. Pross, S. Schouten, L. Tauxe, C. E. Stickley, et al. 2013a. "Eocene Cooling Linked to Early Flow across the Tasmanian Gateway." *Proceedings of the National Academy of Sciences of the United States of America* 110 (24): 9645–50. doi:10.1073/pnas.1220872110.
- Bijl, P K. 2011. "Environmental and Climatological Evolution of the Early Paleogene Southern Ocean." *Utrecht University PhD Thesis, LPP Contribution Series*.
- Bijl, Peter K., Appy Sluijs, and Henk Brinkhuis. 2013b. "A Magneto- and Chemostratigraphically Calibrated Dinoflagellate Cyst Zonation of the Early Palaeogene South Pacific Ocean." *Earth-Science Reviews* 124. Elsevier B.V.: 1–31. doi:10.1016/j.earscirev.2013.04.010.
- Bijl, Peter K, Stefan Schouten, Appy Sluijs, Gert-Jan Reichart, James C Zachos, and Henk Brinkhuis. 2009. "Early Palaeogene Temperature Evolution of the Southwest Pacific Ocean." *Nature* 461 (7265). Nature Publishing Group: 776–79. doi:10.1038/nature08399.
- Bowen, Gabriel J, Bianca J Maibauer, Mary J Kraus, Ursula Röhl, Thomas Westerhold, Amy Steimke, Philip D Gingerich, Scott L Wing, and William C Clyde. 2014. "Two Massive, Rapid Releases of Carbon during the Onset of the Palaeocene–Eocene Thermal Maximum." *Nature Geoscience* 8: 44–47. doi:10.1038/ngeo2316.

- Brinkhuis, H, S Sengers, Appy Sluijs, Jeroen Warnaar, and Graham L. Williams. 2003. "Latest Cretaceous to Earliest Oligocene, and Quaternary Dinoflagellate Cysts from ODP Site 1172, East Tasman Plateau." *Proceedings of the Ocean Drilling Program, Scientific Results* 189: 1–48.
- Brinkhuis, Henk. 1994. "Late Eocene to Early Oligocene Dinoflagellate Cysts from the Priabonian Type-Area (Northeast Italy): Biostratigraphy and Paleoenvironmental Interpretation." *Palaeogeography, Palaeoclimatology, Palaeoecology* 107 (1–2): 121–63.
- Caballero, R., and M. Huber. 2013. "State-Dependent Climate Sensitivity in Past Warm Climates and Its Implications for Future Climate Projections." *Proceedings of the National Academy of Sciences* 110 (35): 14162–67.
- Contreras, L., J. Pross, P. K. Bijl, R. B. O'Hara, J. I. Raine, A. Sluijs, and H. Brinkhuis. 2014. "Southern High-Latitude Terrestrial Climate Change during the Palaeocene–Eocene Derived from a Marine Pollen Record (ODP Site 1172, East Tasman Plateau)." *Climate of the Past* 10 (4). Copernicus GmbH: 1401–20. doi:10.5194/cp-10-1401-2014.
- Crouch, Erica M., and Henk Brinkhuis. 2005. "Environmental Change across the Paleocene–Eocene Transition from Eastern New Zealand: A Marine Palynological Approach." *Marine Micropaleontology* 56 (August): 138–60.
- Crouch, Erica M., Gerald R. Dickens, Henk Brinkhuis, Marie Pierre Aubry, Christopher J. Hollis, Karyne M. Rogers, and Henk Visscher. 2003. "The Apectodinium Acme and Terrestrial Discharge during the Paleocene-Eocene Thermal Maximum: New Palynological, Geochemical and Calcareous Nannoplankton Observations at Tawanui, New Zealand." *Palaeogeography, Palaeoclimatology, Palaeoecology* 194: 387–403. doi:10.1016/S0031-0182(03)00334-1.
- Crouch, Erica M., Claus Heilmann-Clausen, Henk Brinkhuis, Hugh E.G. Morgans, Karyne M. Rogers, Hans Egger, and Birger Schmitz. 2001. "Global Dinoflagellate Event Associated with the Late Paleocene Thermal Maximum." *Geology* 29 (4): 315–18. doi:10.1130/0091-7613(2001)029.
- Crouch, Erica M., Pi Suhr Willumsen, Denise K. Kulhanek, and Samantha J. Gibbs. 2014. "A Revised Paleocene (Teurian) Dinoflagellate Cyst Zonation from Eastern New Zealand." *Review of Palaeobotany and Palynology* 202. Elsevier B.V.: 47–79. doi:10.1016/j.revpalbo.2013.12.004.
- Dale, B., and A. Fjellså. 1994. "Dinoflagellate Cysts as Paleoproductivity Indicators: State of the Art, Potential and Limits." In: *Carbon Cycling in the Glacial Ocean: Constraints on the Ocean's Role in Global Change*, Edited by: Zahn, R., Pedersen, T. F., Kaminski, M. A., and Labeyrie, L., Springer, Berlin, 521–537.
- De Jonge, Cindy, Ellen C. Hopmans, Claudia I. Zell, Jung Hyun Kim, Stefan Schouten, and Jaap S. Sinninghe Damsté. 2014a. "Occurrence and Abundance of 6-Methyl Branched Glycerol Dialkyl Glycerol Tetraethers in Soils: Implications for Palaeoclimate Reconstruction." *Geochimica et Cosmochimica Acta* 141: 97–112.
- De Jonge, Cindy, Ellen C Hopmans, Alina Stadnitskaia, W. Irene C Rijkstra, Ron Hofland, Erik Tegelaar, and Jaap S Sinninghe Damsté. 2013. "Identification of Novel Penta- and Hexamethylated Branched Glycerol Dialkyl Glycerol Tetraethers in Peat Using HPLC-MS2, GC-MS and GC-SMB-MS." *Organic Geochemistry* 54: 78–82. doi:10.1016/j.orggeochem.2012.10.004.
- De Jonge, Cindy, Alina Stadnitskaia, Ellen C Hopmans, Georgy Cherkashov, Andrey Fedotov, and Jaap S Sinninghe Damsté. 2014b. "In Situ Produced Branched Glycerol Dialkyl Glycerol Tetraethers in Suspended Particulate Matter from the Yenisei River, Eastern Siberia." *Geochimica et Cosmochimica Acta* 125: 476–91.
- De Jonge, Cindy, Alina Stadnitskaia, Ellen C Hopmans, Georgy Cherkashov, Andrey Fedotov, Irina D Streletskaia, Alexander A Vasiliev, and Jaap S Sinninghe Damsté. 2015. "Drastic Changes in the Distribution of Branched Tetraether Lipids in Suspended Matter and Sediments from the Yenisei River and Kara Sea (Siberia): Implications for the Use of brGDGT-Based Proxies in Coastal Marine Sediments." *Geochimica et Cosmochimica Acta* 165: 200–225.
- Dickens, Gerald R., Maria M. Castillo, and James C. G. Walker. 1997. "A Blast of Gas in the Latest Paleocene: Simulating First-Order Effects of Massive Dissociation of Oceanic Methane Hydrate." *Geology* 25 (3): 259–62. doi:10.1130/0091-7613(1997)025.
- Dunkley Jones, Tom, Daniel J. Lunt, Daniela N. Schmidt, Andy Ridgwell, Appy Sluijs, Paul J. Valdes, and Mark Maslin. 2013. "Climate Model and Proxy Data Constraints on Ocean Warming across the Paleocene-Eocene Thermal Maximum." *Earth-Science Reviews* 125. Elsevier B.V.: 123–45. doi:10.1016/j.earscirev.2013.07.004.
- Exon, N. F., J. P. Kennett, M. J. Malone, and Et Al. 2001. "Proc. ODP, Initial Reports Volume 189." Available from: *Ocean Drill. Prog., College Station TX, 77845-9547, USA*, 1–98.
- Fensome, R.A., and G.L. Williams. 2004. "The Lentin and Williams Index of Fossil Dinoflagellates 2004 Edition." *American Association of Stratigraphic Palynologists Foundation Contribution Series*.
- Fensome, Robert A., H Gocht, and G L Williams. 1996. "The Eisenack Catalog of Fossil Dinoflagellates New

- Series Vol. 4." *E. Schweizerbart'sche Verlagsbuchhandlung, Stuttgart, Germany*. E. Schweizerbart'sche Verlagsbuchhandlung, 2009–2548.
- Firth, J. V. 1996. "Upper Middle Eocene to Oligocene Dinoflagellate Biostratigraphy and Assemblage Variations in Hole 913B, Greenland Sea." *Proceedings of the Ocean Drilling Program. Scientific Results* 151. Ocean Drilling Program: 203–42.
- Freymond, Chantal V, Francien Peterse, Lorena V Fischer, Florin Filip, Liviu Giosan, and Timothy I Eglinton. 2017. "Branched GDGT Signals in Fluvial Sediments of the Danube River Basin: Method Comparison and Longitudinal Evolution." *Organic Geochemistry* 103: 88–96.
- Frieling, Joost. n.d. "Personal Contact."
- . 2016. "Climate, Carbon Cycling and Marine Ecology during the Paleocene-Eocene Thermal Maximum."
- Frieling, Joost, Holger Gebhardt, Matthew Huber, Olabisi A. Adekeye, Samuel O. Akande, Gert-Jan Reichart, Jack J. Middelburg, Stefan Schouten, and Appy Sluijs. 2017. "Extreme Warmth and Heat-Stressed Plankton in the Tropics during the Paleocene-Eocene Thermal Maximum." *Science Advances* 3: e1600891.
- Frieling, Joost, Alina I. Iakovleva, Gert Jan Reichart, Galina N. Aleksandrova, Zinaida N. Gnibidenko, Stefan Schouten, and Appy Sluijs. 2014. "Paleocene-Eocene Warming and Biotic Response in the Epicontinental West Siberian Sea." *Geology* 42 (9). Geological Society of America: 767–70. doi:10.1130/G35724.1.
- Gradstein, F.M., J.G. Ogg, M. Schmitz, and G. Ogg. 2012. "The Geologic Time Scale." *Boston Elsevier*.
- Greenwood, D R, P T Moss, a I Rowett, a J Vadala, and R L Keefe. 2003. "Plant Communities and Climate Change in Southeastern Australia during the Early Paleogene." *Geological Society of America Special Pa*: 365–380. doi:10.1130/0-8137-2369-8.365.
- Greenwood, David R, Peter Wilf, Scott L Wing, and David C Christophel. 2004. "Paleotemperature Estimation Using Leaf-Margin Analysis: Is Australia Different?" *Palaeos* 19 (2): 129–42. doi:10.1669/0883-1351(2004)019<0129:PEULAI>2.0.CO;2.
- Hobbs, Richard, Brian Huber, and Kara A. Bogus. 2016. "International Ocean Discovery Program Expedition 369 Scientific Prospectus: Australia Cretaceous Climate and Tectonics." *International Ocean Drilling Program*.
- Holdgate, G. R., and S. J. Gallagher. 2003. "Chapter 10: Tertiary, in: *Geology of Victoria*," 289–324.
- Hollis, C J, B R Hines, K Littler, V Villasante-Marcos, D K Kulhanek, C P Strong, J C Zachos, S M Eggins, L Northcote, and A Phillips. 2015. "The Paleocene-Eocene Thermal Maximum at DSDP Site 277, Campbell Plateau, Southern Pacific Ocean." *Climate of the Past* 11: 1009–25. doi:10.5194/cp-11-1009-2015.
- Hollis, Christopher J, Michael J S Tayler, Benjamin Andrew, Kyle W. Taylor, Pontus Lurcock, Peter K. Bijl, Denise K. Kulhanek, et al. 2014. "Organic-Rich Sedimentation in the South Pacific Ocean Associated with Late Paleocene Climatic Cooling." *Earth-Science Reviews*. doi:10.1016/j.earscirev.2014.03.006.
- Hollis, Christopher J, Kyle W R Taylor, Luke Handley, Richard D. Pancost, Matthew Huber, John B. Creech, Benjamin R. Hines, et al. 2012. "Early Paleogene Temperature History of the Southwest Pacific Ocean: Reconciling Proxies and Models." *Earth and Planetary Science Letters* 349–350: 53–66. doi:10.1016/j.epsl.2012.06.024.
- Hopmans, Ellen C., Stefan Schouten, and Jaap S. Sinninghe Damsté. 2016. "The Effect of Improved Chromatography on GDGT-Based Palaeoproxies." *Organic Geochemistry* 93: 1–6. doi:10.1016/j.orggeochem.2015.12.006.
- Hopmans, Ellen C, Johan W H Weijers, Enno Schefuß, Lydie Herfort, Jaap S Sinninghe Damsté, and Stefan Schouten. 2004. "A Novel Proxy for Terrestrial Organic Matter in Sediments Based on Branched and Isoprenoid Tetraether Lipids." *Earth and Planetary Science Letters* 224: 107–16. doi:10.1016/j.epsl.2004.05.012.
- Huber, Brian T., and Frédéric Quillevéré. 2005. "Revised Paleogene Planktonic Foraminiferal Biozonation for the Austral Realm." *The Journal of Foraminiferal Research* 35 (4): 299–314.
- Huber, M., and R. Caballero. 2011. "The Early Eocene Equable Climate Problem Revisited." *Climate of the Past* 7 (2): 603–33. doi:10.5194/cp-7-603-2011.
- Huber, Matthew, Henk Brinkhuis, Catherine E. Stickley, Kristofer Döös, Appy Sluijs, Jeroen Warnaar, Stephen A. Schellenberg, and Graham L. Williams. 2004. "Eocene Circulation of the Southern Ocean: Was Antarctica Kept Warm by Subtropical Waters?" *Paleoceanography* 19 (4): 1–12. doi:10.1029/2004PA001014.
- Huurdeman, Emiel. 2017. "Late Paleocene - Early Eocene Long and Short- Term Environment and Climate Change in Southeast Australia."
- Iakovleva, Alina I, Henk Brinkhuis, and Carla Cavagnetto. 2001. "Late Palaeocene-Early Eocene

- Dinoflagellate Cysts from the Turgay Strait, Kazakhstan; Correlations across Ancient Seaways." *Palaeogeography, Palaeoclimatology, Palaeoecology* 172: 243–68. doi:10.1016/S0031-0182(01)00300-5.
- IPCC. 2014. "Synthesis Report."
- Keating, K. 1993. "The Lithostratigraphy, Palynology and Sequence Stratigraphy of the Pebble Point Formation." *La Trobe University, Bundoora, Victoria*.
- Kennett, J. P., and L. D. Stott. 1991. "Abrupt Deep-Sea Warming, Palaeoceanographic Changes and Benthic Extinctions at the End of the Palaeocene." *Nature* 353: 225–29.
- Kim, Jung Hyun, Jaap van der Meer, Stefan Schouten, Peer Helmke, Veronica Willmott, Francesca Sangiorgi, Nalân Koç, Ellen C. Hopmans, and Jaap S. Sinninghe Damsté. 2010. "New Indices and Calibrations Derived from the Distribution of Crenarchaeal Isoprenoid Tetraether Lipids: Implications for Past Sea Surface Temperature Reconstructions." *Geochimica et Cosmochimica Acta* 74: 4639–54.
- Koch, Paul L., James C. Zachos, and Philip D. Gingerich. 1992. "Correlation between Isotope Records in Marine and Continental Carbon Reservoirs near the Palaeocene/Eocene Boundary." *Nature* 358: 319–22. doi:10.1038/358319a0.
- Liu, Zhangui, Mark Pagani, David Zinniker, Robert DeConto, Matthew Huber, Henk Brinkhuis, Sunita R. Shah, R. Mark Leckie, and Ann Pearson. 2009. "Global Cooling during the Eocene-Oligocene Climate Transition." *Science* 323 (5918): 1187–90.
- McGowran, B. 1978. "Early Tertiary Biostratigraphy in Southern Australia: A Progress Report." In *The Crespin Volume: Essays in Honour of Irene Crespin, Belford, D.J., & Scheibnerova, V., Editors, Bureau Mineral Resources Australia, Geology & Geophysics, Bulletin* 192: 83–95.
- . 1991. "Mastrichtian and Early Cainozoic, Southern Australia: Foraminiferal Biostratigraphy." In: *Williams M.A.J., De Deckker P. & Kershaw A.P. Eds, The Cainozoic of the Australian Region. Geological Society of Australia, Special Publication* 18: 79–98.
- McGowran, B. 1965. "Two Paleocene Foraminiferal Faunas from the Wangerrip Group, Pebble Point Coastal Section, Western Victoria." *Proc. R. Soc. Victoria* 79: 9–74.
- McGowran, B., G. R. Holdgate, Q. Li, and S. J. Gallagher. 2004. "Cenozoic Stratigraphic Succession in Southeastern Australia." *Australian Journal of Earth Sciences* 51: 459–96.
- Naafs, B. D.A., A. V. Gallego-Sala, G. N. Inglis, and R. D. Pancost. 2017a. "Refining the Global Branched Glycerol Dialkyl Glycerol Tetraether (brGDGT) Soil Temperature Calibration." *Organic Geochemistry* 106. Elsevier Ltd: 48–56. doi:10.1016/j.orggeochem.2017.01.009.
- Naafs, B. D.A., G. N. Inglis, Y. Zheng, M. J. Amesbury, H. Biester, R. Bindler, J. Blewett, et al. 2017b. "Introducing Global Peat-Specific Temperature and pH Calibrations Based on brGDGT Bacterial Lipids." *Geochimica et Cosmochimica Acta* 208: 285–301. doi:10.1016/j.gca.2017.01.038.
- Panchuk, K., A. Ridgwell, and L.R. Kump. 2008. "Sedimentary Response to Paleocene-Eocene Thermal Maximum Carbon Release: A Model-Data Comparison." *Geology* 36 (4): 315. doi:10.1130/G24474A.1.
- Pancost, Richard D., Kyle W.R. Taylor, Gordon N. Inglis, Elizabeth M. Kennedy, Luke Handley, Christopher J. Hollis, Erica M. Crouch, et al. 2013. "Early Paleogene Evolution of Terrestrial Climate in the SW Pacific, Southern New Zealand." *Geochemistry, Geophysics, Geosystems* 14 (12): 5413–29. doi:10.1002/2013GC004935.
- Peterse, Francien, Jung Hyun Kim, Stefan Schouten, Dorthe Klitgaard Kristensen, Nalân Koç, and Jaap S. Sinninghe Damsté. 2009. "Constraints on the Application of the MBT/CBT Palaeothermometer at High Latitude Environments (Svalbard, Norway)." *Organic Geochemistry* 40: 692–99.
- Peterse, Francien, Jaap van der Meer, Stefan Schouten, Johan W H Weijers, Noah Fierer, Robert B. Jackson, Jung Hyun Kim, and Jaap S. Sinninghe Damsté. 2012. "Revised Calibration of the MBT-CBT Paleotemperature Proxy Based on Branched Tetraether Membrane Lipids in Surface Soils." *Geochimica et Cosmochimica Acta* 96: 215–29.
- Pross, Jörg, and Henk Brinkhuis. 2005. "Organic-Walled Dinoflagellate Cysts as Paleoenvironmental Indicators in the Paleogene ; a Synopsis of Concepts." *Paläontologische Zeitschrift* 79 (1): 53–59.
- Pross, Jörg, Lineth Contreras, Peter K. Bijl, David R. Greenwood, Steven M. Bohaty, Stefan Schouten, James a. Bendle, et al. 2012. "Persistent near-Tropical Warmth on the Antarctic Continent during the Early Eocene Epoch." *Nature* 488: 73–77.
- Royer, Dana L. 2016. "Climate Sensitivity in the Geologic Past." *Annual Review of Earth and Planetary Sciences* 44 (1): 277–93. doi:10.1146/annurev-earth-100815-024150.
- Schouten, Stefan, Ellen C. Hopmans, Marianne Baas, Henry Boumann, Sonja Standfest, Martin Könneke, David A. Stahl, and Jaap S. Sinninghe Damsté. 2008. "Intact Membrane Lipids of 'Candidatus Nitrosopumilus Maritimus,' a Cultivated Representative of the Cosmopolitan Mesophilic Group I Crenarchaeota." *Applied and Environmental Microbiology* 74 (8): 2433–40. doi:10.1128/AEM.01709-07.

- Schouten, Stefan, Ellen C. Hopmans, and Jaap S. Sinninghe Damsté. 2013. "The Organic Geochemistry of Glycerol Dialkyl Glycerol Tetraether Lipids: A Review." *Organic Geochemistry* 54: 19–61. doi:10.1016/j.orggeochem.2015.07.006.
- Schouten, Stefan, Ellen C Hopmans, Richard D Pancost, and J. S. S. Damste. 2000. "Widespread Occurrence of Structurally Diverse Tetraether Membrane Lipids: Evidence for the Ubiquitous Presence of Low-Temperature Relatives of Hyperthermophiles." *Proceedings of the National Academy of Sciences* 97 (26): 14421–26. doi:10.1073/pnas.97.26.14421.
- Schouten, Stefan, Ellen C Hopmans, Enno Schefuß, and Jaap S. Sinninghe Damsté. 2002. "Distributional Variations in Marine Crenarchaeotal Membrane Lipids: A New Tool for Reconstructing Ancient Sea Water Temperatures?" *Earth and Planetary Science Letters* 204: 265–74. doi:10.1016/S0012-821X(02)00979-2.
- Schouten, Stefan, Martijn Woltering, W. Irene C. Rijpstra, Appy Sluijs, Henk Brinkhuis, and Jaap S Sinninghe Damsté. 2007. "The Paleocene-Eocene Carbon Isotope Excursion in Higher Plant Organic Matter: Differential Fractionation of Angiosperms and Conifers in the Arctic." *Earth and Planetary Science Letters* 258: 581–92.
- Self-Trail, Jean M, David S Powars, David K Watkins, and Gregory A Wandless. 2012. "Calcareous Nannofossil Assemblage Changes across the Paleocene-Eocene Thermal Maximum: Evidence from a Shelf Setting." *Marine Micropaleontology* 92–93: 61–80. doi:10.1016/j.marmicro.2012.05.003.
- Sinninghe Damsté, Jaap S. 2016. "Spatial Heterogeneity of Sources of Branched Tetraethers in Shelf Systems: The Geochemistry of Tetraethers in the Berau River Delta (Kalimantan, Indonesia)." *Geochimica et Cosmochimica Acta* 186: 13–31. doi:10.1016/j.gca.2016.04.033.
- Sinninghe Damsté, Jaap S, W. Irene C Rijpstra, Ellen C Hopmans, Johan W H Weijers, Bärbel U Foesel, Jörg Overmann, and Svetlana N Dedys. 2011. "13,16-Dimethyl Octacosanedioic Acid (Iso-Diabolic Acid), a Common Membrane-Spanning Lipid of Acidobacteria Subdivisions 1 and 3." *Applied and Environmental Microbiology* 77 (12): 4147–54. doi:10.1128/AEM.00466-11.
- Sinninghe Damsté, Jaap S, Marc Strous, W Irene C Rijpstra, Ellen C Hopmans, Jan a J Geenevasen, Adri C T van Duin, Laura a van Niftrik, and Mike S M Jetten. 2002. "Linearly Concatenated Cyclobutane Lipids Form a Dense Bacterial Membrane." *Nature* 419 (6908): 708–12. doi:10.1038/nature01128.
- Slotnick, B S, V Lauretano, J Backman, G R Dickens, A Sluijs, and L Lourens. 2015. "Early Paleogene Variations in the Calcite Compensation Depth: New Constraints Using Old Borehole Sediments from across Ninetyeast Ridge, Central Indian Ocean." *Climate of the Past* 11: 473–93. doi:10.5194/cp-11-473-2015.
- Sluijs, A., P. K. Bijl, S. Schouten, U. Röhl, G. J. Reichert, and H. Brinkhuis. 2011. "Southern Ocean Warming, Sea Level and Hydrological Change during the Paleocene-Eocene Thermal Maximum." *Climate of the Past* 7 (1): 47–61. doi:10.5194/cp-7-47-2011.
- Sluijs, A., and H. Brinkhuis. 2009. "A Dynamic Climate and Ecosystem State during the Paleocene-Eocene Thermal Maximum – Inferences from Dinoflagellate Cyst Assemblages at the New Jersey Shelf." *Biogeosciences Discussions* 6 (3): 5163–5215.
- Sluijs, A, G J Bowen, H Brinkhuis, L J Lourens, and E Thomas. 2007a. "The Palaeocene-Eocene Thermal Maximum Super Greenhouse: Biotic and Geochemical Signatures, Age Models and Mechanisms of Global Change." *Geological Society Special Publication*, 323–49. doi:1747-602X/07/\$15.00.
- Sluijs, A, H Brinkhuis, C E Stickley, J Warnaar, G L Williams, and M Fuller. 2003. "Dinoflagellate Cysts from the Eocene-Oligocene Transition in the Southern Ocean: Result from ODP Leg 189." *Proceedings of the Ocean Drilling Program, Scientific Results* 189: 1–42. doi:10.2973/odp.proc.sr.189.104.2003.
- Sluijs, Appy, Henk Brinkhuis, Erica M. Crouch, Cédric M. John, Luke Handley, Dirk Munsterman, Steven M. Bohaty, et al. 2008. "Eustatic Variations during the Paleocene-Eocene Greenhouse World." *Paleoceanography* 23 (December): 18. doi:10.1029/2008PA001615.
- Sluijs, Appy, Henk Brinkhuis, Stefan Schouten, Steven M Bohaty, Cédric M John, James C Zachos, Gert-Jan Reichert, Jaap S Sinninghe Damsté, Erica M Crouch, and Gerald R Dickens. 2007b. "Environmental Precursors to Rapid Light Carbon Injection at the Palaeocene/Eocene Boundary." *Nature* 450: 1218–21. doi:10.1038/nature06400.
- Sluijs, Appy, Henk Brinkhuis, Graham L. Williams, and Rob A. Fensome. 2009. "Taxonomic Revision of Some Cretaceous–Cenozoic Spiny Organic-Walled Peridiniacean Dinoflagellate Cysts." *Review of Palaeobotany and Palynology* 154: 34–53. doi:10.1016/j.revpalbo.2008.11.006.
- Sluijs, Appy, and Gerald R. Dickens. 2012. "Assessing Offsets between the $\delta^{13}\text{C}$ of Sedimentary Components and the Global Exogenic Carbon Pool across Early Paleogene Carbon Cycle Perturbations." *Global Biogeochemical Cycles* 26 (4): 1–14. doi:10.1029/2011GB004224.
- Sluijs, Appy, Jörg Pross, and Henk Brinkhuis. 2005. "From Greenhouse to Icehouse; Organic-Walled Dinoflagellate Cysts as Paleoenvironmental Indicators in the Paleogene." *Earth-Science Reviews* 68

- (3–4): 281–315. doi:10.1016/j.earscirev.2004.06.001.
- Thomas, Deborah J., James C. Zachos, Timothy J. Bralower, Ellen Thomas, and Steven Bohaty. 2002. "Warming the Fuel for the Fire: Evidence for the Thermal Dissociation of Methane Hydrate during the Paleocene-Eocene Thermal Maximum." *Geology* 30 (12): 1067–70.
- Tierney, Jessica E, and James M Russell. 2009. "Distributions of Branched GDGTs in a Tropical Lake System: Implications for Lacustrine Application of the MBT/CBT Paleoproxy." *Organic Geochemistry* 40: 1032–36.
- Utescher, Torsten, and Volker Mosbrugger. 2015. "Terrestrial Climate Evolution in Northwest Germany Over the Last 25 Million Years." *The Palaeoflora Database*. at <http://www.geologie.unibonn.de/Palaeoflora>.
- Van Hinsbergen, Douwe J.J., Lennart V. De Groot, Sebastiaan J. Van Schaik, Wim Spakman, Peter K. Bijl, Appy Sluijs, Cor G. Langereis, and Henk Brinkhuis. 2015. "A Paleolatitude Calculator for Paleoclimate Studies." *PLoS ONE* 10: 1–21. doi:10.1371/journal.pone.0126946.
- Wall, David, Barrie Dale, G. P. Lohmann, and Woollcott K. Smith. 1977. "The Environmental and Climatic Distribution of Dinoflagellate Cysts in Modern Marine Sediments from Regions in the North and South Atlantic Oceans and Adjacent Seas." *Marine Micropaleontology* 2: 121–200. doi:10.1016/0377-8398(77)90008-1.
- Weber, Yuki, Cindy De Jonge, W. Irene C Rijpstra, Ellen C Hopmans, Alina Stadnitskaia, Carsten J Schubert, Moritz F Lehmann, Jaap S Sinninghe Damsté, and Helge Niemann. 2015. "Identification and Carbon Isotope Composition of a Novel Branched GDGT Isomer in Lake Sediments: Evidence for Lacustrine Branched GDGT Production." *Geochimica et Cosmochimica Acta* 154: 118–29.
- Weijers, Johan W.H., Elda Panoto, Judith van Bleijswijk, Stefan Schouten, W. Irene C. Rijpstra, Melike Balk, Alfons J M Stams, and Jaap S. Sinninghe Damsté. 2009. "Constraints on the Biological Source(s) of the Orphan Branched Tetraether Membrane Lipids." *Geomicrobiology Journal* 26: 402–14. doi:10.1080/01490450902937293.
- Weijers, Johan W H, Stefan Schouten, Ellen C. Hopmans, Jan A J Geenevasen, Olivier R P David, Joanna M. Coleman, Rich D. Pancost, and Jaap S. Sinninghe Damsté. 2006a. "Membrane Lipids of Mesophilic Anaerobic Bacteria Thriving in Peats Have Typical Archaeal Traits." *Environmental Microbiology* 8 (4): 648–57. doi:10.1111/j.1462-2920.2005.00941.x.
- Weijers, Johan W H, Stefan Schouten, Appy Sluijs, Henk Brinkhuis, and Jaap S Sinninghe Damsté. 2007a. "Warm Arctic Continents during the Palaeocene-Eocene Thermal Maximum." *Earth and Planetary Science Letters* 261: 230–38. doi:10.1016/j.epsl.2007.06.033.
- Weijers, Johan W H, Stefan Schouten, Otto C Spaargaren, and Jaap S Sinninghe Damsté. 2006b. "Occurrence and Distribution of Tetraether Membrane Lipids in Soils: Implications for the Use of the TEX86 Proxy and the BIT Index." *Organic Geochemistry* 37: 1680–93. doi:10.1016/j.orggeochem.2006.07.018.
- Weijers, Johan W H, Stefan Schouten, Jurgen C. van den Donker, Ellen C. Hopmans, and Jaap S. Sinninghe Damsté. 2007b. "Environmental Controls on Bacterial Tetraether Membrane Lipid Distribution in Soils." *Geochimica et Cosmochimica Acta* 71: 703–13. doi:10.1016/j.gca.2006.10.003.
- Westerhold, T, and U Röhl. 2009. "High Resolution Cyclostratigraphy of the Early Eocene – New Insights into the Origin of the Cenozoic Cooling Trend." *Climate of the Past* 5: 309–27. doi:10.5194/cpd-5-495-2009.
- Wilson, GJ. 1988. "Paleocene and Eocene Dinoflagellate Cysts from Waipawa, Hawkes Bay, New Zealand." *New Zealand Geological Survey Paleontological Bulletin* 57: 96.
- Wing, Scott L, Guy J. Harrington, Francesca A. Smith, Jonathan I. Bloch, Doug M. Boyer, and Katherine H. Freeman. 2005. "Transient Floral Change and Rapid Global Warming at the Paleocene-Eocene Boundary." *Science* 310: 993–96. doi:10.1126/science.1116913.
- Zachos, James C., David K. Rea, Koji Seto, Ritsuo Nomura, and Nobuaki Niitsuma. 1992. "Paleogene and Early Neogene Deep Water Paleooceanography of the Indian Ocean as Determined from Benthic Foraminifer Stable Carbon and Oxygen Isotope Records." In *In: Synthesis of Results from Scientific Drilling in the Indian Ocean; Geophysical Monograph* 70, 351–85. American Geophysical Union. doi:10.1029/GM070p0351.
- Zachos, James C, Gerald R Dickens, and Richard E Zeebe. 2008. "An Early Cenozoic Perspective on Greenhouse Warming and Carbon-Cycle Dynamics." *Nature* 451 (7176): 279–83.
- Zachos, J, M Pagani, L Sloan, E Thomas, and K Billups. 2001. "Trends, Rhythms, and Aberrations in Global Climate 65 Ma to Present." *Science (New York, N.Y.)* 292 (5517): 686–93. doi:10.1126/science.1059412.
- Zeebe, Richard E., James C. Zachos, and Gerald R. Dickens. 2009. "Carbon Dioxide Forcing Alone Insufficient to Explain Palaeocene–Eocene Thermal Maximum Warming." *Nature Geoscience* 2 (8).

Nature Publishing Group: 576–80. doi:10.1038/ngeo578.

Zell, Claudia, Jung Hyun Kim, David Hollander, Laura Lorenzoni, Paul Baker, Cleverson Guizan Silva, Charles Nittrouer, and Jaap S Sinninghe Damsté. 2014. "Sources and Distributions of Branched and Isoprenoid Tetraether Lipids on the Amazon Shelf and Fan: Implications for the Use of GDGT-Based Proxies in Marine Sediments." *Geochimica et Cosmochimica Acta* 139: 293–312.

Zhu, Chun, Johan W H Weijers, Thomas Wagner, Jian Ming Pan, Jian Fang Chen, and Richard D Pancost. 2011. "Sources and Distributions of Tetraether Lipids in Surface Sediments across a Large River-Dominated Continental Margin." *Organic Geochemistry* 42: 376–86.

Appendix C

Table 1: The adjusted global soil data set from De Jonge et al. (2014). The samples are ordered by sample name. MAT (°C), soil pH C-org (%) and MAP (mm/year) are present-day values. The other indices shown are calculated using Eqs 9-16.

ID	Sample name	MAT	pH	C-org	MAP	Sum tetra	Sum penta	Sum hexa	IR penta	IR hexa	#rings tetra	#rings penta	#rings penta'
1	Australia-17	13.90	6.40		624	59.3	34.2	6.4	0.50	0.50	0.25	0.04	0.15
2	Australia-4	19.00	6.60	2.90	677	54.2	40.7	5.1	0.33	0.51	0.05	0.03	0.06
3	Brazil-12	24.90	6.20		2060	88.3	10.9	0.8	0.54	0.70	0.41	0.41	0.30
4	Brazil-13	24.90	3.90			95.8	3.8	0.4	0.08	0.28	0.05	0.00	0.00
5	Brazil-14	21.20	4.00			91.4	7.8	0.8	0.21	0.56	0.01	0.00	0.00
6	Brazil-28	25.60	5.90		1570	92.8	6.6	0.6	0.61	0.62	0.14	0.12	0.30
7	Cameroon-1	21.70	6.40	3.00	1950	83.6	15.1	1.3	0.56	0.50	0.43	0.31	0.30
8	Canada-14	6.10	4.00		1474	61.7	36.6	1.7	0.00	0.06	0.11	0.04	
9	Canada-17	2.40	7.70		505	23.8	54.5	21.8	0.59	0.68	0.46	0.45	0.36
10	Canada-24	9.50	5.00		2031	51.6	38.6	9.8	0.04	0.12	0.07	0.05	0.12
11	China-19	22.40	4.60	2.22	2006	95.7	4.3	0.0	0.16		0.03	0.00	0.00
12	China-20	24.70	3.90	1.87	1600	91.8	7.8	0.4	0.15	0.00	0.04	0.00	0.00
13	China-23	18.20	4.50	0.58	1590	87.6	10.5	1.9	0.36	0.61	0.03	0.07	0.07
14	China-25	17.20	5.50	0.82	1670	80.5	17.5	2.0	0.52	0.54	0.11	0.10	0.09
15	China-27	17.80	4.70	5.18	1590	85.7	13.1	1.2	0.16	0.35	0.04	0.02	0.10
16	China-31	19.60	6.10	4.22	1720	87.0	12.0	1.0	0.47	0.51	0.27	0.17	0.24
17	China-32	20.80	4.30	1.36	1690	91.7	7.1	1.2	0.22	0.55	0.04	0.06	0.25
18	China-49	14.00	6.50	3.66	1210	57.0	35.9	7.1	0.76	0.59	0.74	0.39	0.65
19	China-6	19.20	7.10	2.93	1876	76.7	21.0	2.3	0.59	0.62	0.35	0.23	0.15
20	China-MG1180	14.32	7.90			44.4	45.6	10.1	0.65	0.64	0.17	0.09	0.18
21	China-MG1220	14.08	7.30			65.3	30.9	3.8	0.61	0.60	0.24	0.17	0.27
22	China-MG1515	12.31	6.40			84.0	15.2	0.8	0.06	0.19	0.01	0.00	0.00
23	China-MG1645	11.53	7.50			39.5	47.8	12.7	0.61	0.68	0.58	0.51	0.43
24	China-MG1740	10.96	6.70			49.3	41.7	9.0	0.62	0.65	0.37	0.38	0.36
25	China-MG1800	10.60	7.10			32.1	51.4	16.5	0.65	0.72	0.44	0.40	0.32
26	China-MG1850	10.30	7.50			33.3	51.8	14.9	0.63	0.64	0.47	0.39	0.38
27	China-MG1915	9.91	6.90			55.3	39.2	5.5	0.35	0.37	0.25	0.11	0.20
28	China-MG1973	9.56	7.70			24.0	55.1	20.9	0.68	0.77	0.61	0.64	0.42
29	China-MG2005	9.37	7.50			40.3	48.3	11.4	0.45	0.58	0.28	0.22	0.26
30	China-MG2115	8.71	7.10			24.8	52.3	22.9	0.59	0.69	0.66	0.61	0.52
31	China-MG2160	8.44	7.90			35.6	48.7	15.6	0.58	0.65	0.47	0.38	0.30
32	China-MG2220	8.08	6.60			37.2	48.7	14.0	0.42	0.53	0.25	0.15	0.19
33	China-MG2300	7.60	6.70			41.9	43.8	14.4	0.33	0.42	0.13	0.05	0.14
34	China-MG2350	7.30	6.90			37.1	47.2	15.7	0.49	0.63	0.26	0.19	0.26
35	China-MG2420	6.88	7.20			28.6	47.5	23.9	0.43	0.57	0.27	0.19	0.27
36	China-MG2470	6.58	7.90			26.8	50.0	23.2	0.59	0.70	0.32	0.24	0.26
37	China-MG2540	6.16	7.80			24.9	48.9	26.3	0.59	0.68	0.42	0.50	0.48
38	China-MG2620	5.68	6.50			34.7	47.0	18.3	0.44	0.51	0.40	0.35	0.31
39	China-MG2742	4.95	4.40			67.5	29.1	3.3	0.03	0.08	0.07	0.07	0.05
40	China-MG2764	4.82	5.90			44.4	44.7	10.9	0.11	0.11	0.12	0.07	0.07
41	China-MG2808	4.55	5.00			57.4	35.8	6.8	0.07	0.18	0.09	0.08	0.07
42	China-MG2960	3.64	7.20			34.5	48.5	17.0	0.37	0.41	0.41	0.29	0.21
43	China-MG3049	3.11	4.50			47.8	43.2	9.0	0.00	0.04	0.06	0.05	
44	China-MG3065	3.01	6.40			30.5	48.6	20.9	0.21	0.27	0.08	0.07	0.25
45	China-MG3119	2.69	5.60			39.6	47.6	12.8	0.12	0.05	0.06	0.06	0.10
46	China-MG3140	2.56	4.90			58.5	36.5	5.0	0.04	0.13	0.04	0.03	0.05
47	China-MG3145	2.53	7.30			21.9	48.3	29.7	0.35	0.49	0.18	0.22	0.32
48	China-MG3188	2.27	5.30			43.1	43.4	13.5	0.05	0.03	0.06	0.04	0.04
49	China-MG3209	2.15	5.00			33.3	42.0	24.7	0.09	0.03	0.07	0.03	0.04
50	China-MG3676	-0.66	6.60			36.4	43.5	20.1	0.24	0.13	0.05	0.05	0.04
51	China-MG3769	-1.21	6.30			38.0	45.1	16.9	0.10	0.06	0.05	0.03	0.03

52	China-MG3819	-1.51	5.00			38.6	43.9	17.5	0.07	0.04	0.06	0.04	0.05
53	Colombia-12	13.80	4.80			85.1	13.9	1.0	0.19	0.26	0.05	0.05	0.07
54	Colombia-14	6.60	5.50	750		44.6	42.9	12.5	0.06	0.06	0.11	0.09	0.06
55	Colombia-7	26.20	4.20	2900		98.0	1.9	0.1	0.06	0.00	0.04	0.17	0.00
56	Colombia-9	26.20	3.80	2900		98.7	1.3	0.0	0.07		0.02	0.04	0.00
57	Ecuador-19	12.70	6.60	2900		49.3	43.7	7.0	0.59	0.60	0.51	0.38	0.31
58	Ecuador-6	26.20	4.90	2900		93.1	6.7	0.3	0.32	0.44	0.09	0.04	0.13
59	Ecuador-7	26.20	4.60	2900		94.7	5.1	0.2	0.36	0.63	0.07	0.14	0.17
60	Egypt-1	25.00	7.60	30		62.3	33.6	4.1	0.89	0.87	0.53	0.55	0.31
61	France-15	8.30	4.70	6.00	664	46.9	43.1	10.0	0.10	0.09	0.07	0.03	0.07
62	France-TESO1	4.00	4.92		1009	43.1	44.8	12.1	0.09	0.05	0.12	0.03	0.05
63	France-TESO10	8.40	6.46		758	23.4	42.2	34.5	0.50	0.70	0.24	0.14	0.10
64	France-TESO11	12.90	6.83		556	22.9	43.5	33.6	0.58	0.75	0.35	0.22	0.17
65	France-TESO12	11.70	6.59		719	23.8	46.2	30.0	0.57	0.72	0.31	0.18	0.15
66	France-TESO13	12.80	6.32		568	31.5	53.1	15.5	0.48	0.54	0.49	0.38	0.32
67	France-TESO14	12.80	7.68		552	19.3	47.8	32.8	0.65	0.77	0.33	0.15	0.17
68	France-TESO14B	12.80	7.81		552	21.6	49.8	28.7	0.72	0.79	0.38	0.32	0.30
69	France-TESO15	11.50	6.39		770	24.8	45.3	29.9	0.54	0.68	0.30	0.16	0.21
70	France-TESO16	11.50	6.39		770	29.9	47.9	22.2	0.44	0.56	0.37	0.18	0.18
71	France-TESO18	10.10	5.52		959	45.8	41.6	12.6	0.13	0.11	0.06	0.04	0.06
72	France-TESO19	14.20	7.87		633	23.9	52.3	23.7	0.84	0.83	0.46	0.52	0.26
73	France-TESO2	3.90	4.67		1053	35.3	47.8	16.9	0.07	0.05	0.09	0.04	0.12
74	France-TESO22B	14.30	8.48		637	29.0	46.4	24.6	0.59	0.70	0.37	0.25	0.24
75	France-TESO24	14.60	7.77		648	24.9	45.7	29.4	0.60	0.68	0.27	0.15	0.21
76	France-TESO25	14.50	7.90		646	26.3	52.8	20.9	0.82	0.84	0.33	0.26	0.30
77	France-TESO26	14.90	7.26		648	27.3	50.2	22.6	0.60	0.64	0.50	0.33	0.35
78	France-TESO28	13.50	8.43		633	28.0	48.5	23.5	0.65	0.73	0.43	0.37	0.28
79	France-TESO3	3.60	4.65		1052	41.4	48.3	10.3	0.06	0.06	0.09	0.06	0.05
80	France-TESO30	14.30	7.40		637	36.1	48.3	15.6	0.52	0.58	0.24	0.13	0.22
81	France-TESO31	15.30	7.51		634	32.0	46.4	21.6	0.89	0.80	0.48	0.31	0.39
82	France-TESO34	15.30	8.11		617	32.1	48.5	19.4	0.51	0.60	0.67	0.47	0.55
83	France-TESO36	15.40	7.47		577	25.9	52.1	21.9	0.63	0.67	0.36	0.33	0.30
84	France-TESO43	15.20	6.90		605	26.6	52.0	21.4	0.51	0.53	0.30	0.24	0.26
85	France-TESO43B	15.20	7.47		605	24.1	52.6	23.3	0.53	0.58	0.31	0.17	0.27
86	France-TESO47	10.50	6.98		549	36.6	46.5	16.9	0.67	0.75	0.45	0.38	0.35
87	France-TESO48	6.40	4.64		728	39.1	45.5	15.4	0.09	0.08	0.11	0.04	0.08
88	France-TESO49	7.70	4.82		790	42.1	48.1	9.8	0.04	0.06	0.11	0.07	0.00
89	France-TESO5	3.60	4.18		1098	45.3	40.0	14.8	0.14	0.14	0.13	0.10	0.07
90	France-TESO51	8.50	6.90		613	22.3	44.4	33.3	0.56	0.73	0.34	0.20	0.20
91	France-TESO6	4.60	4.87		1054	35.2	50.9	13.9	0.14	0.07	0.09	0.04	0.03
92	France-TESO7	12.60	7.48		553	30.0	50.0	19.9	0.55	0.67	0.65	0.68	0.43
93	France-TESO8	9.20	5.42		574	43.1	45.8	11.1	0.30	0.27	0.09	0.03	0.10
94	Gabon-4	25.80	5.30	2.73	2158	96.7	3.1	0.2	0.37	0.77	0.05	0.00	0.07
95	Gabon-5	26.30	5.10	2.22	2158	98.0	2.0	0.0	0.15		0.01	0.00	0.00
96	Gabon-6	26.00	5.90	2.45	1969	88.7	10.6	0.6	0.65	0.54	0.28	0.33	0.23
97	Galapagos	24.00	4.40		451	92.4	7.3	0.2	0.12	0.42	0.04	0.01	0.04
98	Germany-G1	5.40	7.40		805	47.4	35.8	16.8	0.25	0.47	0.09	0.21	0.39
99	Germany-G2	5.80	7.30		805	20.3	45.1	34.6	0.37	0.52	0.46	0.57	0.39
100	Germany-H1	8.70	6.10		768	41.1	46.6	12.3	0.20	0.24	0.51	0.22	0.30
101	Greece-13	12.10	5.40		458	52.8	38.1	9.0	0.16	0.18	0.00	0.00	0.00
102	Greece-5	15.70	7.40	3.74	446	22.2	50.1	27.8	0.81	0.80	0.58	0.50	0.17
103	Greenland-5	-0.40	5.50		984	37.2	47.0	15.8	0.34	0.18	0.08	0.10	0.02
104	Iceland-6	3.50	6.10	6.59	706	38.3	49.1	12.5	0.29	0.22	0.32	0.13	0.20
105	Iceland-sa	3.50	5.30		706	37.0	48.0	15.0	0.05	0.09	0.13	0.05	0.00
106	Ireland-9	8.80	3.80	24.00	928	58.1	38.0	3.9	0.00	0.06	0.12	0.07	
107	Italy-1	14.00	6.20	2.90	811	50.5	41.2	8.3	0.55	0.50	0.15	0.08	0.07
108	Italy-11	15.40	5.40	1.94	1007	51.4	40.4	8.2	0.35	0.31	0.04	0.02	0.08
109	Italy-14	14.20	5.60	3.69	1007	47.8	43.2	8.9	0.49	0.42	0.09	0.04	0.06

110	Italy-17	15.40	7.60	1.63	1007	36.3	43.3	20.4	0.70	0.70	0.48	0.47	0.41
111	Netherlands-B	9.50	7.70		761	20.5	52.9	26.5	0.83	0.77	0.61	0.55	0.56
112	Netherlands-T7	9.40	3.70		752	56.6	38.5	4.9	0.02	0.10	0.09	0.08	0.00
113	Nigeria-19	26.80	7.30	2.20	1507	78.7	20.1	1.2	0.70	0.64	0.65	0.64	0.47
114	Norway-1	5.00	7.60	1.85	1048	22.4	52.8	24.8	0.62	0.70	0.43	0.42	0.36
115	Norway-3	5.30	4.30	5.98	892	57.1	37.1	5.8	0.00	0.00	0.08	0.05	
116	Peru-10	25.50	4.40		1350	95.0	4.6	0.4	0.15	0.24	0.02	0.19	0.08
117	Peru-13	26.20			2900	99.7	0.3	0.0	0.08		0.14	0.00	0.00
118	Peru-14	26.20			2900	98.5	1.5	0.0	0.06		0.06	0.32	0.00
119	Rarotonga	23.80	5.40		2112	95.8	4.0	0.2	0.24	0.52	0.04	0.26	0.09
120	Scotland-D	8.20	5.40		991	49.1	43.6	7.3	0.06	0.06	0.12	0.05	0.13
121	Seychelles	26.60	5.20		235	98.6	1.4	0.0	0.14		0.03	0.00	0.00
122	South Africa-12	18.40	5.50	2.91	759	84.4	14.8	0.7	0.21	0.39	0.04	0.00	0.00
123	South Africa-16	19.90	6.00	2.75	759	84.5	14.4	1.1	0.46	0.53	0.08	0.07	0.00
124	South Africa-3	18.40	4.40	3.29	759	89.3	10.3	0.4	0.14	0.26	0.08	0.00	0.00
125	Spain-6	16.40	6.60	0.80	486	42.3	45.6	12.2	0.48	0.37	0.11	0.04	0.06
126	Svalbard-LB1	-6.00	4.35		190	19.9	54.8	25.3	0.49	0.43	0.13	0.13	0.14
127	Svalbard-MP1	-6.00	7.11		190	27.9	51.1	20.9	0.53	0.54	0.09	0.09	0.09
128	Svalbard-MP2	-6.00	8.29		190	14.3	46.4	39.3	0.68	0.72	0.32	0.28	0.27
129	Svalbard-MP3	-6.00	5.50		190	30.1	53.6	16.3	0.39	0.30	0.10	0.08	0.03
130	Svalbard-MP4	-6.00	8.34		190	13.7	54.1	32.2	0.76	0.77	0.37	0.29	0.36
131	Svalbard-MP5	-6.00	8.25		190	14.4	49.5	36.1	0.70	0.75	0.38	0.35	0.36
132	Svalbard-MP6	-6.00	9.34		190	12.2	39.4	48.4	0.57	0.58	0.37	0.28	0.36
133	Svalbard-NA1	-6.00	7.42		190	11.4	41.0	47.6	0.58	0.66	0.19	0.25	0.12
134	Svalbard-NA2	-6.00	6.32		190	26.9	54.7	18.4	0.48	0.33	0.04	0.06	0.03
135	Sweden-15	0.70	4.50	2.13	569	56.1	39.4	4.5	0.04	0.07	0.06	0.07	0.00
136	Sweden-4	7.70	7.70	0.92	578	24.8	53.0	22.2	0.69	0.70	0.40	0.44	0.33
137	Sweden-B	5.30	4.00		641	41.2	48.5	10.3	0.35	0.43	0.52	0.33	0.31
138	Netherlands-A the	9.00	6.70		720	31.2	51.1	17.7	0.64	0.73	0.39	0.32	0.31
139	Netherlands-F the	9.00	6.70		720	33.7	51.5	14.8	0.51	0.52	0.33	0.18	0.25
140	Netherlands-J the	9.00	6.40		720	30.9	51.3	17.8	0.65	0.72	0.38	0.28	0.29
141	Netherlands-M	9.00	6.90		720	24.8	50.6	24.6	0.71	0.78	0.44	0.40	0.36
142	Turkey-12	10.40	8.00	1.05	547	28.3	41.5	30.3	0.83	0.85	0.35	0.59	0.15
143	Turkey-8	10.50	8.00	1.06	340	22.0	25.1	52.9	0.93	0.96	0.13	0.00	0.00
144	Uganda-1	12.00	3.60		1483	70.9	26.3	2.8	0.00	0.07	0.03	0.04	
145	Uganda-2	2.00	5.10		1483	16.4	40.9	42.7	0.07	0.05	0.01	0.02	0.04
146	Uganda-3	24.00	7.10		1483	66.7	29.5	3.8	0.77	0.60	0.58	0.46	0.47
147	Uruguay-7	17.30	5.60	0.39	1133	83.7	13.6	2.7	0.35	0.39	0.06	0.00	0.00
148	Uruguay-8	17.30	5.30	3.72	1133	83.9	15.4	0.8	0.28	0.32	0.04	0.01	0.00
149	USA-10	24.20	5.10	3.98	1093	92.9	6.7	0.3	0.17	0.49	0.09	0.09	0.19
150	USA-13	10.00	5.90	2.11	493	64.9	31.4	3.7	0.42	0.53	0.11	0.06	0.11
151	USA-17	-2.90	7.10	3.98	277	25.2	50.6	24.3	0.45	0.45	0.26	0.18	0.27
152	USA-BB1	6.10	4.25	12.84	1200	64.6	31.0	4.4	0.02	0.08	0.05	0.04	0.06
153	USA-BB2	6.10	4.60	5.22	1200	59.7	34.1	6.2	0.05	0.12	0.10	0.04	0.09
154	USA-BF1	7.80	4.05	6.44	1000	64.0	31.7	4.3	0.03	0.09	0.06	0.04	0.09
155	USA-BP1	6.60	7.53	3.10	450	24.9	52.6	22.5	0.66	0.67	0.37	0.25	0.23
156	USA-BZ2	-2.90	5.16	3.03	260	32.9	51.0	16.1	0.21	0.09	0.03	0.04	0.02
157	USA-BZ3	-2.90	5.36	3.73	260	39.9	45.5	14.6	0.03	0.02	0.02	0.02	0.04
158	USA-CA1	10.30	7.27	1.67	400	18.3	56.3	25.4	0.66	0.60	0.34	0.09	0.14
159	USA-CA2	10.30	8.02	2.15	400	15.6	54.7	29.7	0.72	0.64	0.33	0.11	0.11
160	USA-CC1	5.80	6.06	1.91	720	65.4	30.8	3.9	0.32	0.35	0.13	0.07	0.10
161	USA-CF1	5.30	3.92	2.56	1300	61.4	33.2	5.4	0.05	0.07	0.11	0.07	0.09
162	USA-CF2	5.30	3.63	4.06	1300	70.3	27.2	2.6	0.02	0.16	0.06	0.06	0.04
163	USA-CF3	5.30	3.56	4.33	1300	78.9	19.8	1.4	0.02	0.21	0.06	0.07	0.00
164	USA-CL1	15.90	5.68	2.33	1250	73.6	23.2	3.2	0.34	0.47	0.11	0.05	0.23

165	USA-CL2	15.90	5.57	2.27	1250	75.9	21.8	2.3	0.30	0.32	0.09	0.06	0.10
166	USA-CL3	15.90	4.89	1.21	1250	78.9	18.6	2.4	0.13	0.30	0.04	0.02	0.17
167	USA-CM1	18.50	7.85	2.99	850	47.7	40.7	11.6	0.59	0.61	0.70	0.49	0.43
168	USA-CO1	-3.00	6.13	1.59	600	26.0	53.0	21.1	0.37	0.27	0.18	0.05	0.07
169	USA-CO2	6.10	5.68	1.81	350	33.7	49.4	16.9	0.33	0.22	0.07	0.00	0.00
170	USA-CO3	9.30	6.02	0.82	322	40.7	49.1	10.3	0.39	0.41	0.09	0.04	0.08
171	USA-DF1	14.60	5.37	2.78	1100	73.7	22.9	3.4	0.10	0.10	0.06	0.02	0.15
172	USA-DF3	14.60	5.05	1.70	1100	76.1	21.5	2.4	0.06	0.18	0.04	0.00	0.00
173	USA-GB2	2.00	7.57	6.89	400	12.0	44.4	43.6	0.82	0.82	0.54	0.62	0.28
174	USA-GB3	2.00	7.18	5.71	400	20.5	52.6	26.9	0.80	0.74	0.22	0.21	0.17
175	USA-GB4	2.00	6.85	3.62	400	21.1	53.0	25.9	0.57	0.48	0.24	0.17	0.08
176	USA-GB5	4.80	8.22	1.68	400	9.9	35.9	54.3	0.82	0.87	0.32	0.21	0.11
177	USA-GB6	2.00	7.23	2.24	400	16.7	52.2	31.1	0.76	0.77	0.31	0.33	0.17
178	USA-HF2	7.00	3.98	9.55	1100	68.1	29.4	2.4	0.02	0.10	0.03	0.03	0.00
179	USA-HI3	22.80	6.53	18.24	1000	57.9	37.2	4.9	0.46	0.60	0.40	0.25	0.32
180	USA-HJ1	9.40	5.41	6.95	2000	43.4	41.2	15.4	0.32	0.21	0.05	0.00	0.00
181	USA-IE2	8.60	5.52	4.07	1200	58.8	36.2	5.0	0.18	0.15	0.15	0.07	0.06
182	USA-IE3	8.60	5.72	6.41	1200	48.0	44.3	7.8	0.37	0.37	0.28	0.11	0.17
183	USA-IE4	8.60	6.29	3.27	1200	48.0	44.6	7.5	0.51	0.56	0.50	0.42	0.30
184	USA-IE5	8.60	5.57	5.29	1200	59.4	35.4	5.2	0.17	0.16	0.19	0.08	0.09
185	USA-IT1	3.00	5.78	6.31	750	46.7	45.5	7.8	0.23	0.24	0.15	0.07	0.16
186	USA-IT2	3.00	5.42	3.91	750	48.3	43.8	7.9	0.11	0.12	0.09	0.04	0.12
187	USA-KP1	12.50	6.37	6.12	835	58.6	36.4	5.1	0.41	0.44	0.33	0.21	0.15
188	USA-KP2	12.50	6.50	4.62	835	64.7	31.2	4.2	0.44	0.46	0.24	0.14	0.10
189	USA-LQ2	21.50	5.03	4.11	3500	94.2	5.5	0.3	0.15	0.29	0.07	0.01	0.09
190	USA-MP1	8.80	4.56	10.70	2200	34.8	45.2	20.1	0.05	0.03	0.04	0.04	0.03
191	USA-MP2	8.80	4.38	9.87	2200	35.3	44.0	20.8	0.04	0.02	0.03	0.03	0.07
192	USA-R-1	8.00	6.60		918	38.4	43.3	18.3	0.76	0.32	0.56	0.33	0.48
193	USA-R-2	8.60	6.50		876	43.3	48.5	8.2	0.27	0.37	0.51	0.33	0.38
194	USA-R-3	7.10	7.70		815	41.3	47.2	11.5	0.51	0.60	0.57	0.44	0.43
195	USA-R-4	7.20	7.70		719	31.4	50.4	18.2	0.47	0.56	0.50	0.37	0.37
196	USA-R-5	3.80	8.10		307	21.5	43.3	35.2	0.79	0.79	0.32	0.58	0.17
197	USA-R-6	8.50	7.40		419	26.3	46.8	26.9	0.60	0.51	0.20	0.15	0.11
198	USA-RT1	18.10	7.92	3.94	840	48.2	41.7	10.1	0.79	0.68	0.73	0.36	0.55
199	USA-RT2	18.10	8.07	3.75	840	46.8	43.2	10.0	0.81	0.64	0.70	0.27	0.55
200	USA-SA1	10.30	6.90	2.29	400	24.8	50.2	25.0	0.50	0.32	0.09	0.05	0.06
201	USA-SB1	15.00	7.92	2.65	550	13.2	56.1	30.7	1.00	0.97	0.15		0.05
202	USA-SN1	3.60	4.95	4.25	600	22.3	49.7	28.1	0.23	0.17	0.18	0.00	0.00
203	USA-SN3	3.60	5.74	1.66	600	24.1	52.9	23.0	0.25	0.18	0.09	0.03	0.03
204	USA-SP1	12.70	6.25	1.68	650	35.4	50.1	14.5	0.48	0.33	0.11	0.06	0.07
205	USA-SP2	3.60	5.13	8.10	750	37.2	47.8	14.9	0.10	0.06	0.07	0.04	0.01
206	USA-SR1	17.20	6.84	4.59	500	22.3	54.4	23.3	0.53	0.48	0.11	0.05	0.09
207	USA-SR2	17.20	8.00	1.46	500	12.6	44.8	42.6	0.84	0.74	0.27	0.33	0.10
208	USA-SR3	17.20	6.95	3.30	500	16.1	53.9	30.1	0.57	0.50	0.13	0.03	0.06
209	USA-SV1	13.50	8.31	0.30	210	11.8	56.1	32.1	1.00	0.94	0.10		0.03
210	USA-SV2	13.50	8.44	0.23	210	17.7	55.8	26.5	0.96	0.92	0.15	0.00	0.05
211	USA-SV4	13.50	8.29	0.27	210	24.9	51.2	23.8	0.90	0.93	0.07	0.07	0.03
212	USA-VC1	2.50	5.55	5.67	500	37.6	50.3	12.2	0.31	0.36	0.06	0.02	0.07
213	USA-VC2	2.50	5.99	3.44	500	38.0	51.5	10.5	0.34	0.29	0.19	0.12	0.08
214	USA-W	9.90	4.50		1239	76.0	22.4	1.7	0.04	0.21	0.04	0.05	0.00
215	Zaire-1	24.60	3.90		1871	91.6	7.7	0.7	0.11	0.00	0.03	0.00	0.00
216	Zaire-2	24.60	4.10	1.26	1871	97.7	2.3	0.0	0.09		0.04	0.00	0.00

Table 2: The adjusted global peat data set from (Naafs, Inglis, Zheng, Amesbury, Biester, Bindler, Blewett, Burrows, del Castillo Torres, Chambers, Cohen, Evershed, Feakins, Gallego-Sala, et al., 2017). Annual mean temperature (°C) and pH are present-day values. The number of samples is used to calculate an average of the peat and from this the indices are calculated, using Eqs 9-16.

	Country	Peat location/name	# samples	Annual mean Temp.	pH	Sum tetra	Sum penta	Sum hexa	#rings Tetra	#rings Penta	#rings Penta'	IR penta	IR hexa
1	Ireland	Ballyduff Bog	9	8.3	4	58.69	36.58	4.73	0.11	0.08		0.00	0.05
2	UK	Butterburn Flow	7	8.0	4.15	58.65	36.32	5.03	0.07	0.06		0.00	0.00
3	Germany	Bissendorfer Moor	8	8.9	4	56.04	40.37	3.60	0.11	0.06		0.00	0.01
4	Finland	Kontolanrahka	5	4.4	4	58.31	38.39	3.29	0.05	0.01		0.00	0.00
5	Peru	Maquía	4	25.8	6.1	94.96	4.88	0.16	0.06	0.14	0.10	0.35	0.37
6	Peru	Buena Vista del Maquía	8	25.8	6	94.44	5.33	0.23	0.05	0.07		0.00	0.00
7	Peru	Nueva Alianza	4	26.4	5.7	90.63	9.19	0.17	0.07	0.06	0.16	0.40	0.00
8	Peru	Tacshacocho	4	26.7	5.1	94.40	5.50	0.10	0.05	0.05		0.00	0.00
9	France	Fransne, Jura Mountains	16	9.6	3.5	57.85	37.10	5.05	0.05	0.03		0.00	0.02
10	Switzerland	Lörmoos	2	9.0	4.32	59.08	37.91	3.01	0.03	0.01		0.00	0.00
11	Switzerland	Praz Rodet	2	9.6	4.26	66.51	30.43	3.05	0.05	0.03		0.00	0.00
12	Switzerland	Sortel	2	4.3	4.82	53.78	37.68	8.54	0.05	0.03		0.00	0.01
13	Switzerland	Hochrajen	2	1.5	4.55	54.86	39.20	5.94	0.06	0.02		0.00	0.00
14	Tanzania	Kyambangunguru	4	24.4	5.4	77.77	20.05	2.18	0.06	0.04	0.08	0.33	0.41
15	Poland	Kojle Lake	2	6.3		64.95	32.49	2.57	0.08	0.07		0.00	0.01
16	Latvia	Teici Bog	2	5.0		63.27	34.28	2.44	0.04	0.02		0.00	0.00
17	Romania	Poiana Siol	2	2.3		58.14	37.09	4.76	0.04	0.05		0.00	0.00
18	China	Tibetean Plateau	8	-1.0	5.5	34.18	51.91	13.91	0.15	0.04	0.13	0.07	0.13
19	Argentina	Andorra	13	4.5	5.4	40.23	48.46	11.31	0.04	0.02	0.00	0.04	0.07
20	Queensland	Bomfield Swamp	14	21.1	6.5	85.61	13.24	1.15	0.11	0.10	0.04	0.07	0.13
21	Chile	SKY1	6	6.5	4.25	45.27	43.97	10.75	0.06	0.05	0.00	0.10	0.00
22	USA	Okefenokee Swamp	3	20.5	4	90.57	8.88	0.55	0.09	0.07		0.00	0.13
23	USA	Dismal Swamp	1	15.7	4	81.96	17.25	0.79	0.18	0.09		0.00	0.00
24	USA	North Carolina Peat	1	17.1	3.7	84.33	15.11	0.56	0.18	0.08		0.00	0.00
25	USA	Shark River peat	1	24.5	6.51	70.78	25.63	3.59	0.49	0.34	0.31	0.60	0.46
26	USA	Tamiami Sawgrass Peat	1	23.9	7.14	68.43	28.53	3.04	0.48	0.33	0.35	0.30	0.47
27	USA	Loxahatchee Sawgrass Peat	1	24.7	6.65	82.95	15.85	1.20	0.20	0.16	0.13	0.23	0.23
28	USA	Loxahatchee Nymphaea Peat	1	24.7	7.94	79.84	18.39	1.77	0.25	0.16	0.17	0.22	0.42
29	USA	Snuggedy Swamp Peat	1	19.3		79.55	18.92	1.53	0.30	0.35		0.00	0.03
30	USA	New York Peat (Fort Drum)	1	6.5	7.85	35.16	45.86	18.98	0.62	0.39	0.37	0.38	0.43
31	USA	Maine Sphagnum peat	1	5.7	4.28	59.75	36.67	3.58	0.11	0.07		0.00	0.10
32	Spain	Chao de Veiga Mol	8	12.4	4.1	58.09	37.38	4.53	0.09	0.08		0.00	0.02
33	Spain	Borralleiras da Cal Grande	6	13.9	4.1	59.09	36.76	4.15	0.12	0.08		0.00	0.03
34	Spain	Zalama	8	12.1	4.65	56.63	39.91	3.46	0.14	0.09		0.00	0.01
35	Iran	Peat near Neor Lake	7	4.8		25.00	50.26	24.66	0.46	0.18	0.24	0.24	0.24
36	Brazil	Pau de Fruta	6	19.4	3.8	87.15	11.81	1.04	0.07	0.05		0.00	0.00
37	Brazil	São João da Chapada	5	19.4	3.9	89.41	9.74	0.84	0.07	0.08		0.00	0.05
38	Brazil	Sempre Viva	5	19.4	3.3	88.91	10.53	0.55	0.11	0.05		0.00	0.02
39	Brazil	Pinheiros	6	19.4	3.7	82.90	15.81	1.29	0.06	0.04		0.00	0.02
40	Russia	Igarka Site 1+2	6	-8.3		30.55	48.13	21.32	0.16	0.06	0.13	0.28	0.26
41	UK	Walton Moss	6	8.1		59.37	36.20	4.43	0.05	0.06		0.00	0.01
42	Belgium	Poleur	2	7.5		41.39	40.24	18.37	0.09	0.07		0.00	0.00
43	UK	Bodmin Moor	2	8.6		52.16	38.01	9.83	0.05	0.05		0.00	0.00
44	Argentina	Harberton	8	4.0		50.01	41.68	8.31	0.10	0.04		0.00	0.07
45	Poland	Kosova mire	2	7.8		75.19	21.70	3.11	0.02	0.02		0.00	0.00
46	France	OHM Vicdessos	3	3.8		59.03	33.81	7.16	0.05	0.04		0.00	0.00
47	Switzerland	Simplon	2	5.5		60.48	33.07	6.45	0.04	0.03		0.00	0.00
48	Iceland	Fjallsjökull	2	4.0		9.88	35.46	54.67	0.31	0.12	0.14	0.78	0.93
49	Switzerland	Fachepremont	2	3.5		74.46	23.89	1.65	0.04	0.02		0.00	0.00

50	France	Pinet Fosse	3	8.4		62.04	34.97	2.99	0.06	0.03		0.00	0.00
51	Poland	Linje mire	2	8.1		68.80	25.40	5.81	0.07	0.01		0.00	0.00
52	Norway	N. Norway	1	1.6		50.31	43.04	6.65	0.06	0.02		0.00	0.00
53	Iceland	S. Iceland	2	11.3		21.96	49.86	28.18	0.25	0.20	0.11	0.67	0.68
54	Switzerland	Flesch	2	5.5		58.35	38.23	3.42	0.03	0.02	0.00	0.06	0.16
55	Switzerland	Hängstli	1	10.8		83.30	15.00	1.70	0.04	0.02		0.00	0.00
56	Kenya	Nyabuiyabui	3	9.8		53.69	40.57	5.74	0.09	0.08	0.04	0.03	0.04
57	Kenya	Shidodo	6	22.5		75.81	21.58	2.61	0.09	0.10	0.05	0.16	0.28
58	Kenya	Marula	2	14.3		65.30	28.82	5.87	0.09	0.14	0.00	0.09	0.17
59	Tanzania	Kitulu	4	17.4		54.12	37.66	8.22	0.17	0.11	0.13	0.10	0.14
60	Japan	Piyashiri	6	14.3		51.95	39.33	8.72	0.06	0.03		0.00	0.02
61	Germany	Harz, Odersprung Bog	19	6.2	4.25	51.35	42.33	6.31	0.10	0.10		0.00	0.02
62	Canada	Chénéville	2	6.2		64.35	31.87	3.78	0.07	0.05		0.00	0.00
63	Canada	Parc-des-grands-Jardins	2	3.2		40.77	47.52	11.70	0.06	0.04		0.00	0.00
64	Canada	Peace river	2	-0.3		35.08	46.54	18.39	0.07	0.10	0.32	0.10	0.30
65	Canada	Radisson	5	-3.0		39.18	46.01	14.81	0.04	0.04		0.00	0.00
66	Canada	Sainte-Eulalie	2	5.3		72.55	25.83	1.62	0.07	0.04		0.00	0.01
67	Canada	Seba beach	2	2.7		51.93	41.10	6.97	0.08	0.04		0.00	0.00
68	Canada	Shippagan 527	2	4.9		71.40	26.73	1.86	0.05	0.04		0.00	0.00
69	Canada	SS70-14	2	-3.6		18.62	51.48	29.90	0.53	0.35	0.40	0.59	0.24
70	Canada	Waswanipi	3	0.4		65.51	31.54	2.95	0.06	0.04		0.00	0.00
71	Scotland	Kentra Bay 007G	9	5.8	5	49.60	43.82	6.58	0.16	0.07		0.00	0.00
72	Scotland	Kentra Bay 004D	11	5.8	4.85	48.89	46.12	4.99	0.13	0.05		0.00	0.00
73	Scotland	Kentra Bay 001A	10	5.8	6.12	49.00	44.00	7.00	0.16	0.10	0.50	0.05	0.14
74	Scotland	Kentra Bay M3	9	5.8	4.70	53.00	40.51	6.50	0.15	0.09	0.09	0.06	0.02
75	Scotland	Kentra Bay M4	10	5.8	4.74	57.02	37.33	5.66	0.08	0.05		0.00	0.00
76	Scotland	Kentra Bay M1	9	5.8	5.49	44.08	46.01	9.90	0.19	0.13	0.14	0.22	0.20
77	Scotland	Kentra Bay 009I	10	5.8	4.87	51.27	43.27	5.47	0.13	0.08		0.00	0.00
78	N-Ireland	Fallahogy Bog	6	9.4		59.98	35.19	4.83	0.09	0.10		0.00	0.00

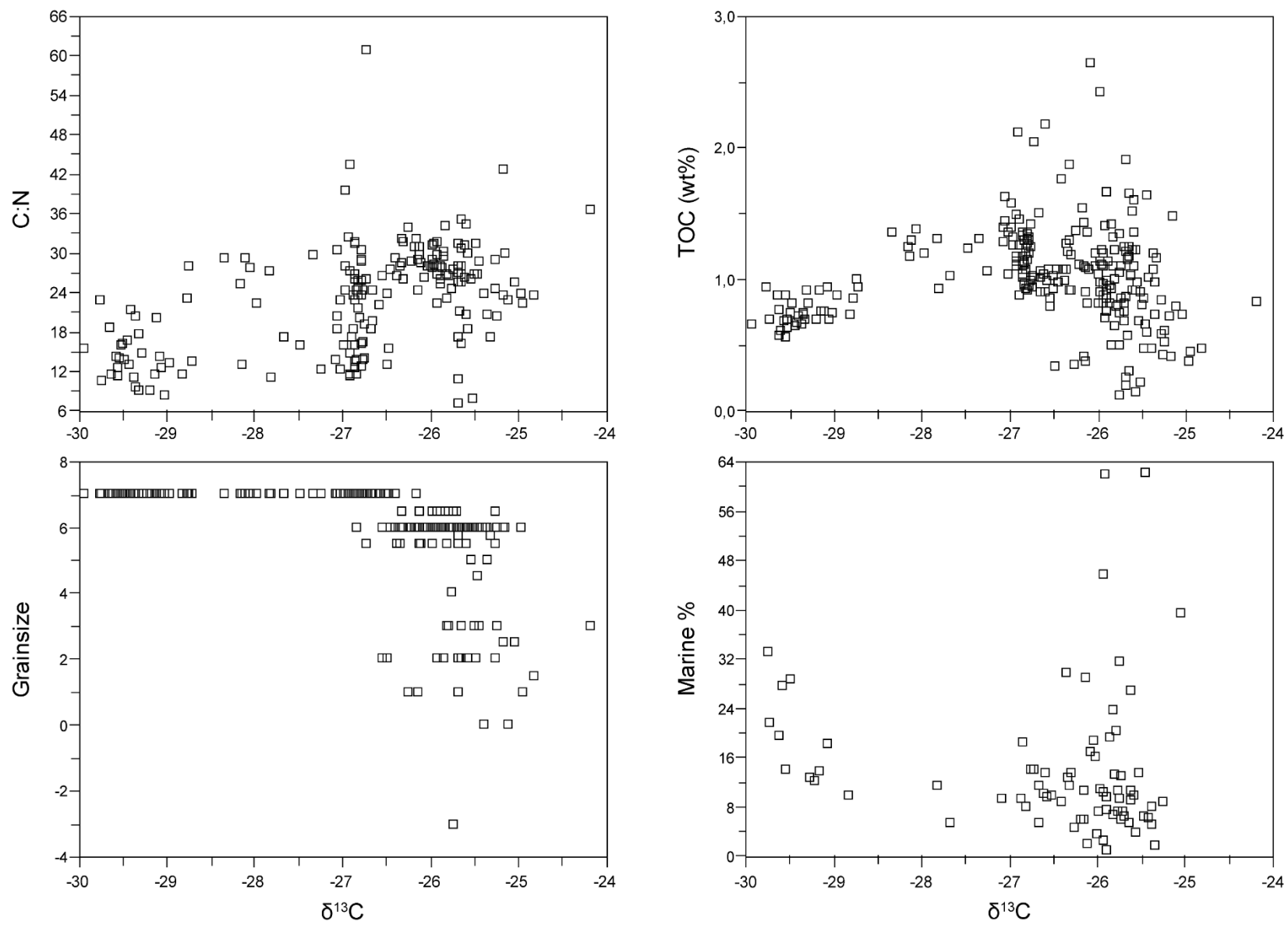


Figure 1: Comparison of $\delta^{13}C_{org}$ with different environmental variables a) C:N b) TOC (wt%) c) grainsize d) marine %. The grainsize of each sample has been determined by looking at the log (Fig. 3) and the marine % has been determined by taking the ratio between the actual abundance of dinocysts and terrestrial palynomorphs.

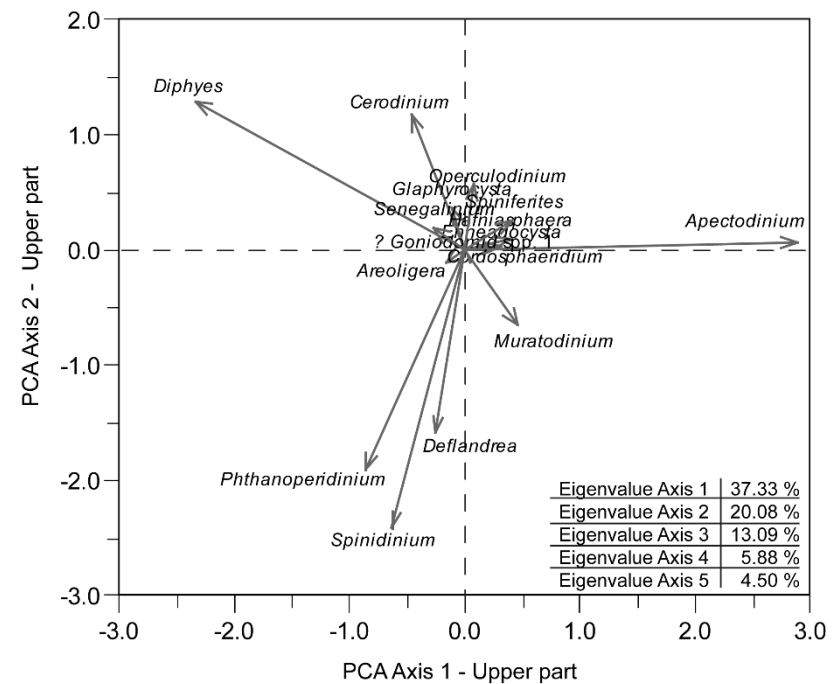
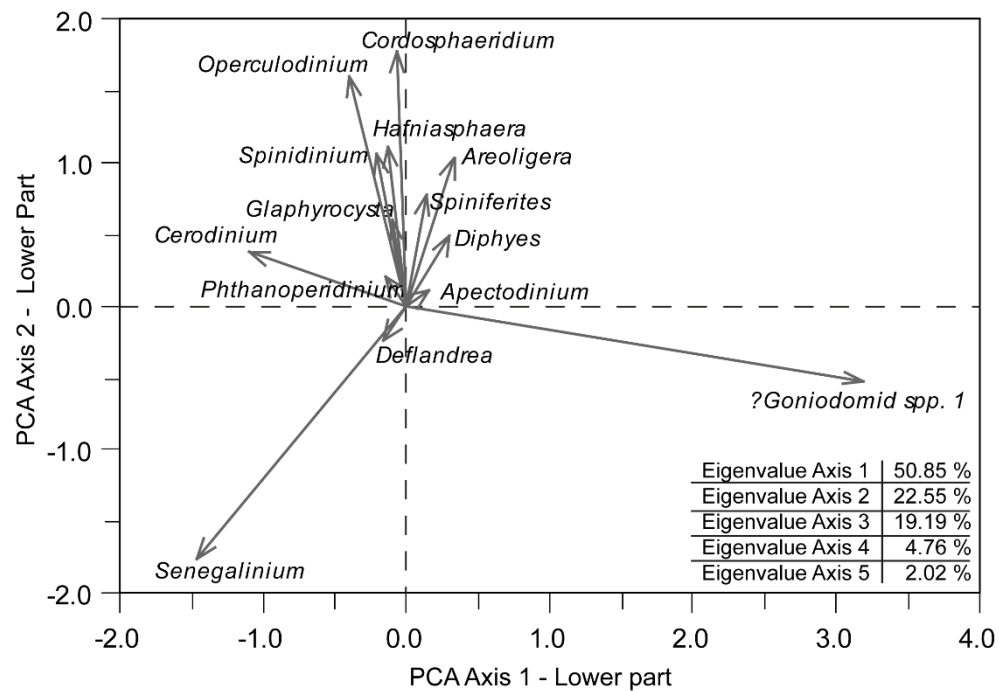


Figure 2: Principal component analysis (PCA) performed separately on the lower (1.7-32.5) and upper (> 32.5) part of Margaret Point, a square root transformation was performed

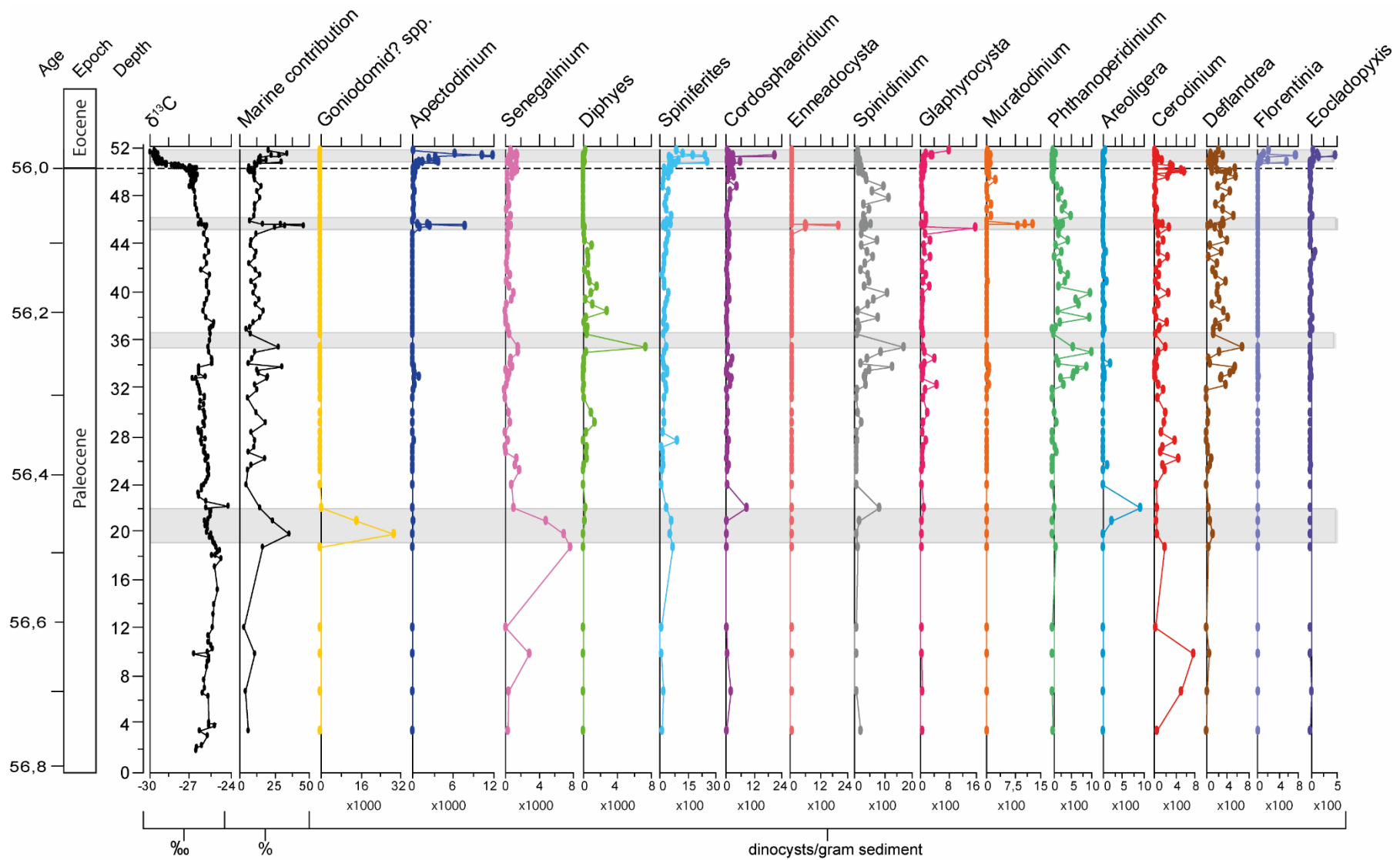


Figure 3: Absolute dinocysts abundances plotted against depth and age of the section. All species with more than 400 species per gram sediment somewhere in the section was selected. $\delta^{13}\text{C}$ and the marine contribution, the part of the sample that has a marine origin, are also plotted. The grey bands in the figure show the four phases where there was a peak of high absolute abundance of a dinocysts species. These are Goniodomid? spp., Diphyes and two times Apectodinium respectively, from the bottom to the top of the section. The dotted line shows the depth of the onset of the negative CIE.